POLITECNICO DI MILANO

Scuola di Ingegneria Industriale e dell'Informazione

Master of Science in Automation and Control Engineering

TUNING AND CONTROLLING OPTICAL TELECOMMUNICATION CHANNELS BASED ON RING RESONATOR MODULATORS

SUPERVISOR: Prof. Alberto Leva

Master thesis by:

Seyed Alireza Tabatabaei Mashayekh

Student ID: 833196

Academic Year 2016 – 2017

Dedicated to my mother

Acknowledgments

I would like to express my special appreciation to my advisor Prof. Alberto Leva for supporting me by a valuable guidance and encouragement.

I would like to appreciate Prof. Dr. Jeremy Witzens, Dr. Florian Merget and Dr. Alvaro Moscoso Martier about supporting me during the 1 year hardworking on this project by providing a very precious practical and theoretical guidance in IPH- Integrated Photonics at RWTH- Aachen university by sharing a valuable achievements and infrastructures to realize this master project.

Special thanks to my parents for their support and attention throughout my whole life in general.

Abstract

Silicon micro ring resonators have been hailed for their potential use in next-generation optical interconnects. However, the functionality of silicon micro ring based devices suffer from susceptibility to thermal fluctuations that is often overlooked in their demonstrated results, but must be resolved for their future implementation in microelectronic applications. In this work we survey the emerging efforts that have been put forth to resolve these thermal susceptibilities and provide a comprehensive discussion of their advantages and disadvantages. The growing bandwidth needs within data applications have motivated the replacement of traditional electronic links with optical links for information networks as diverse as data centers, supercomputers, and fiber-optic access networks. Applications such as these stress the traditional portfolio of optical components, rebalancing the emphasis from expensive high-performance components towards low-cost high-volume components that can be closely integrated with electronics. With these considerations in mind, the silicon photonics platform has received wide attention for its ability to deliver the necessary bandwidth required at an economy-of-scale that will be enabled by its compatibility with CMOS fabrication processes. Online controlling of the micro rings is the main goal of the project presented in this thesis, not only to obtain a production-grade package in commercialized scale and take advantage of the optical telecommunication facilities in a feasible way but also to achieve user friendliness and independence of the used PC/Spectrometer in tuning the optical telecommunication channels while in data transmission.

Table of Contents

I. Chapter1: Introduction 13
Optical telecommunication 13
Overview 13
Optical Data modulation 14
Silicon photonics 17
Silicon photonics towards silicon Laser 17
Laser 18
Key Optical Components 22
Overview 22
Interconnection 23
Receiver 29
Optical Amplification 31
Optical filters 34
Multiplexer & De-Multiplexer 36
Motivation and goals of this project 37
Organization of content 38
II. Chapter 2: WDM System subject to control 40
Overview 40
WDM in Macro Scale 41
WDM System Architecture in Micro Scale 43
Laser 44
Transmitter 45
Receiver 47
WDM Control System 48
III. Chapter 3: Hardware 50
Overview 50
Microcontroller – Xmega256A3BU 51
Analog to Digital Convertor (ADS1158) 54
Digital to Analog Convertor (MAX5732) 56
Power supply 58
Trans-Impedance Amplifier (TIA) 69
Output Buffers (OPA4251) 73
High Current Output Buffer (OPA567) 76
IV. Chapter 4: Software 79
Overview 79

System Under control 80
The closed-loop transfer function 82
Analog disturbances in a digital system 83
Analog sub system evaluation 84
Data Acquisition and Identification 91
PID Controller Simulation 99
Simulation of PID for receiver side 102
Approaches to control System 104
Approaches for Realization of Control Methods by Hardware 112
V. Chapter 5: Measurement Results and Conclusion 117
Overview 117
Measurement Results 117
..... 121
Conclusion and Prospects 123

I. Chapter1: Introduction

Optical telecommunication

Overview

Optical communication is any type of communication in which light is used to carry the signal to the remote end, instead of electrical current. Optical communication relies on optical fibers to carry signals to their destinations [1]. A modulator/demodulator, a transmitter/receiver, a light signal and a transparent channel are the building blocks of the optical communications system. Because of its numerous advantages over electrical transmission, optical fibers have largely replaced copper wire communications in core networks in the developed world.

Since the development of low-loss optical fiber cables in the 1970s, optical communications became one of the most popular methods of communication. Optical communication systems consist of the following components:

1. Transmitter: Converts and transmits an electronic signal into a light signal. The most commonly used transmitters are semiconductor devices, such as light-emitting diodes (LEDs) and laser diodes.
2. Receivers: Typically consist of a photo-detector, which converts light into electricity using the photoelectric effect. The photo detector is typically a semiconductor-based photodiode.
3. Optical Fiber: Consists of a core, cladding and a buffer through which the cladding guides the light along the core by using total internal reflection.

The main benefits of optical communication include high bandwidth, exceptionally low loss, great transmission range and no electromagnetic interference. The cons of optic communication include the high cost of cable, transmitter/receiver and other support equipment, and the skill and expertise required during cable installation and interconnection.

An overview of optical telecommunication data transmission cycle is shown in Figure 1.1(A) which contains Input & Output Data, Transmitter/Receiver, Optical fiber and Detectors. A sample of an Optical Telecommunication Network is shown in Figure 1.1 (B).

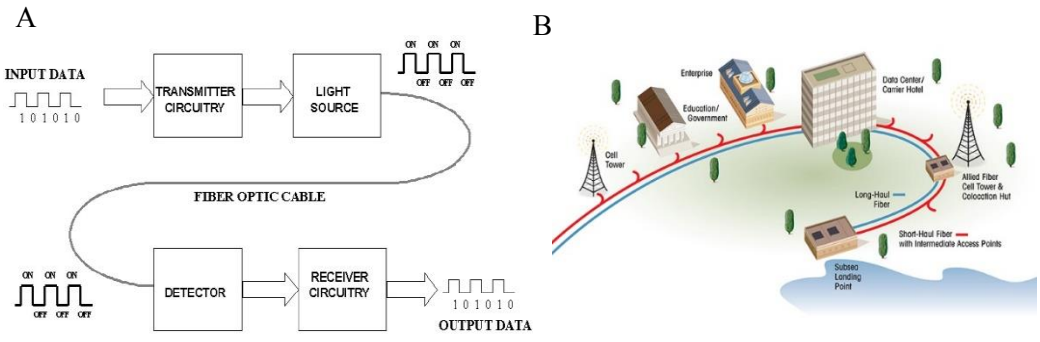

Figure 1.1 – (A) Block Diagram of Optical Telecommunication Cycle (B) Optical Telecommunication Network

Optical Data modulation

Overview

a) Direct Modulation

Digital signals consist of logical 1s and 0s, which readily corresponds to electrical ON and OFF states, or to two discrete voltage (or current) levels. The typical optical communications light source is a laser diode, which is easily modulated by controlling its current. Several factors limit the upper frequency at which a laser diode can be modulated. These include the time constants (frequency response) of the driving circuitry, the physics of the diode itself, and the characteristics of the transmission medium, which is typically an optical fiber. Microwave design and layout techniques have been used to assure performance of driving circuitry well into the GHz range, removing this as a major limitation [2]. Optical fibers have a certain amount of dispersion, which introduces uncertainty at the detector, related mainly to transmission distance [3]. This uncertainty is worse at high data rates—integration can help solve the uncertainty, and there is less integration time with the shorter highspeed pulses.

Ultimately, direct modulation is limited by the characteristics of the diode itself. A full turn-on/turn-off cycle represents a significant electrical and thermal stress, which can result in a frequency shift (chirp), transients (ringing), as well as reduced operational lifetime, of the laser diode. One method of dealing with these effects is to apply a modulated "radio signal" to the diode. The current swing is reduced, which improves reliability, and the bandwidth is greatly increased because the diode's drift and transient responses are reduced. But this technique also greatly reduces the signal-to- noise ratio, which reduces the range, and it requires more complex driver and detector circuitry.

b) Indirect Modulation

Modulation of a continuous light beam removes the laser diode-related problems at the cost of greater complexity. It also eliminates the signal-to-noise problems of applying a modulated subcarrier. The stable light source allows maximum transmission distance for a given amount of dispersion in the fiber. Established methods include delivering the data to electrically modulated crystalline materials such as lithium neonate. These devices can rapidly switch the light beam between a direct signal path, or split the beam into two paths with 180-degree phase shift, which cancel when recombined. This provides electrically controlled on-off transitions that do not affect the light source. The other common method uses electro-absorption (EA) modulators, usually a semiconductor material that can be switched between trans missive and opaque states to provide the on-off transitions. Materials used in these modulators can be conveniently integrated with the laser diode. As with direct modulation, the driving circuitry uses microwave design and layout to couple high speed data streams to the modulating devices. The latest methods of achieving indirect modulation are fully integrated onto a single substrate. The latest developments in solid state optical switching are faster than EA, so switched optical paths are used, integrated onto the same substrate, with optical paths typically using transparent versions of the same material. Figure 1.2 is a block diagram of such an optical modulator, which can be further integrated with a detector onto a microprocessor or other device, as on-chip optical interface.

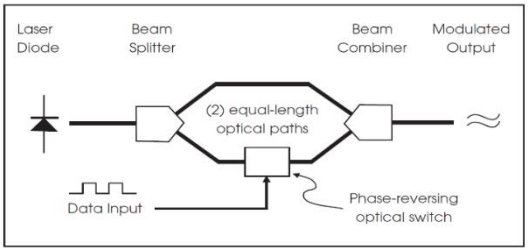

Figure 1.2- Functional diagram of an optical modulator

Wavelength Division Modulation WDM

Wavelength division multiplexing is a kind of *frequency division multiplexing* – a technique where optical signals with different wavelengths are combined, transmitted together, and separated again [4]. It is mostly used for optical fiber communications to transmit data in several (or even many) channels with slightly different wavelengths. In this way, the transmission capacities of fiber-optic links can be increased strongly, so that most efficient use is made not only of the fibers themselves but also of the active components such as fiber amplifiers. Apart from telecom, wavelength division multiplexing is also used for, e.g., interrogating multiple fiber-optic sensors within a single fiber.

Theoretically, the full data transmission capacity of a fiber could be exploited with a single data channel of very high data rate, corresponding to a very large channel bandwidth. However, given the enormous available bandwidth (tens of terahertz) of the low-loss transmission window of silica single-mode fibers, this would lead to a data rate which is far higher than what can be handled by optoelectronic senders and receivers. Also, various types of dispersion in the transmission fiber would have very detrimental effects on such wide-bandwidth channels, so that the transmission distance would be strongly restricted. Wavelength division multiplexing solves these problems by keeping the transmission rates of each channel at reasonably low levels (e.g. 10 Gbit/s or 100 Gbit/s) and achieving a high total data rate by combining several or many channels.

Two different versions of WDM, defined by standards of the International Telecommunication Union (ITU), are distinguished:

- *Coarse wavelength division multiplexing* (CWDM, ITU standard G.694.2 [6]) uses a relatively small number of channels, e.g. four or eight, and a large channel spacing of 20 nm. The nominal wavelengths range from 1310 nm to 1610 nm. The wavelength tolerance for the transmitters is fairly large, e.g. ±3 nm, so that unstabilized DFB lasers can be used. The single-channel bit rate is usually between 1 and 3.125 Gbit/s. The resulting total data rates are useful e.g. within metropolitan areas, if broadband technologies are not widespread in household.

- *Dense wavelength division multiplexing* (DWDM, ITU standard G.694.1 [7]) is the extended method for very large data capacities, as required e.g. in the Internet backbone. It uses many channels (e.g. 40, 80, or 160), and a correspondingly small channel spacing of 12.5, 25, 50 or 100 GHz. All optical channel frequencies refer to a reference frequency which has been fixed at 193.10 THz (1552.5 nm). The transmitters should meet tight wavelength tolerances. Typically, they are temperature-stabilized DFB lasers. The single-channel bit rate can be between 1 and 100 Gbit/s, and in the future even higher.

Due to the wide amplification bandwidth of EDFA (erbium-doped fiber amplifiers), all channels can often be amplified in a single device (except in cases where e.g. the full range of CWDM wavelengths is used). However, problems can arise from the variation of gain with wavelength or from interaction of the data channels (*crosstalk*, *channel interference*) e.g. via fiber nonlinearities. Enormous progress has been achieved with a combination of various techniques, such as the development of very broadband (double-band) fiber amplifiers, gain flattening filters, nonlinear data regeneration and the like. The system

parameters such as channel bandwidth, channel spacing, transmitted power levels, fiber and amplifier types, modulation formats, dispersion compensation schemes, etc., need to be well balanced to achieve optimum overall performance.

Even for existing fiber links with only one or a few channels per fiber, it can make sense to replace senders and receivers for operation with more channels, as this can be cheaper than replacing the whole system with a system with a higher transmission capacity. In fact, this approach often eliminates the need to install additional fibers, even though the demand on transmission capacities is increasing enormously.

Apart from increasing the transmission capacity, wavelength division multiplexing also adds flexibility to complex communication systems. In particular, different data channels can be injected at different locations in a system, and other channels can be extracted. For such operations, *add–drop multiplexers* can be used, which allow one to add or drop data channels based on their wavelengths. Reconfigurable add–drop multiplexers make it possible to reconfigure the system flexibly to provide data connections between many different stations. In Figure 1.3 we can see a basic scheme of WDM.

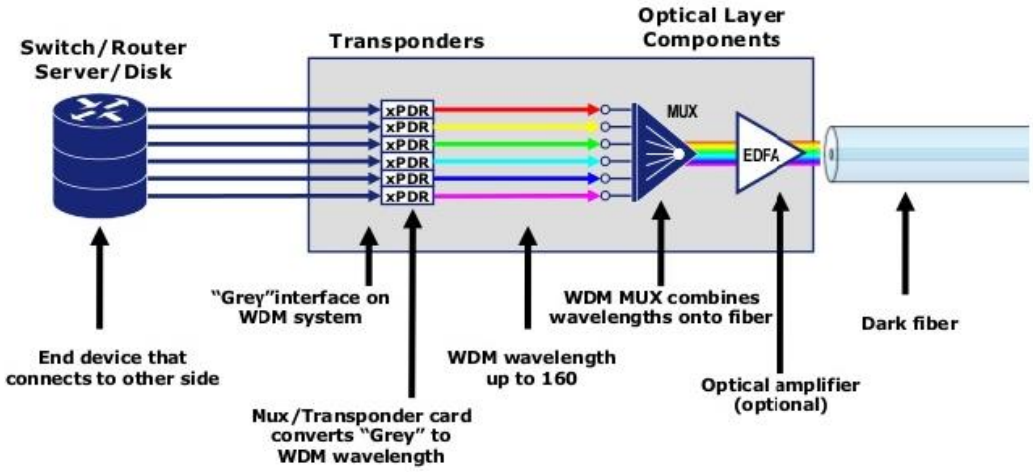

Figure 1. 3 - Basic Scheme of WDM

Silicon photonics

Overview

Silicon photonics can reuse the huge technology base and supply chain from electronics industry. Photonic components (i.e. modulators, detectors, sources) are fully compatible with CMOS technology [5]. Photonic links may replace copper links for very short distances and co-exist electronics in functional optoelectronic chips. The main role of silicon chip is bolded in optical telecommunication as interface of the data centers and optical fiber used in optical telecommunication. Figure 1.4 is an overview of the silicon photonic as an interface in optical data transmission cycle.

To summarize the pros and cons of the silicon photonic features we can introduce them as table 1.1.

Advantage	Disadvantage
Take advantage of CMOS platform	Indirect bandgap material
High index contrast (strong light confinement, small footprint)	Weak electro optic effect
Transparent in 1.3 – 1.6 μm region	Relatively lossy waveguides
Devices with sub-wavelength dimension feasible	Lacks efficient light emission – No electrically pumped Si laser

Table 1.1 – Pros and cons of Silicon photonics

Silicon photonics towards silicon Laser

There are different approaches to have integrated laser sources on silicon chips but in practice there exist lots of non-ideal behavior of the light sources. Also, it is needed to control the affecting parameters on the laser sources which makes use of them difficult. Here we briefly introduce the approaches of the integration of laser sources on silicon chips.

- **Hybrid silicon photonic integrated circuit technology**
  Bonding of functional III-V active components onto silicon-on-insulator substrates
- **Bonding of III-V epitaxial layers**
  Wafer or die bonding of III-V films on Si and processing thereof
- **hetero-epitaxial growth of III-V on Si**
  selectively grow III-V crystals on Si substrate
- **selective growth of Germanium on Si**
  Growth of Ge layers on silicon oxide trenches

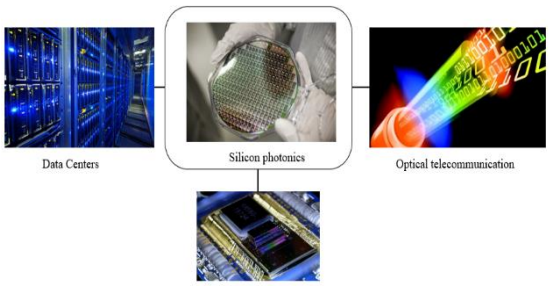

Figure 1.4 – Silicon Photonics in Optical data

Laser integration could be counted as challenges of silicon photonics because of alignment of laser structure and wave guides, CW operation at desired wave length, Key Enabling technology for integrated multi-lambda sources, up to 10mW coupled power. Next section will be a brief introduction about the basics of a laser source as main part of the silicon photonics.

Laser

Overview

Lasers are devices that produce intense beams of light which are *monochromatic*, *coherent*, and *highly collimated*. The wavelength (color) of laser light is extremely pure (monochromatic) when compared to other sources of light, and all the photons (energy) that make up the laser beam have a fixed phase relationship (coherence) with respect to one another [8]. Light from a laser typically has very low divergence. It can travel over great distances or can be focused to a very small spot with a brightness which exceeds that of the sun. Because of these properties, lasers are used in a wide variety of applications in all walks of life. The term "laser" is an acronym for (L)ight (A)mplification by (S)timulated (E)mission of (R)adiation. To understand the laser, one needs to understand the meaning of these terms. The term "light "is generally accepted to be electromagnetic radiation ranging from 1 nm to 1000 mm in wavelength. The visible spectrum (what we see) ranges from approximately 400 to 700 nm. The wavelength range from 700 nm to 10 mm is considered the near infrared (NIR), and anything beyond that is the far infrared (FIR). Conversely, 200 to 400 nm is called ultraviolet (UV); below 200 nm is the deep ultraviolet (DUV).

PHOTONS AND ENERGY

Light is made up of particles called "photons" which exhibit both particle-like and wave-like properties. Each photon has an intrinsic energy determined by the equation:

$$E = h\nu \qquad (1)$$

Where $\nu$the frequency of the light and h is is Planck's constant. Since, for a wave, the frequency and wavelength are related by the equation:

$$\lambda\nu = c \quad (2)$$

Where λ the wavelength of the light and c is the speed of light in a vacuum, equation 1 can be rewritten as:

$$E = \frac{hc}{\lambda} \quad (3)$$

It is evident from this equation that the longer the wavelength of the light, the lower the energy of the photon; consequently, ultraviolet light is much more "energetic" than infrared light.

Returning to the Bohr atom: for an atom to absorb light (i.e., for the light energy to cause an electron to move from a lower energy state E_n to a higher energy state E_m), the energy of a single photon must equal, almost exactly, the energy difference between the two states. Too much energy or too little energy and the photon will not be absorbed. Consequently, the wavelength of that photon must be:

$$\lambda = \frac{hc}{\Delta E} \ (4)$$

Where

$$\Delta E = E_m - E_n \ (5)$$

Likewise, when an electron decays to a lower energy level in a radiative transition, the photon of light given off by the atom must also have an energy equal to the energy difference between the two states.

SPONTANEOUS AND STIMULATED EMISSION

In general, when an electron is in an excited energy state, it must eventually decay to a lower level, giving off a photon of radiation. This event is called "spontaneous emission," and the photon is emitted in a random direction and a random phase. The average time it takes for the electron to decay is called the time constant for spontaneous emission. On the other hand, if an electron is in energy state $E2$, and its decay path is to $E1$, but, before it has a chance to spontaneously decay, a photon happens to pass by whose energy is approximately E_2-E_1, there is a probability that the passing photon will cause the electron to decay in such a manner that a photon is emitted at exactly the same wavelength, in exactly the same direction, and with exactly the same phase as the passing photon. This process is called "stimulated emission." Absorption, spontaneous emission, and stimulated emission are illustrated in Figure 1.5.
in any real population of atoms, the probability for stimulated emission is quite small. Furthermore, not all of the atoms are usually in an excited state; in fact, the opposite is true. Boltzmann's principle, a fundamental law of thermodynamics, states that, when a collection of atoms is at thermal equilibrium, the relative population of any two energy levels is given by:

$$\frac{N2}{N1} = \exp(-\frac{E_2 - E_1}{kT})$$

Where $N2$ and $N1$ are the populations of the upper and lower energy states, respectively, T is the equilibrium temperature, and k is Boltzmann's constant. Substituting $h\nu$ for $E2$ - $E1$ yields:

$$\Delta N = N_1 - N_2 = \left(1 - e^{-\frac{h\nu}{kT}}\right) N_1$$

For a normal population of atoms, there will always be more atoms in the lower energy levels than in the upper ones. Since the probability for an individual atom to absorb a photon is the same as the probability for an excited atom to emit a photon via stimulated emission, the collection of real atoms will be a net absorber, not a net emitter, and amplification will not be possible. Consequently, to make a laser, we have to create a "population inversion."

POPULATION INVERSION

Atomic energy states are much more complex than indicated by the description above. There are many more energy levels, and each one has its own time constants for decay. The four-level energy diagram shown in Figure 1.6 is representative of some real lasers. The electron is pumped (excited) into an upper level $E4$ by some mechanism (for example, a collision with another atom or absorption of high-energy radiation). It then decays to $E3$, then to $E2$, and finally to the ground state E1. Let us assume that the time it takes to decay from $E2$ to $E1$ is much longer than the time it takes to decay from $E2$ to E1. In a large population of such atoms, at equilibrium and with a continuous pumping process, a population inversion will occur between the $E3$ and $E2$ energy states, and a photon entering the population will be amplified coherently.

THE RESONATOR

Although with a population inversion we can amplify a signal via stimulated emission, the overall single-pass gain is quite small, and most of the excited atoms in the population emit spontaneously and do not contribute to the overall output. To turn this system into a laser, we need a positive feedback mechanism that will cause most of the atoms in the population to

contribute to the coherent output. This is the resonator, a system of mirrors that reflects undesirable (off-axis) photons out of the system and reflects the desirable (on-axis) photons back into the excited population where they can continue to be amplified.

Now consider the laser system shown in Figure 1.6. The lasing medium is pumped continuously to create a population inversion at the lasing wavelength. As the excited atoms start to decay, they emit photons spontaneously in all directions. Some of the photons travel along the axis of the lasing medium, but most of the photons are directed out the sides. The photons traveling along the axis have an opportunity to stimulate atoms they encounter to emit photons, but the ones radiating out the sides do not. Furthermore, the photons traveling parallel to the axis will be reflected back into the lasing medium and given the opportunity to stimulate more excited atoms. As the on-axis photons are reflected back and forth interacting with more and more atoms, spontaneous emission decreases, stimulated emission along the axis predominates, and we have a laser.

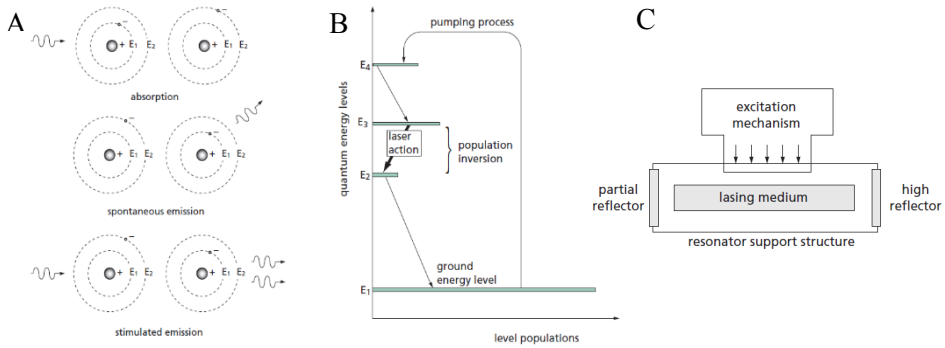

Figure 1.5 - (A) Spontaneous and stimulated emission (B) A four-level laser pumping system (C)

Laser spectrum

The optical spectrum (or *emission spectrum*) of a light source or some beam contains information on how the optical energy or power is distributed over different wavelengths. Usually, it is presented in the form of a diagram where the power spectral density (not necessarily with an absolute calibration) is plotted as a function of the wavelength or optical frequency. As an example, Figure 1.6 shows the numerically simulated optical spectrum of a supercontinuum source. In contrast to that very broad spectrum, the optical spectrum of a single-frequency laser source is often characterized by a very narrow line – in extreme cases, with a linewidth of the order of 1 Hz, corresponding to only ≈ $3 \cdot 10^{-12}$ nm (for 1 µm center wavelength). Other lasers have a spectrum consisting of multiple lines, and some (particularly mode-locked lasers for ultrashort pulses) can have a large spectral width of 100 nm or more with a frequency comb structure.

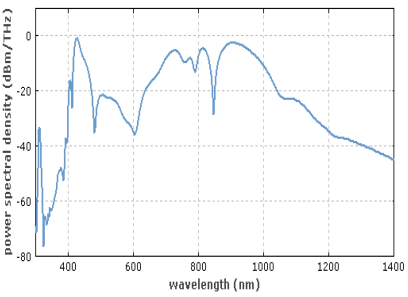

Figure 1.6 - Example of a Laser

Optical spectra can be recorded with different types of spectrometers, which greatly differ in terms of the covered spectral range and the spectral resolution.

The optical spectrum is intimately related to the temporal coherence properties of the light. For example, the temporal coherence function fully determines the spectrum. The optical spectrum is also related

to the Fourier transform of the electric field, although the latter is in most cases not directly accessible. Therefore, it is also called the *Fourier spectrum* of the optical field.

The optical bandwidth is essentially the width of the optical spectrum. There are different definitions, but the full width at half maximum (FWHM) is often used.

Single-Mode vs. Multi-Mode Laser

The term *single-mode operation*, which usually applies to lasers, is ambiguous, as it is used with different meanings:

- It can mean *single-transverse-mode operation*, where a laser operates on a single kind of *transverse* resonator mode, which is almost always a Gaussian mode (although operation on a single higher-order mode is also possible, e.g. by using some diffractive element in the laser resonator). If operation indeed occurs in a Gaussian mode, the laser's beam quality is diffraction-limited. However, laser oscillation may then still occur on multiple *axial* (longitudinal) modes, which have essentially the same transverse shape but differing optical frequencies, separated by the free spectral range.

- In other cases, the term really indicates operation on a single resonator mode, which is then also usually an axial (Gaussian) mode. This is more precisely called *single-longitudinal-mode operation* or *single-frequency operation*. In that case, the laser is a single-frequency laser, and the laser linewidth is fairly small (→*narrow-linewidth lasers*).

The number and type of oscillating resonator modes in a laser depends on the circumstances:

- The excitation of higher-order transverse modes can often be avoided by pumping only the volume covered by the axial modes. This is often done e.g. in end-pumped solid-state lasers.
- Multiple axial modes may still be excited, if the gain bandwidth is larger than the axial mode spacing (as is the case in most solid-state lasers). This may be changed by decreasing the gain bandwidth, by inserting an intracavity filter (e.g. an etalon), or by increasing the axial mode spacing (free spectral range), i.e. by using a very short laser resonator.

Single-frequency operation is usually more difficult to achieve than just single-transverse-mode operation, because it is not sufficient to introduce spatially varying loss or gain. Factors which make it more challenging are all those reducing the mode competition, e.g. inhomogeneous saturation via spatial hole burning.

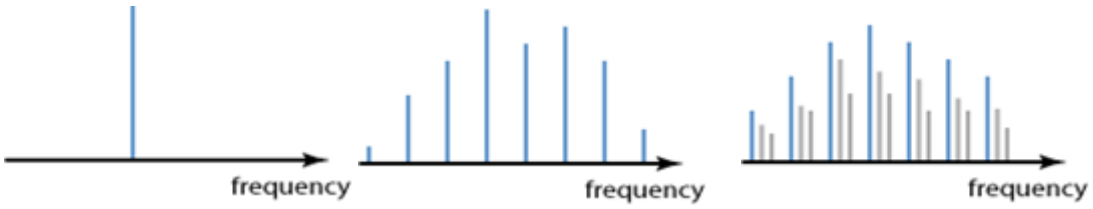

Figure 1.7 - Emission spectra of lasers with single-mode emission (top), multiple axial mode (but single transverse mode) emission (middle), and full multimode emission (bottom).

Key Optical Components

Overview

In this section, we would like to describe the basic optical components used in in an optical transmission system. An exemplary optical network identifying the key optical components shown in Figure 1.8 [9]. The end-to-end optical transmission involves both electrical and optical signal paths. To perform conversion from electrical to optical domain, the optical transmitters are used, while to perform conversion in opposite direction (optical to electrical conversion), the optical receivers are used. The optical fibers serve as foundation of an optical transmission system because the optical fiber is used as a medium to transport the optical signals from source to destination. The optical fibers attenuate the signal during transmission, and someone has to use optical amplifiers, such as erbium-doped fiber amplifiers (EDFAs), Raman amplifiers, or parametric amplifiers, to restore the signal quality. However, the process of amplification is accompanied with noise addition. The simplest optical transmission system employs only one wavelength. The wavelength division multiplexing (WDM) can be considered as an upgrade of the single-wavelength system.

During transmission of WDM signals, occasionally one or several wavelengths are to be added or dropped, which is performed by the optical component known as optical add–drop multiplexer (OADM). To combine several distinct wavelength channels into composite channel, the wavelength multiplexers are used. On the other hand, to split the composite WDM channel into distinct wavelength channels, the wavelength demultiplexers are used. To impose the information signal, optical modulators are used. The optical modulators are commonly used in combination with semiconductor lasers.

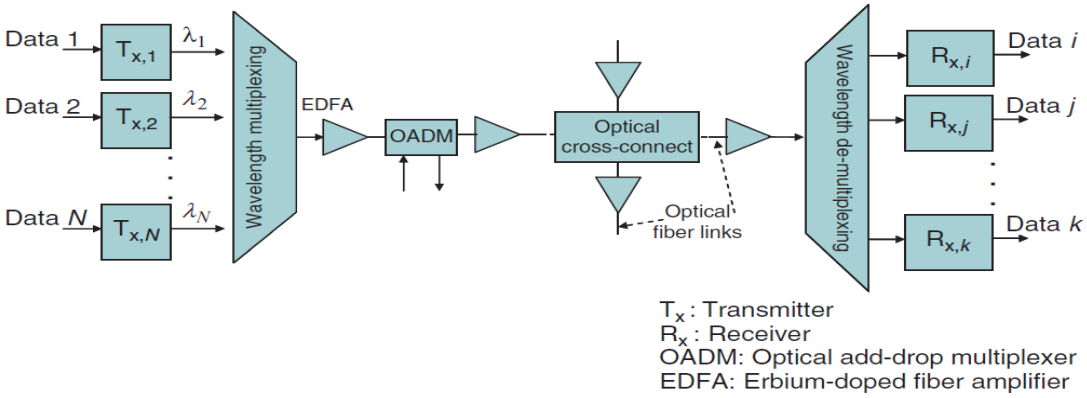

Figure 1.8 - An exemplary optical network identifying key optical components

Interconnection

c) Grating coupler and Edge Coupler

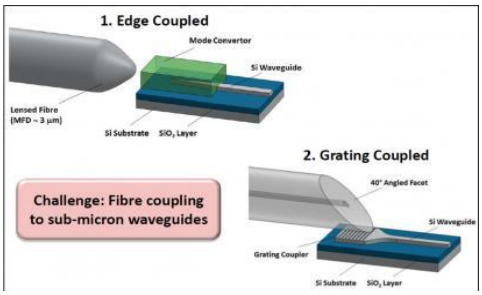

Figure 1.11 – Edge coupler vs. Grating Coupler

Materials with a high refractive index contrast are useful for high-density photonic integrated circuits. The basic building blocks of those circuits are nanophotonic waveguides such as photonic-crystal or photonic-wire waveguides. Examples of materials with a high refractive index contrast are silicon-on-insulator (SOI) or indium phosphide (InP) membranes with an air cladding [10]. However, a difficulty is coupling light between optical fibers and integrated waveguides. Because the waveguide core layer is only 100 – 300 nm thick and the guided mode is strongly confined in that core, there is a large mismatch between the waveguide mode and a single-mode fiber mode. This coupling problem is important and several groups have recently demonstrated1,2) coupling losses below 1 dB using an inverted lateral taper with a polymer overlay. Although this is a very elegant solution to the coupling problem, it may be beneficial to have a surface coupler that can be placed anywhere on a chip, not only at the edges. Such a coupler does not require polishing of facets and allows wafer-scale testing of photonic integrated circuits because light can be coupled in and out of the surface of the chip. Waveguide grating couplers are suitable for this task. The grating coupler can be fabricated using one additional lithography and etching step. Standard single-mode fibers and fiber arrays can be used for the packaging. The grating, which couples light from an out-of-plane fiber into a planar waveguide, is followed by an in-plane taper to couple to a single-mode photonic wire waveguide. The grating coupler can be shown schematically according to Figure 1.9.

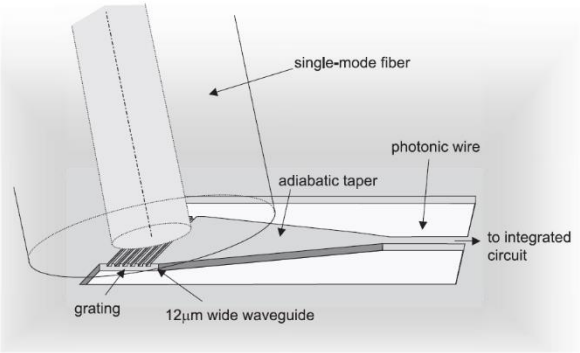

Figure1. 9 - principle of grating coupler for coupling

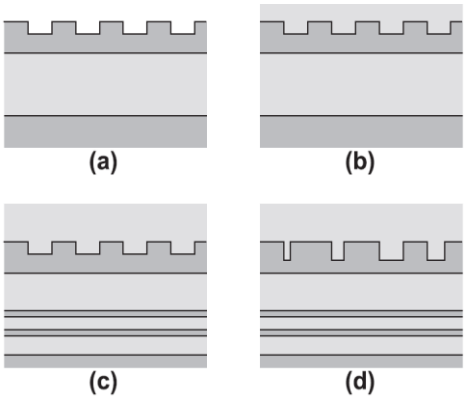

Figure 1.10 - Schematic drawing of different types of couplers: Uniform grating in (a) SOI with air top cladding, (b) SOI with oxide top cladding, (c) SOI With bottom Si/SiO2 mirror, (d) a grating coupler with varying groove widths is shown. Dark gray represents Si and light gray SiO2.

As shown in Figure 1.10, the difference among the grating coupler and edge coupler is obvious. In grating coupler, the fiber with a certain angle is approaching to the grating coupler and coupling is happening. However, in edge coupler lensed fiber is in the same level as wave guide and in sub-micron distance without any angle coupling is performed.

d) Waveguide

An optical waveguide is a spatially inhomogeneous structure for guiding light, i.e. for restricting the spatial region in which light can propagate. Usually, a waveguide contains a region of increased refractive index, compared with the surrounding medium (called cladding) [11]. However, guidance is also possible, e.g., using reflections, e.g. at metallic interfaces. Some waveguides also involve plasmonic effects at metals.

The applications of waveguides are manifold. Some examples are:

- Optical fibers allow the transmission of light over long distances, e.g. for optical fiber communications.
- On *photonic integrated circuits*, as used e.g. in *silicon photonics*, waveguides guide light between different optical components.
- In the future, silicon waveguides on digital processor chips and polymer waveguides in circuit boards may be used for fast optical data transmission between components of computers.
- Some waveguides are used for maintaining high optical intensities over appreciable lengths, e.g. in nonlinear devices [12] [13] such as frequency doublers and Raman lasers. Active (amplifying) waveguides are used in waveguide lasers and amplifiers. Important examples are fiber lasers and fiber amplifiers.
- A waveguide can be used for stripping off higher-order transverse modes, thus acting as a *mode cleaner*.
- In some cases, an interaction of the guided light with material in the evanescent field is used, e.g. in certain *waveguide sensors*.
- Waveguides can also be employed for splitting and combining light beams, e.g. in integrated optical interferometers.

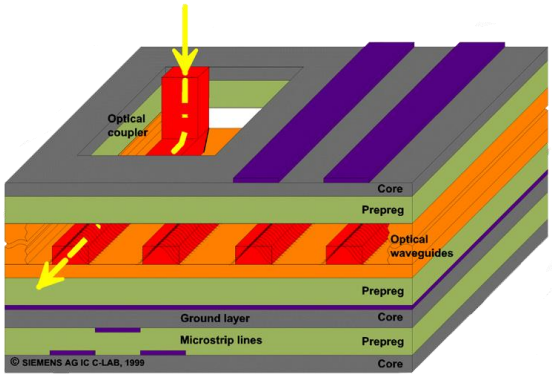

Figure 1.12 - Wave guide schematics in photonic devices

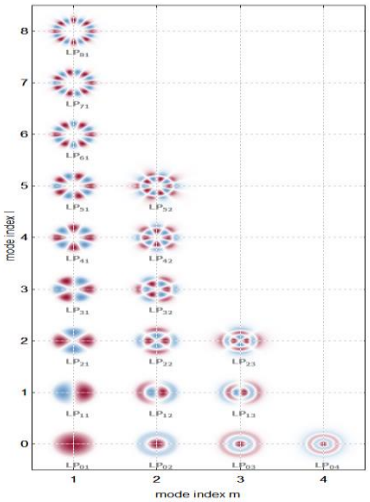

Figure 1.13 - Electric field amplitude profiles for all the

Waveguide structures are spatially inhomogeneous structures which can guide waves. For light propagating in a waveguide, the self-consistency condition for a mode is stricter than for free-space modes: the shape of the complex amplitude profile in the transverse dimensions must remain exactly constant. Any re-scaling is not allowed, only an overall phase change and a loss or gain of total optical power, which are both described by the *propagation constant*.

A waveguide has only a finite number of *guided propagation modes*, the intensity distributions of which have a finite extent around the waveguide core. The number of guided modes, their transverse amplitude profiles and their propagation constants depend on the details of the waveguide structure and on the optical frequency. A single-mode waveguide (e.g. a single-mode fiber) has only a single guided mode per polarization direction. As an example of a multimode waveguide, Figure 1.12 shows the transverse profiles of all the LP modes of a multimode fiber.

A waveguide also has *cladding modes*, the intensity distributions of which essentially fill the whole cladding (and core) region. Optical fibers (even single-mode fibers) have a large number of cladding modes, which often exhibit substantial propagation losses at the outer interface of the cladding.

Optical fibers (except for photonic crystal fibers) usually have a radially symmetric refractive index profile and also a relatively small refractive index contrast between core and cladding. In that case, one can quite accurately describes the mode as LP modes, which are mathematically simpler to describe and are therefore usually used in practice.

For radially symmetric refractive index profiles, there is also the interesting phenomenon of *orbital angular momentum modes* [12] [13].Those carry an angular momentum which is *not* related to the photon spin, also not to a rotating polarization direction. The wave fronts exhibit a helical structure. This is possible only for modes having zero intensity at the beam center – for example, LP modes with non-zero *l*.

Modes of fiber and other waveguides can be numerically calculated numerically with so-called *mode solvers*, which can be part of a fiber simulation software. Depending on whether the waveguides have radially symmetric profiles and are weakly guiding, mode solver algorithms with a different level of complexity and quite different computation times are required. A mode solver for optical fibers, when restricted to pure LP modes, can be numerically much simpler and faster than a general 2D mode solver.

Transmitter

e) Overview

For high-speed communication (10 GBit/s and beyond) it becomes extremely difficult to modulate the laser directly, therefore external optical modulators are used. The electro absorption modulator is such a modulator [9]. It can be understood as a reverse-biased PIN detector. Although it improves the chirp performance considerably compared to direct modulation of the laser, there is still enough chirp to make long haul high speed transmission impossible. More importantly, the modulator chirp is dynamic and changes with the actual drive voltage. Here we briefly describe the main modulation methods which contains MZI, EAM and finally RRM method.

f) Mach-Zender Modulators (MZM)

The optical signal generated by semiconductor laser has to be modulated by information signal before being transmitted over the optical fiber [14]. This can be achieved by directly modulating the bias current of semiconductor laser, which can be done even at high speed (even up to 40 Gb/s in certain lasers). Unfortunately, this concept although conceptually simple is

rarely used in practice because of the frequency chirp introduced by direct modulation, nonuniform frequency response, and large current swing needed to provide operation. For transmitters operating at 10 Gb/s and above, instead, the semiconductor laser diode (LD) is commonly biased at constant current to provide continuous wave (CW) output, and external modulators are used to impose the information signal to be transmitted. The most popular modulators are electro-optic optical modulators, such as Mach–Zehnder modulators, and electro absorption modulators [9] [15]. The principle of the external modulator is illustrated in Figure 1.15(A). Through the external modulation process, a certain parameter of the CW signal, used as a signal carrier, is varied in accordance with the information-bearing signal

There are two types of external modulators commonly used in practice: Mach– Zehnder modulator (MZM) and electro absorption modulator (EAM), whose operational principle is illustrated in Figure 1.15. The MZM is based on electro-optic effect, the effect that in certain materials (such as LiNbO3) where the refractive index n changes with respect to the voltage V applied across electrodes:

$$\Delta n = -\frac{1}{2}\,\Gamma\, n^3\, r_{33}\left(\frac{V}{d_e}\right) \;>>\; \Delta\varphi = \frac{2\pi}{\lambda}\,\Delta n\, L$$

Where Δn denotes the refractive index change, $\Delta\varphi$ is corresponding phase change, r_{33} is the electro-optic coefficient, d_e is separation of electrode length, and λ is the wavelength the light. The MZM (see Fig. 1.15(A)) is a planar waveguide structure deposited on the substrate, with two pairs of electrodes (1) for high-speed ac voltage representing the modulation data (RF) signal and (2) for dc bias voltage. Let V1.t / and V2.t / denote the electrical drive signals on the upper and lower electrodes, respectively. The output electrical field Eout.t / of the second Y-branch can be related to the input electrical filed Ein by:

$$E_{out}(t) = \frac{1}{2}\left[\exp\left(j\,\frac{\pi}{V_\pi}\,V_1(t)\right) + \exp\left(j\,\frac{\pi}{V_\pi}\,V_2(t)\right)\right] E_{in}$$

Where V_π is differential drive voltage. V1 -V2 = V_π resulting in differential phase shift of π rad between two waveguides. Possible modulation formats that can be used with this MZM include: on–off keying (OOK) with zero/nonzero chirp, binary phase-shift keying (BPSK), differential phase-shift keying (DPSK), quadrature phase-shift keying (QPSK), differential QPSK (DQPSK), and return-to-zero (RZ) with duty cycle 33%, 50%, or 67.

The electro absorption modulator (EAM) is a semiconductor-based planar waveguide composed of multiple p-type and n-type layers that form multiple quantum wells (MQWs). The basic design of EAM is similar to that of semiconductor lasers. The MQW is used to support the quantum-confined Stark effect (the absorption spectrum being a function of applied field) more effectively. Because of similarities of EAMs and semiconductor lasers design it is possible to fabricate them on the same substrate (see Figure 1.15 (B)), providing that EAM and laser are electrically isolated. Bandgap of quantum wells is larger than photon energy, so that the light is completely transmitted in the absence of bias, which corresponds to the ON state. When the reverse bias is applied the input signal is absorbed, which corresponds to the OFF state. The modulation speed of EAMs is typically comparable to the modulation speed of MZMs. However, the extinction ratio (the ratio of average powers corresponding to symbol 1 and symbol 0) is lower.

g) Electro Absorption Modulators (EAM)

An electro absorption modulator (or electro-absorption modulator) is a semiconductor device which can be used for controlling (modulating) the intensity of a laser beam via an electric voltage –*optical modulators*) [15] [9]. Its principle of operation is based on the *Franz–Meldish effect* [1, 2], i.e., a change in the absorption spectrum caused by an applied electric field, which changes the bandgap energy (thus the photon energy of an absorption edge) but usually does not involve the excitation of carriers by the electric field. Most electro absorption modulators are made in the form of a waveguide with electrodes for applying an electric field in a direction perpendicular to the modulated light beam. For achieving a high extinction ratio, one usually exploits the quantum-confined Stark effect in a quantum well structure.

Compared with electro-optic modulators, electro absorption modulators can operate with much lower voltages (a few volts instead of hundreds of thousands of volts). They can be operated at very high speed; a modulation bandwidth of tens of gigahertz can be achieved, which makes these devices useful for optical fiber communications [15] [9]. A convenient feature is that an electro absorption modulator can be integrated with a distributed feedback laser diode on a single chip to form a data transmitter in the form of a photonic integrated circuit. Compared with direct modulation of the laser diode, a higher bandwidth and reduced chirp can be obtained.

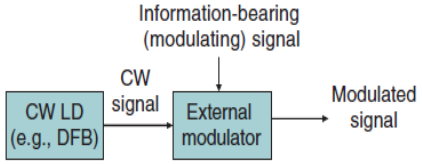

Figure 1.14 – An illustration of external modulation principle. DFB distributed

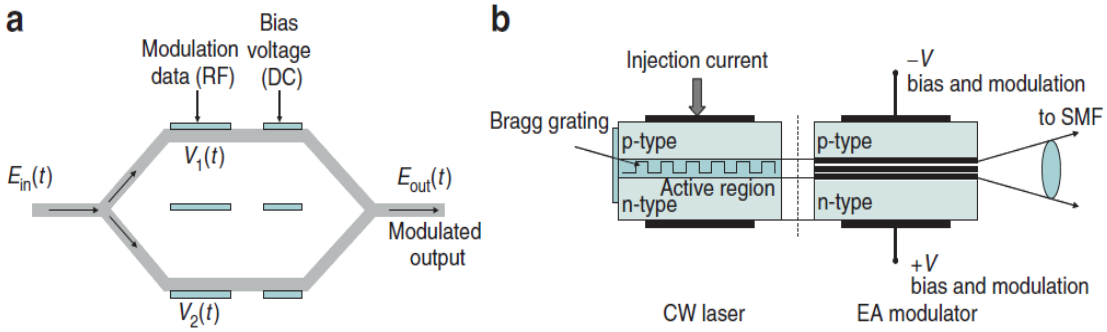

Figure 1.15 – (a) Mach–Zehnder modulator (b) Electro Absorption Modulator

h) Ring Resonator Modulators (RRM)

The silicon modulator is a key component for CMOS-compatible optical interconnection systems. Recently, high-speed modulators based on free-carrier plasma dispersion effect have been demonstrated using either Mach-Zehnder interferometers (MZI) or micro-ring resonators in silicon and III-V materials [16]. Comparing to the mm-long MZI-based modulators, the advantages of the ring-resonator-based modulator include its small size (~10μm) and low-power consumption. In the ring resonator, in contrast to single-pass devices like MZI, light at the resonant wavelength travels many round trips in the resonator, and interacts with the carriers many times. As a result, the total number of carriers needed to change the optical transmission of the ring resonator is much less than that needed in MZI-modulators, and therefore much less RF power is needed to drive these carriers in and out of the active region.

The key components of the WDM interconnection system are the cascaded modulators shown in the shadowed area of Figure 1.16, which are fabricated on a SOI substrate. The device structure is based on the micro-ring modulator we presented inn next sections. They consist of ring resonators embedded with PIN junctions used to inject and extract free carriers, which in turn modify the refractive index of the silicon and the resonant wavelength of the ring resonator using the mechanism of the plasma dispersion effect. The waveguides and rings are formed by silicon strips with the height of 200 nm and the width of 450 nm on top of a 50-nm-thick slab layer. The speed of the modulator was limited to 400 Mbps under non-return-to-zero (NRZ) coding. The reason for this limitation is that the p-i-n junction is formed on only part of the ring resonator, while carriers diffuse into the section of the ring that is not part of the p-i-n junction, where they cannot be efficiently extracted during the reverse biased period, leading to a longer fall time following consecutive '1's.

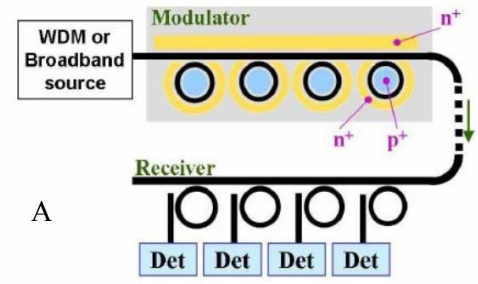

A

Figure 1.16 - Schematics of a WDM optical interconnection system with cascaded silicon ring resonators as a WDM modulator and demultiplexer. Det: detector.

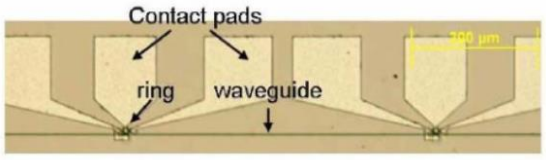

B

Figure 1.17- Top-view microscopic picture of the fabricated modulators, showing two of the four ring modulators coupled to a straight waveguide.

Receiver

i) OVERVIEW

The purpose of the optical receiver is to convert the optical signal into electrical domain and to recover the transmitted data. The typical OOK receiver configuration is already given in Figure 1.18. We can identify three different stages: front-end stage, the linear channel stage, and data recovery stage [9]. The front-end stage is composed of a photodetector and a preamplifier. The most commonly used front-end stages are high-impedance front-end and transimpedance front-end, both shown in Figure 1.18. High-impedance front end employs a large value load resistance to reduce the level of thermal noise and has a good receiver sensitivity. However, the bandwidth of this scheme is low because the RC constant is large. To achieve both the high receiver sensitivity and large bandwidth, the transimpedance frontend scheme, shown in Figure 1.16 is used. Even though the load resistance is high, the negative feedback reduces the effective input resistance by a factor of G - 1, where G is the front-end amplifier gain. The bandwidth is increased for the same factor compared to high-impedance front-end scheme.
The photodiode is an integral part of both front-end stage schemes [9]. The key role of the photodiode is to absorb photons in incoming optical signal and convert them back to the

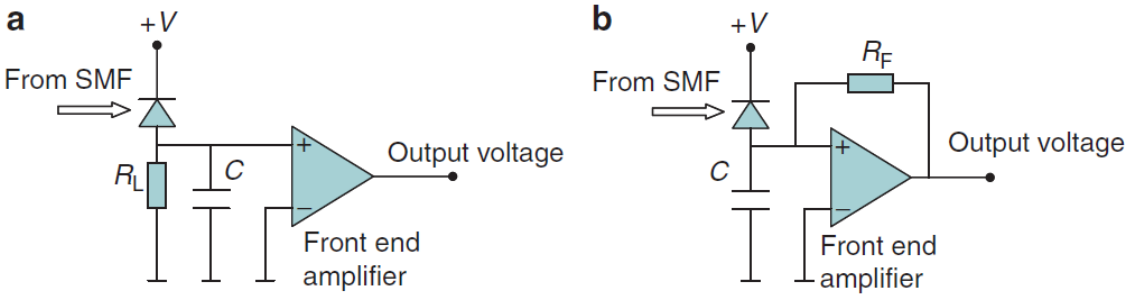

Figure 1.18 - Optical receiver front-end stage schemes (A) high-impedance front-end (B) trans impedance front-end

electrical level through the process opposite to the one taking place in semiconductor lasers.

The incoming optical signal may be preamplified by an optical amplifier and further processed by an optical filter to reduce the level of amplified spontaneous emission (ASE) noise or by wavelength demultiplexer to select a desired wavelength channel. The optical signal is converted into electrical domain by using a photodetector, followed by an electrical post amplifier. The clock recovery circuit is most commonly implemented using the phase-lock loop (PLL). Finally, the purpose of decision circuit is to provide the binary sequence being transmitted by comparing the sampled signal to a predetermined threshold. Whenever the received sample is larger than the threshold, the decision circuit decides in favor of bit 1, otherwise in favor of bit 0

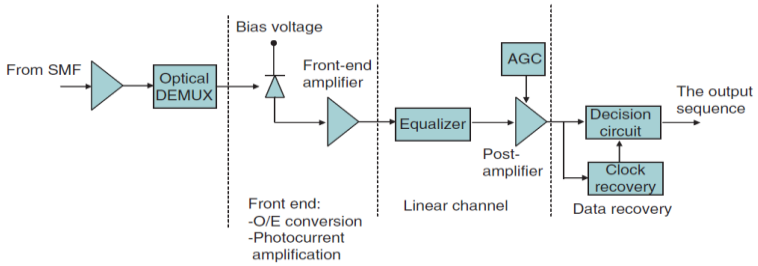

Figure 1.19 – A typical direct detection architecture. O/E optical to electrical and AGC

A silicon photodiode is a solid-state device which converts incident light into an electric current. It consists of a shallow diffused p-n junction, normally a p-on-n configuration although "P-type" devices (n-on-p) are available for enhanced responsivity in the 1μm region [17]. Modern day silicon [18]photodiodes are generally made by planar diffusion or ion-implantation methods. In the p-on-n planar diffused configuration, shown in the Figure 1.20, the junction edge emerges on the top surface of the silicon chip, where it is passivated by a thermally grown oxide layer.

The equivalent circuit of a photodiode is shown in the Figure 1.20. The photodiode behaves as a current source when illuminated. When operated without bias, this current is distributed between the internal shunt resistance and external load resistor. In this mode, a voltage develops which creates a forward bias, thus reducing its ability to remain a constant current source. When operated with a reverse voltage bias, the photodiode becomes an ideal current source. Parameters of shown equivalent circuit of photodiode in Figure 1.20 can be defined according to table 1.2.

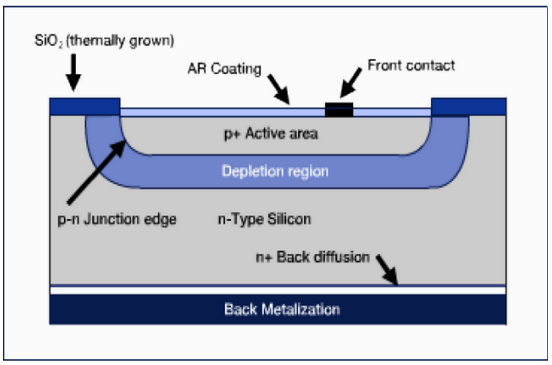

Figure 1.20– Cross section view a Photodiode

A silicon photodiode can be operated in either the *photovoltaic* or *photoconductive* mode. In the photovoltaic mode, the photodiode is unbiased; while for the photoconductive mode, an external reverse bias is applied. Mode selection depends upon the speed requirements of the application, and the amount of dark current that is tolerable. In the photovoltaic mode, dark current is at a minimum. Photodiodes exhibit their fastest switching speeds when operated in the photoconductive mode. Photodiodes and Op-Amps can be coupled such that the photodiode operates in a short circuit current mode. The op-amp functions as a simple current to voltage converter, these structures are shown in Figure 1.22.

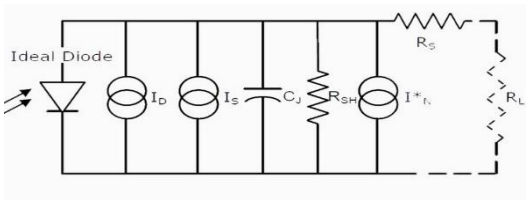

Figure 1.21 – Equivalent circuit of photodiode

Parameters	Description	Unit
I_D	Dark current	Amps
Is	Light Signal Current (I_S=RPo)	Amps
R	Photodiode responsivity at wavelength of irradiance	Amps/Watt
Po	Light power incident on photodiode active area	Watts
R_{SH}	Shunt Resistance	Ohms
I_N	Noise Current	Amps rms
C	Junction Capacitance	Farads
R_S	Series Resistance	Ohms
R_L	Load Resistance	Ohms

Table 1.2 - PD equivalent circuit Parameters

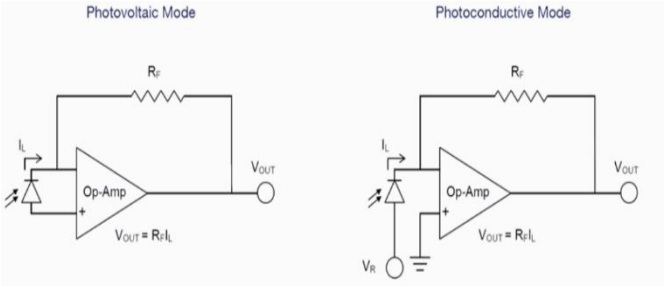

Figure 1.22 – Conversion circuits of PD Current to Voltage

Optical Amplification

Overview

An optical amplifier is a device which receives some input signal and generates an output signal with higher optical power. Typically, inputs and outputs are laser beams, either propagating as Gaussian beams in free space or in a fiber. The amplification occurs in a so-called gain medium, which has to be "pumped" (i.e., provided with energy) from an external source. Most optical amplifiers are either optically or electrically pumped [18].

Important parameters of an optical amplifier include:

- the maximum gain, specified as an amplification factor or in decibels (dB)
- the saturation power, which is related to the gain efficiency
- the saturated output power (for a given pump power)
- the power efficiency and pump power requirements
- the saturation energy
- the time of energy storage (→*upper-state lifetime*)
- the gain bandwidth (and possibly smoothness of gain spectrum)
- the noise figure and possibly more detailed noise specifications
- the sensitivity to back-reflections
- the number of modes it can amplify

Different kinds of amplifiers differ very much e.g. in terms of saturation properties. For example, rare-earth-doped gain media can store substantial amounts of energy, whereas optical parametric amplifiers provide amplification only as long as the pump beam is present. As another example, semiconductor optical amplifiers store much less energy than fiber amplifiers, and this has important implications for optical fiber communications.

EDFA

Erbium-doped fiber amplifiers are the by far most important fiber amplifiers in the context of long-range optical fiber communications; they can efficiently amplify light in the 1.5-nm wavelength region, where telecom fibers have their loss minimum.

A typical setup of a simple erbium-doped fiber amplifier (EDFA) is shown in Figure 1.23. Its core is the erbium-doped optical fiber, which is typically a single-mode fiber. In the shown case, the *active fiber* is "pumped" with light from two laser diodes (bidirectional pumping), although unidirectional pumping in the forward or backward direction (co-directional and counter-directional pumping) is also very common. The pump light, which most often has a wavelength around 980 nm and sometimes around 1450 nm, excites the erbium ions (Er^{3+}) into the $^4I_{13/2}$ state (in the case of 980-nm pumping via $^4I_{11/2}$), from where they can amplify light in the 1.5-nm wavelength region via stimulated emission back to the ground-state manifold $^4I_{15/2}$.

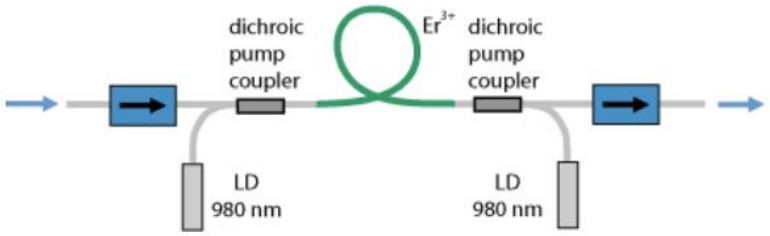

Figure 1.23 - Schematic setup of a simple erbium-doped fiber amplifier. Two laser diodes (LDs) provide the pump power for the erbium-doped fiber. The pump light is injected via dichroic fiber couplers. Pig-tailed optical isolators reduce the sensitivity of the device to back-reflections.

The setup shown also contains two "pig-tailed" (fiber-coupled) optical isolators. The isolator at the input prevents light originating from amplified spontaneous emission from disturbing any previous stages, whereas that at the output suppresses lasing (or possibly even destruction) if output light is reflected back to the amplifier. Without isolators, fiber amplifiers can be sensitive to back-reflections.

Apart from optical isolators, various other components can be contained in a commercial fiber amplifier. For example, there can be fiber couplers and photodetectors for monitoring optical power levels, pump laser diodes with control electronics and gain-flattening filters. For particularly compact packages, various passive optical components can be combined into a photonic integrated circuit (*planar light wave circuit*).

Very high signal gains, as used, e.g., for the amplification of ultrashort pulses to high energies, are usually realized with amplifier chains, consisting of several amplifier stages with additional optical elements (e.g. isolators, filters, or modulators) in between.

EDFAs can serve various functions in systems for optical fiber communications; the most important applications are the following:

- The power of a data transmitter may be boosted with a high-power EDFA before entering a long fiber span, or a device with large losses, such as a fiber-optic splitter. Such splitters are widely used e.g. in cable-TV systems, where a single transmitter is used to deliver signals into many fibers.
- A fiber amplifier may also be used in front of a data receiver, if the arriving signal is weak. Despite the introduction of amplifier noise, this can improve the signal-to-noise ratio and thus the possible data transmission rate, since the amplifier noise may be weaker than the input noise of the receiver. It is more common, however, to use avalanche photodiodes, which have some built-in signal amplification.
- In-line EDFAs are used between long spans of passive transmission fiber. Using multiple amplifiers in a long fiber-optic link has the advantage that large transmission losses can be compensated without (a) letting the optical power drop to too low levels, which would spoil the signal-to-noise ratio, and (b) without transmitting excessive optical powers at other locations, which would cause detrimental nonlinear effects due to the unavoidable fiber nonlinearities. Many of these in-line EDFAs are operated even under difficult conditions, e.g. on the ocean floor, where maintenance would be hardly possible.
- Although data transmitters are normally not based on erbium-doped devices, EDFAs are often part of equipment for testing transmission hardware. They are also used in the context of optical signal processing.

These functions can be realized in the telecom C and L bands. Other types of fiber amplifiers, e.g. based on praseodymium, have been considered for other bands, but none can compete with erbium-based devices in terms of gain and gain efficiency.

A particular attraction of EDFAs is their large gain bandwidth, which is typically tens of nanometers and thus actually more than enough to amplify data channels with the highest data rates without introducing any effects of gain narrowing. A single EDFA may be used for simultaneously amplifying many data channels at different wavelengths within the gain region; this technique is called *wavelength division multiplexing*. Before such fiber amplifiers were available, there was no practical method for amplifying all channels e.g. between long fiber spans of a fiber-optic link: one had to separate all data channels, detect and amplify them electronically, optically resubmit and again combine them. The introduction of fiber amplifiers thus brought an enormous reduction in the complexity, along with a corresponding increase in reliability. Very long lifetimes are possible by using redundant down-rated pump diodes.

The only competitors to erbium-doped fiber amplifiers in the 1.5-μm region are Raman amplifiers, which profit from the development of higher power pump lasers. Raman amplification can also be done in the transmission fiber. Nevertheless, EDFAs remain very dominant.

SOA

A semiconductor optical amplifier is an optical amplifier based on a semiconductor gain medium. It is essentially like a laser diode where the end mirrors have been replaced with anti-reflection coatings; a tilted waveguide can be used to further reduce the end reflectivity's. The signal light is usually sent through a semiconductor single-mode waveguide with transverse dimensions of e.g. 1–2 nm and a length of the order of 0.5–2 mm. The waveguide mode has significant overlap with the active (amplifying) region, which is pumped with an electric current [20] [21]. The injection current creates a certain carrier density in the conduction band, allowing for optical transitions from the conduction band to the valence band. The gain maximum occurs for photon energies slightly above the bandgap energy.

In principle, one can also use a semiconductor optical amplifier where the end reflectivity's are not minimized. One has to operate such a *Fabry–Pérot amplifier* (*FP amplifier*) slightly below the laser threshold; in that regime, the output power depends strongly on the input power, i.e., one obtains a high effective signal gain. However, the available optical bandwidth is then very small, and the occurrence of strong reflections may be detrimental to the system in which such a device is used. For these reasons, in most cases one uses traveling-wave amplifiers, where the end reflectivity's are suppressed as far as possible.

The amplification is intrinsically polarization-sensitive, but amplifier designs have been developed which provide nearly polarization-independent characteristics. For example, one may use two identical amplifiers in series, where the second one is rotated against the first one by 90°. There are also configurations with two parallel amplifiers for the two polarization directions, with polarizing beam splitters before and after these amplifiers. Another possibility is to use a double pass through a single amplifier, where there is a Faraday rotator between the device and the reflecting mirror.

SOAs can be used in telecom systems in the form of fiber-pigtailed components (with either normal single-mode fibers or polarization-maintaining fibers), operating at signal wavelengths near 1.3 um or 1.5 um, and offering a gain of up to 30 dB, limited essentially by amplified spontaneous emission (ASE). The strong gain saturation in SOAs can be a problem for some applications, but it can also be exploited for nonlinear signal processing in telecom systems – for example, for channel translation in a wavelength division multiplexing system.

The technology of semiconductor amplifiers competes with that of erbium-doped fiber amplifiers (EDFAs). The main differences compared with EDFAs are:

- The setup is much more compact, containing only a small semiconductor chip with electrical and fiber connections. A compact housing may even contain additional polarization-insensitive Faraday isolators at the input, output, or both ports.
- The output powers are substantially smaller, particularly when comparing with high-power fiber amplifiers.
- The required operation power is also smaller; typical drive currents a few hundred milliamperes.
- The gain bandwidth can be similar. Devices operating in different wavelength regions can be made.
- The upper-state lifetime and thus the stored energy are much smaller, so that the gain reacts to changes in pump power or signal power within nanoseconds (instead of milliseconds). Changes in gain also cause phase changes (*linewidth enhancement factor*).
- SOAs exhibit much stronger nonlinear distortions in the form of self-phase modulation and four-wave mixing. These are often unwanted, but can also be used e.g. for optical signal processing (see below).
- The noise figure is typically higher.
- The amplification is intrinsically polarization-dependent, as far as that is not avoided with special designs (see above).

Optical filters

Overview

An optical filter is usually meant to be a component with a wavelength-dependent (actually frequency-dependent) transmission or reflectivity, although there are also filters where the dependence is on polarization or spatial distribution, or some uniform level of attenuation is provided [21]. Filters with particularly weak wavelength dependence of the transmittance are called neutral density filters.

There are many different types of optical filters, based on different physical principles. Some examples of optical filters are:

- Absorbing glass filters, dye filters, and color filters are based on wavelength-dependent absorption in some material such as a glass dopant, dye, pigment or semiconductor. As the absorbed light is converted into heat, such filters are usually not suitable for high-power optical radiation.
- Various kinds of optical filters are based on interference effects, combined with wavelength-dependent phase shifts during propagation. Such filters exhibit wavelength-dependent reflection and transmission, and the light which is filtered out can be sent to some beam dump, which can tolerate high optical powers. An important class of interference-based filters contains dielectric coatings. Such coatings are used in dielectric mirrors (including dichroic mirrors), but also in thin-film polarizers, and in polarizing and non-polarizing beam splitters. Via thin-film design it is possible to realize edge filters, low-pass, high-pass and band-pass filters, notch filters, etc. The same physical principle is used in fiber Bragg gratings and other optical Bragg gratings such as volume Bragg gratings. Apart from step-index structures, there are also gradient-index filters, called *rugate filters*. That approach allows one to make high-quality notch filters, for example.

- Fabry–Pérot interferometers, etalons and arrayed waveguide gratings are also based on interference effects, but typically exploiting larger path length differences. Therefore, they can have sharper spectral features.
- Lyot filters involve wavelength-dependent polarization changes. Similar devices are used as birefringent tuners in tunable lasers.
- Other filters are based on wavelength-dependent refraction in prisms (or prism pairs) or on wavelength-dependent diffraction at gratings, combined with an aperture.
- There are acousto-optic tunable filters, where it is exploited that Bragg reflection at an acoustic wave works only within a narrow frequency range.

Concerning the shape of the transmission curve, there are:

- bandpass filters, transmitting only a certain wavelength range
- notch filters, eliminating light of a certain wavelength range
- edge filters, transmitting only wavelengths above or below a certain value (*high-pass and low-pass filters*)

Crow Filter

Coupled resonator optical waveguide devices (CROWs) are microscopic structures that are formed by cascading or putting in parallel a number of (micro) ring resonators (also called microcavities) - which are essentially waveguides shaped in the form of a ring - in a way that light can be coupled into the structure, resonates through the rings and is coupled out again at a different number of ports depending on the wavelength. Their basic functionality is that of an

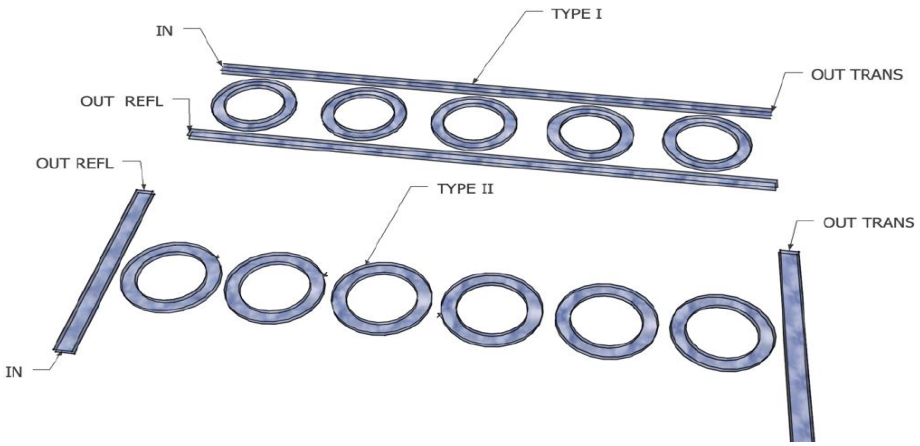

Figure 1.24 - Schematic description of possible ring formations.

optical filter. Figure 1.24 shows two basic formations of how these rings can be put together. The structure above named Type I contains rings that aren't mutually coupled but coupled periodically to two parallel waveguides. Light can be inputted at the upper left of downright, and outputted at the down left or upright. This structure is comparable with a distributed feedback Filter. The second structure, Type II, shows and array of rings mutually coupled and connected at both ends to waveguide busses. Down left light can be put in, and extracted at the top-left or right-bottom. The direction in which the light is output at the right depends on the quantity of rings. This type of filter could be compared to a stack of reaction Bragg-mirrors or Fabry-Perot cavities. Because of the comparison with these types of filters with other already well-known Filter types, certain properties can be copied and applied those these filters. Take into account that a uniform shape of the ring resonators was assumed, this means all the rings have the same circumference.

Multiplexer & De-Multiplexer

OADM

An **optical add-drop multiplexer** (**OADM**) is a device used in wavelength-division multiplexing systems for multiplexing and routing different channels of light into or out of a single mode fiber (SMF) [22]. This is a type of optical node, which is generally used for the formation and the construction of optical telecommunications networks. "Add" and "drop" here refer to the capability of the device to add one or more new wavelength channels to an existing multi-wavelength WDM signal, and/or to drop (remove) one or more channels, passing those signals to another network path. An OADM may be a specific type of optical cross-connect.

A traditional OADM consists of three stages: an optical demultiplexer, an optical multiplexer, and between them a method of reconfiguring the paths between the demultiplexer, the multiplexer and a set of ports for adding and dropping signals. The demultiplexer separates wavelengths in an input fiber onto ports. The reconfiguration can be achieved by a fiber patch panel or by optical switches which direct the wavelengths to the multiplexer or to drop ports. The multiplexer multiplexes the wavelength channels that are to continue on from de-multiplexer ports with those from the add ports, onto a single output fiber.

All the light paths that directly pass an OADM are termed *cut-through lightpaths*, while those that are added or dropped at the OADM node are termed *added/dropped lightpaths*. An OADM with remotely reconfigurable optical switches (for example 1×2) in the middle stage is called a reconfigurable OADM (ROADM). Ones without this feature are known as *fixed* OADMs. While the term OADM applies to both types, it is often used interchangeably with ROADM.

Physically, there are several ways to make an OADM. There are a variety of demultiplexer and multiplexer technologies including thin film filters, fiber Bragg gratings with optical circulators, free space grating devices and integrated planar arrayed waveguide gratings. The switching or reconfiguration functions range from the manual fiber patch panel to a variety of switching technologies including microelectromechanical systems (MEMS), liquid crystal and thermo-optic switches in planar waveguide circuits.

Although both have add/drop functionality, OADMs are distinct from add-drop multiplexers. The former function in the photonic domain under wavelength-division multiplexing, while the latter are implicitly considered to function in the traditional SONET/SDH networks.

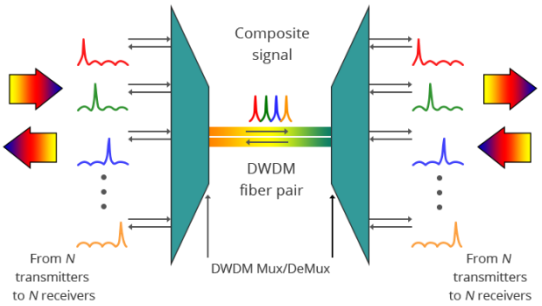

Figure 1.25– Main Scheme of Optical Multiplexer and

Motivation and goals of this project

According to the defined project, we are dealing with an optical telecommunication system based on silicon photonic chips which is fabricated and mounted on a RF board as an interface of electrical and optical signals. This optical telecommunication system contains 8 optical transmitters, receivers and 3 filter which are related to the high frequency part of the system. Ideal performance of this system is modulation of the electrical signals to the optical signals by ring resonator modulators and transmitting data and then multiplexing the different channels by OADM and passing data through optical fibers. This modulated and multiplexed data will be amplified to be detected in receiver part of the high frequency system. By demultiplexing the modulated optical signal and detection by high frequency photodiodes, which convert optical signals to the electrical signals.

In an ideal situation, all the transmitted data should be received in the pair photodiode of the receiver. But in real world the wave length of the transmitter and receiver's ring resonators are not at the same wave length. Also, wavelengths of the ring resonators are not at the same and equal space from each other in wave length domain. To have equal space among the optical channels to avoid cross talk between the channels, and the same wave length of transmitter and receiver side we need an extra feedback control for controlling and tuning the wave length of the ring resonators which are in exposure of temperature fluctuation. Consequently, temperature fluctuation is affecting the wave length of the ring resonators by impact on refractive index of the material. Temperature fluctuation is caused by variation of the ambient temperature, power dissipation in the electronic circuits like delivers, applying data by data generator, etc.

Manipulation of the wave length in ring resonators are performed by fabrication of a micro heater on top of the ring resonators to change the temperature of the ring resonator which has effect in the refractive index of the material. By variation of the refractive index we will have shifting in the wave length of each ring resonator. This manipulation is observed by a low frequency photodiode which are coupled to wave guides and contain at most 3% of the light power inside the ring resonators. By power dissipation in the micro heaters, we have changes in the current generated by photodiodes.

By observation of the monitoring PDs and controlling the power dissipation in the micro heaters, it is desired to control dynamically the wave length of an optical telecommunication system with 8 pair of transmitters and receivers. So main goals for the defined project can be according to:

- Monitoring the currents of the low frequency photodiodes
- Conversion of the analog signal to digital signal
- Processing data and generation of the control law
- Conversion of the generated digital control law to analog signal
- Applying power to dissipate in the micro heater to tune the optical channel

To reach the desired goals of the project, there is a need to design of compatible hardware based on micro controller to be able to process monitoring photodiode signals and generation of the control law for microheaters. Designing a hardware based on microcontroller causes to provide an optimized software to program the microcontroller. Since we need to monitor every channel as fast as possible and generate the control law in an appropriate time. In next section, we will discuss about the organization of the contents which will clarify the steps of the accomplishments during this project.

Organization of content

Regarding the definition of the steps for reaching the desires of the project, we will discuss first about the system which we are dealing with and much more details about it in chapter 2. In this chapter, we will have review on the dealt optical system, WDM system architecture, transmitter of the system which includes RRM, filter and OADM of the system. Moreover, in receiver section we will have discussion about the performance of OADM in receiver part and about the fabricated photodiodes (Ge PD) and flip chip PDs. Next section will be related to WDM control system and the tuning control PCB in the whole architecture of the optical telecommunication system. In this part, we will discuss about the lack of a control system and effect of it on the output signal in receiver part by considering the ideal performance of the other components of the system. Finally, in chapter 2 we will discuss about the solution of the problem raised by lack of control system and non-ideality of data modulation caused by it.

In chapter 3, we will discuss about the designed hardware which is compatible to acquire data, process and generation of control law for microheaters. Designed hardware contains transimpedance amplifier for conversion of photodiodes' current to voltage, an analog to digital convertor, a microcontroller to process data, a digital to analog convertor and finally an output buffer for supporting the power dissipation in micro heaters. In this chapter, there will be detailed discussions about every part and in case of possibility simulation of the designed hardware will be provided. The last part of this chapter will be about the manufactured and assembled hardware and summarization about it.

In chapter 4, the system under control will be studied in terms of control theory. Frist the control system will be defined in aspect of digital control theory and it will be attempted to model the whole system as first order system and the hardware limitations and features affecting on the controlling system will be discussed. Then a static model of the micro ring resonators and micro heaters will be provided then it will be attempted to provide a dynamic model of the system and response time of the system for suitable inputs will be discussed. A comparison of the modeled system in theory and experiments will be studied and the solutions and the approach will be discussed in next section which contains initialization and controlling the system. Final section in this chapter is allocated to the realization of the control solutions by hardware and preparing the driver codes and control codes of the system and implementation of them on the hardware.

In the chapter 5, the measurement result of the optical telecommunication system under control will be presented and will be discussed. Then, we will have summarization and conclusion of the project and the prospects of the project.

II. Chapter 2: WDM System subject to control

Overview

In this section, it is tended to study the optical telecommunication system in macroscopic scale and description of the components and circuits by block diagrams. Furthermore, there will be a discussion about the details of every component in microscale and their responsibility in data transmission. As a macro scale system, we will start from the electrical signal domain which should be modulated to carrier signal. Then we need to guide the electrical signal to the optical interface board by RF cables to be converted to optical domain signal. Conversion of the electrical signal to optical signal is realized by the optical drivers and silicon photonic components which will be discussed in microscopic scale. The optical modulated signal will be amplified and then reversed back into the receiver part of the silicon photonic chip to be detected and converted to electrical domain modulated signal. Converted electrical signal will be analyzed to compare the transmitted and received data by the criteria of bit error rate (BER).

In micro scale study of the system, there will be an evaluation of the optical filter, optical data transmitter which is RRM modulator and structure of the OADM to multiplex of the optical signal to pass it through the optical fiber. Moreover, in receiver part the OADM structure to de-multiplex of the optical modulated signal which has passed through the optical fiber will be discussed. Optical modulated signal is detected by the coupled photodiodes to the receiver ring resonators. The detected electrical signal will be analyzed by data analyzer based on BER and the eye diagram of the transmitted data. A very general scheme of data transmission setup could be shown as Figure 2.1.

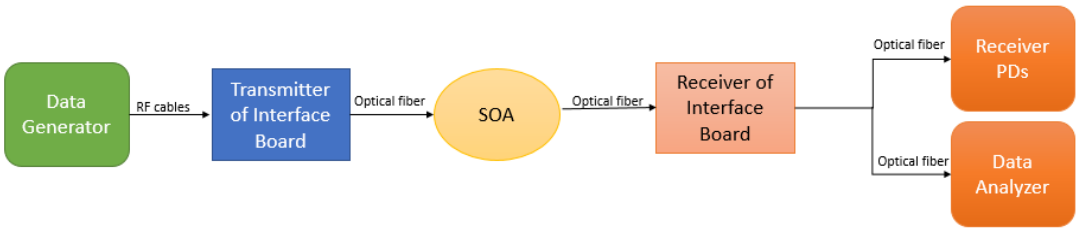

Figure 2.1 – Macroscale of the optical telecommunication system

WDM in Macro Scale

In macroscopic scale dealt optical telecommunication could be shown as Figure 2.2 which contains data generator, an RF interface board, SOA as optical amplifier, data analyzer and photodiode detector. According to Figure 2.2 below we see generated data goes into the input of the transmitter of the RF interface board which are connected to the transmitter side of the silico photonics chips. Signals after modulation in optical domain are amplified by SOA and received back by optical fibers in receiver part of the RF interface board which is connected to receiver of the silicon chips and is analyzed by data analyzer to compare the transmitted data and received data. To vast the system evaluation of the optical data transmission we can present it according to Figure 2.3 which includes transmitter, SOA, and receiver part of the system

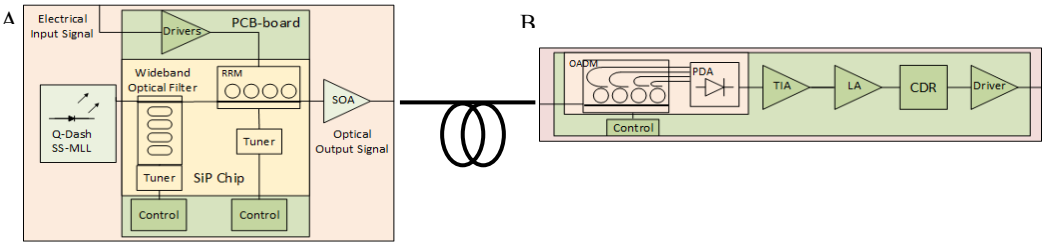

Figure 2.2 – (A) Transmitter structure (B) Receiver Structure

According to the Figure2.2 above, electrical signal is entering to the transmitter, simultaneously laser is injecting light to wave guides and is passing through the optical crow filter in order to have a passband spectrum and attenuate the unwanted wave lengths. Then by RRM modulators electrical signal is modulated to laser. As shown in the Figure 2.3 (A) RRM modulators are tuned by microheaters which is performed by a control loop. Then modulated signal goes through SOA and enters optical fiber. Signal reaches to receiver side and passes through OADM to be demultiplexed. Ring resonator fabricated in receiver part again are under the control by a control loop. Then every channel is detected by photodiodes (PDA), then is amplified by transimpedance amplifier (TIA) to enter the process and analyze data. In process part, clock data recovery block is synchronizing the data click to enter to drivers. Drivers according to the received signal will set and reset which is realization of OOK method of demodulation. In Figure 2.3(A) we can see the aligned fiber array and the modulator driver beside of the silicon photonic chip.in figure 2.3 (B) we can see the test bench of the separated transmitter(Tx) and receiver (Rx) interface boards on the test benches.

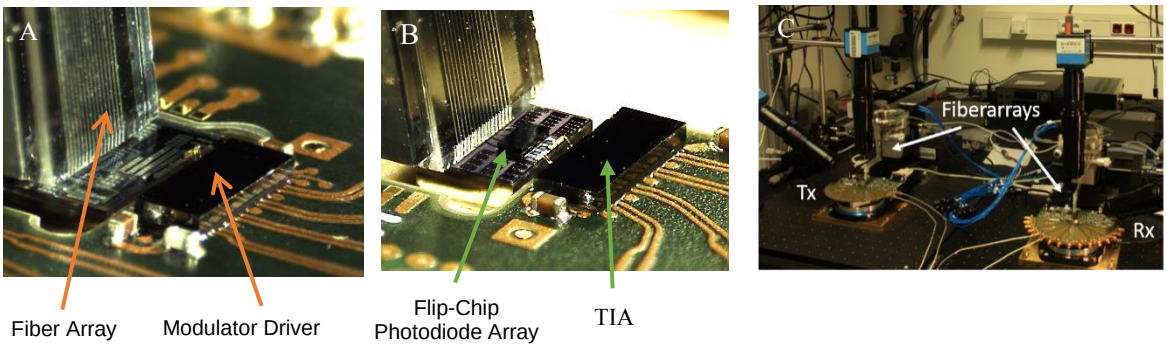

Figure 2.3 – (A) RRM Modulator driver (B) Filip Chip Photodiode array and TIA (C) Tx and Rx configuration on test bench

j) Transmitter

In much more detail, we can describe the transmitter performance according to block diagram shown as Figure 2.4(A) which includes a tunable external laser light (Agilent tunable laser) which is injected by fiber arrays to silicon chip, an interface board for transmitting the signal and external SOA which is amplifying the output signal of the transmitter part. In the figure 2.4 (B) we can see the Q-factor[1] [23]of modulated signal versus BER of the signal in receiver part by sweeping the laser power.

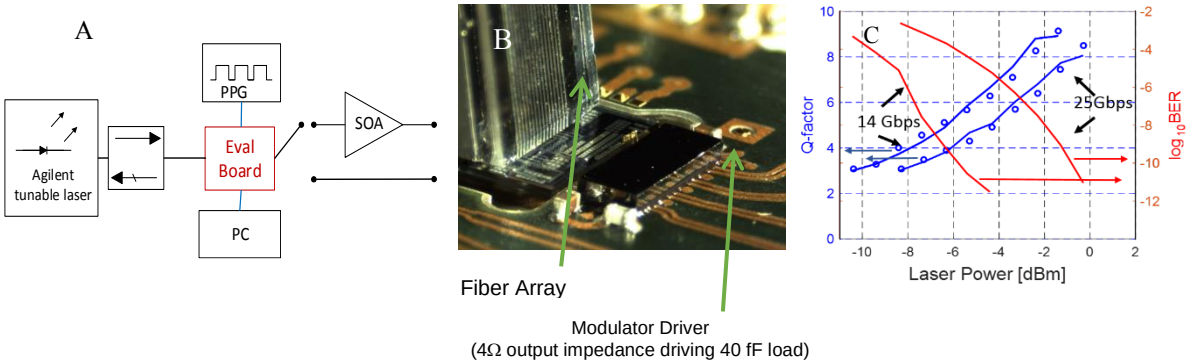

Figure 2.4 - (A) Tx Integration (B) Tx realization on interface board (C) analysis of the transmission data by the criteria of Q-factor and BER by sweeping laser power

k) Receiver

In much more detail, we have described the receiver part according to the block diagram shown in Figure 2.5(A). In Figure 2.5 (B), the realization of the Rx on the evaluation board is shown which contains a flip chip photodiode and TIAs. The responsivity of the photodiodes is reported according the Figure 2.5 (C). In table 2.1, two different photodiodes are studied in terms of cut-off frequency, losses in grating couplers and sensitivity in 14 Gbps and 25 Gbps.

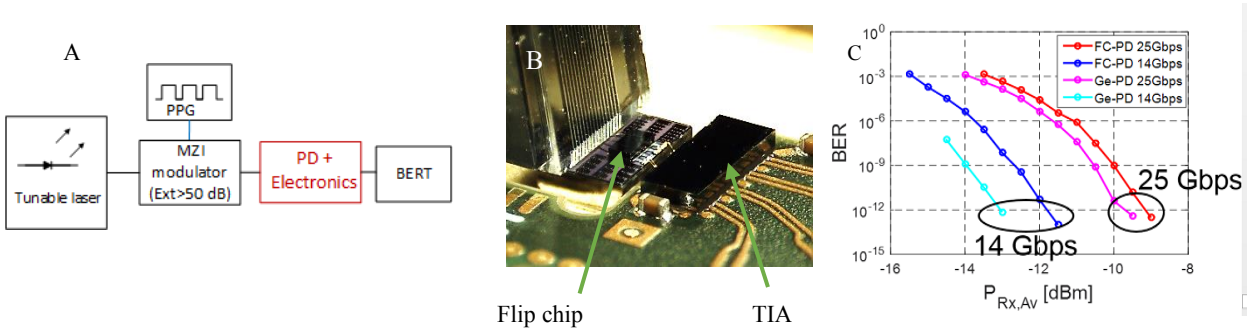

Figure 2.5 – (A) RX Integration (B) Rx realization on interface board (C) Analysis of the receiver data by the criteria of BER vs. average power of the receiver

[1] There are only two possible signal levels in binary digital communication systems and each of these signal levels may have a different average noise associated with it. This means that there are essentially two discrete signals to- noise ratios, which are associated with the two possible signal levels. To calculate the overall probability of bit error, we must account for both signal-to-noise ratios. the two SNRs can be combined into a single quantity – providing a convenient measure of overall system quality – called the Q-factor

	Responsivity	Cut-off Freq.	GC loss	Sens.@14Gbps	Sens.@25Gbps
GE-PD	0.67 A/W	> 30 GHz	3 db	-13 dBm	-9.7dBm
FC-PD	0.84 A/W	18 GHz	2x3dB (2 interface)	-11.8dBm	-9.1dBm

Table 2.1 – Comparison of Ge photodiode and flip chip photodiode sensitivity in 14 and 25 Gbps.

Full Link Configuration

By connection of the transmitter and receiver evaluation boards a full link configuration is obtained which can be defined as block diagram shown in Figure 2.6 (A). The analysis of a measurements of data and modulated data in two 14 and 25 Gbps are shown in the figure 2.6 (B) versus laser power.

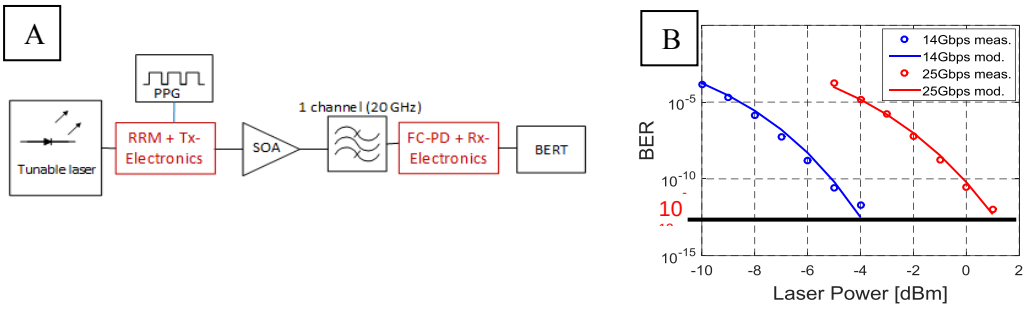

Figure 2.6 – (A) Full link configuration block diagram of TX and RX (B) Analysis of modulated data and measurement data based on the laser power.

WDM System Architecture in Micro Scale

Architecture Overview

In this section, there will be a detailed discussion about the optical components of the silicon photonics chips which are contributing the data modulation and transmission in optical telecommunication system. The overall view of the silicon chips can be described as Figure 2.7.

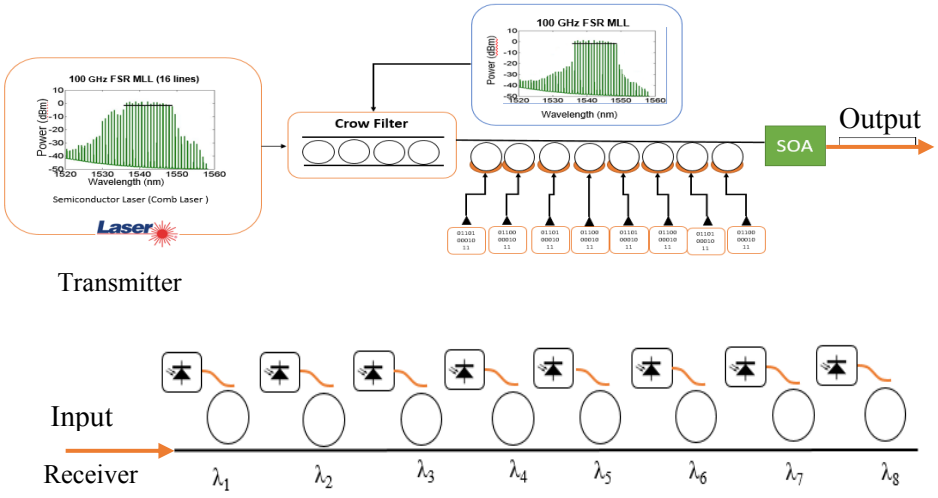

Figure 2.7 – Overall view of the optical transmitter and Receiver

Laser

Laser as a carrier in optical telecommunication is a crucial and key component in this technology which induces some challenges in it. Instability of the laser, incompatibility of the growing materials suitable for laser structure is the most common challenges in this area. In this configuration injection of the laser inside the chip could be realized in two main approach. First approach is the coupling a light laser by interconnections like edge coupler and grating coupler which is providing an experimental situation for the proving concept. Second approach is mounting a flip chip on the considered section of the silicon chips to inject the needed laser inside the waveguides by onboard laser. Here we briefly study about the mounted flip chip laser on the silicon chip, and main characteristics of it.

A 3D schematic of the mounting a flip chip is shown in Figure 2.8 [24] [25].the real experimental view is provided in Figure 2.8(b) which is laser mounted and coupled by the optical fiber to make a characterization process. Characteristics of the laser used in the experiments is reported as Figure 2.8(C).

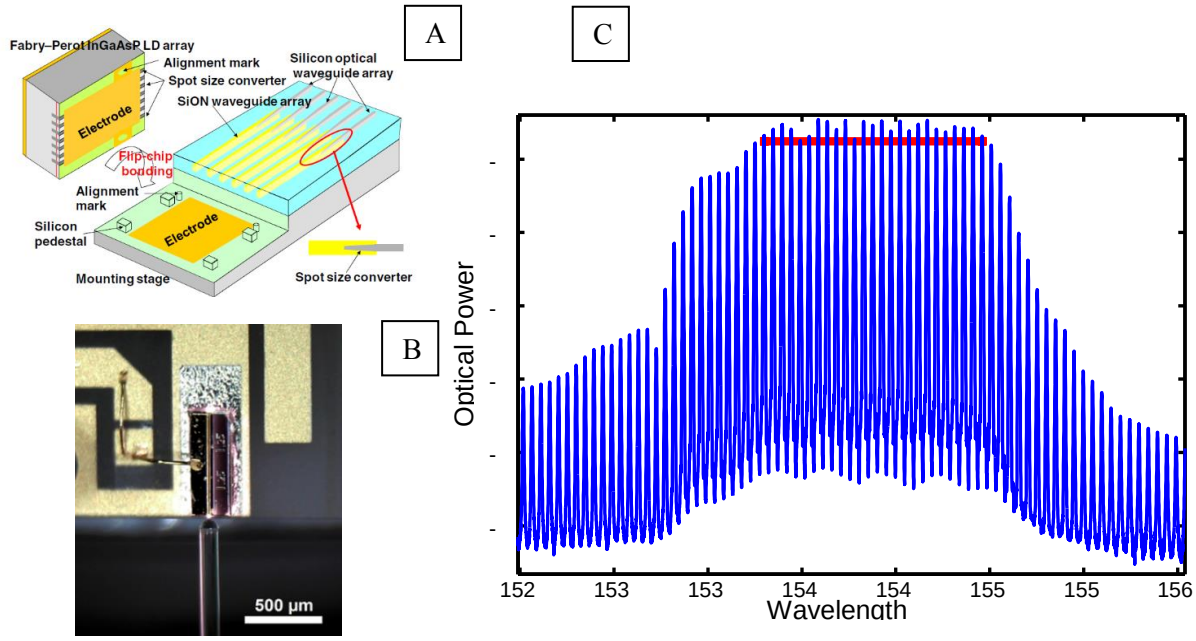

Figure 2.8 – (A) Hybrid Integration structure with an LD array on a silicon Waveguide platform (B) Experimental mounted flip chip Laser (C) Spectrum of the used flip chip in experiments

Laser	System experiment
➢ 60 GHz	➢ 100 GHz FSR
➢ -5 dBm fiber Coupled	➢ 15 consecutive lines
➢ 25 lines within half of peak power	➢ ~2X higher RIN

Table 2.2 – Laser and system under experiments main features

Transmitter

Transmitter as an optical module contain main components which are: Ring Resonator Modulator, Crow Filter. Here we briefly describe about the performance of the RRM modulators and crow filters. Crow filter performance is same as the band pass filter to attenuate the unwanted laser lines. RRM by modulation of the 0s and 1s in wave length domain cause to provide data to transfer. Then, this optical signal is amplified by SOA and is transmitted to receiver.

l) RRM modulator

Since the ring resonators are our main point of interest here we briefly describe about the performance and characteristics of them in system under experiment and vastly will be described and studied to chapter 4 about the behavior and dynamic behavior of it. The picture of fabricated ring resonators and thermal tuner is shown in Figure 2.9 (A). The performance of the RRM modulators based on OMA[2] versus bandwidth is presented as Figure 2.9 (B).

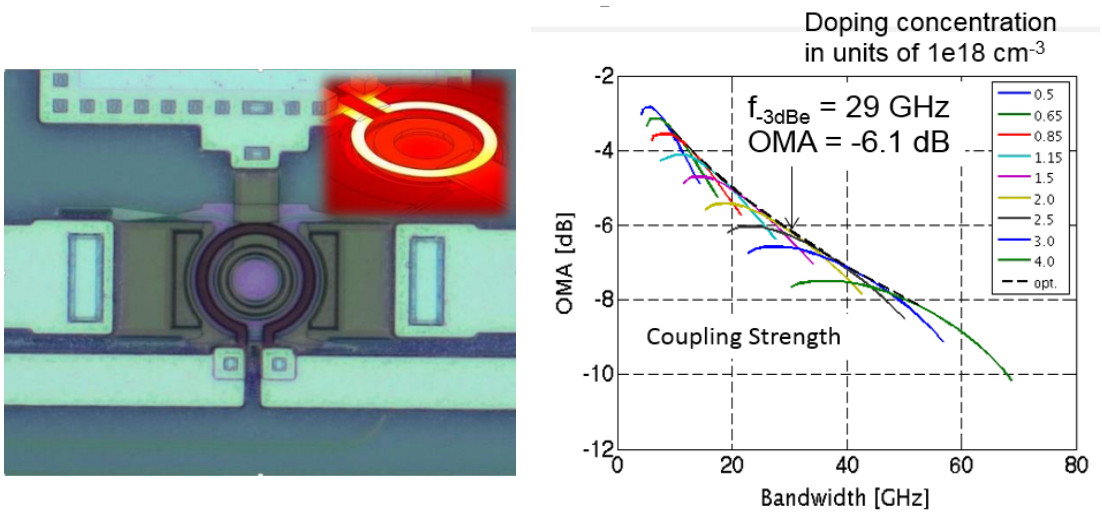

Figure 2.9 - (A) Fabricated RRM with thermal tuner (B) OMA of the RRM vs. Bandwidth.

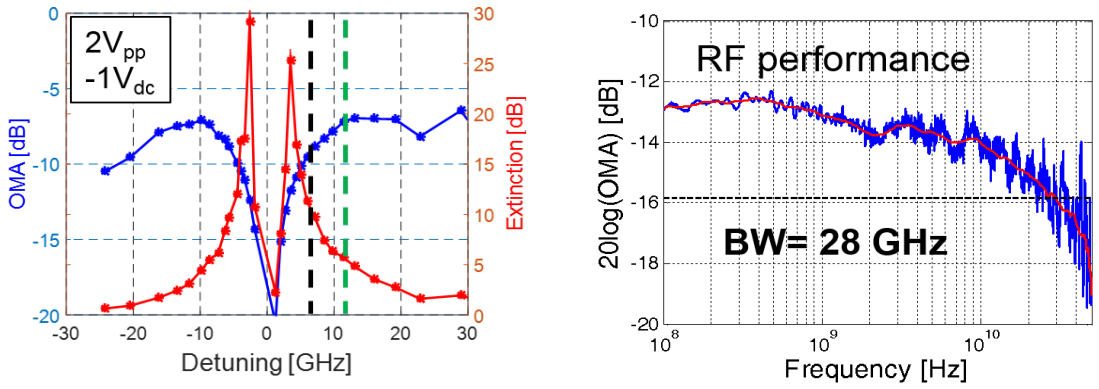

Figure 2.10 – (A) Optical modulation Amplitude of the RRM in system under experiment (B) RF performance of the RRM modulators

[2] Optical Modulation Amplitude

Crow filter

As mentioned, crow filter is used for attenuating laser lines in unwanted wave lengths. This feature is the same as band pass filter in electrical signals. In Figure 2.11 (A) & (B) we can see the structure of the crow filter in 2 scales of 50,200 μm. The transmission of the crow filters is according to the Figure 2.12(A) and the effect of the crow filter on the input laser is shown in Figure 2.12 (B) &(C).

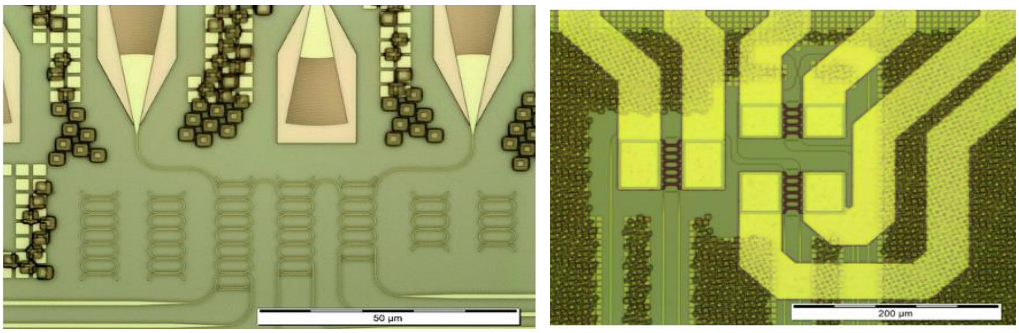

Figure 2.11 - (A) fabricated Crow Filter in 50 μm scale (B) fabricated Crow Filter in 200 μm scale

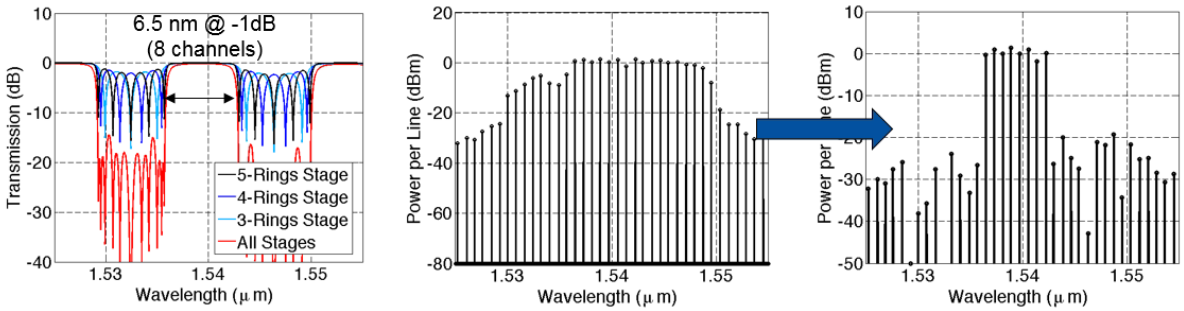

Figure 2.12 – (A) Transmission of the crow filter (B)Input laser spectrum of the crow filter (C) Output Spectrum of the Crow Filter

Receiver

Receiver as an optical component is responsible for demodulation and detection of the transmitted signal. There are different configurations of the photodiodes which are Flip-chip & Germanium photodiodes. The mounted flipchip on the receiver part of the silicon photodiode is according to Figure 2.13(A), bandwidth of the flip chip photodiodes is according the Figure 2.13(B) and the measured responsivity is according to Figure 2.13(C).

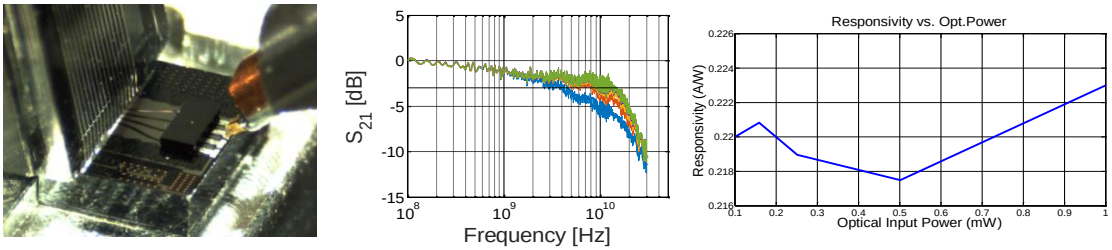

Figure 2.13 – (A) Mounted Flip-chip Photodiode (B)Bandwidth of the Flip-chip Photodiode (C) Responsivity of Flip-chip PD

The second type of the photodiodes used in the receiver part of the optical system is germanium photodiodes. Fabricated Ge photodiodes, cross section view, bandwidth, responsivity is according to Figure 2.14 (A),(B),(C),(D).

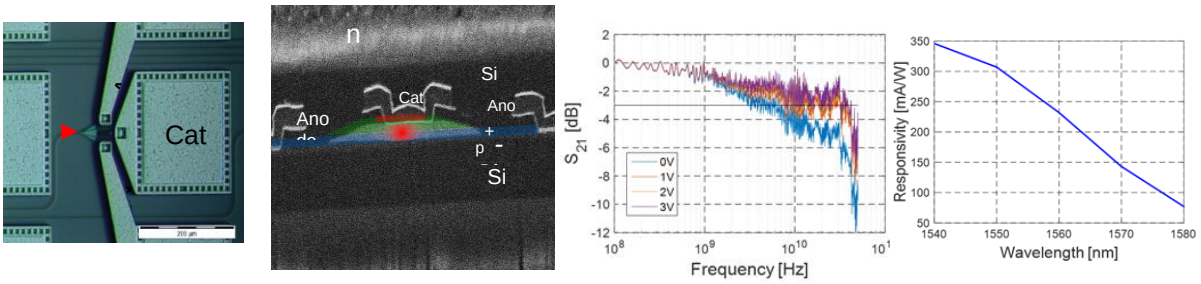

Figure 2.14 – (from left to right) 1) sample fabrication 2) Material Structure 3) Gain Bandwidth 4) Responsivity

By describing the responsibilities of the optical components in much more detail we need to clarify the control PCB in this configuration and the effects and expectations of the control board PCB on the performance of the optical telecommunication channel is subject to evaluate. Next section is allocated to the Control Board PCB in optical telecommunication and its responsibilities in this data transmission cycle. It will be discussed the lack of control on the ring resonators how can have effect on the data transmission process and the contribution of the control board and its advantages will be evaluated.

WDM Control System

Since we need to independently have ability to tune every channel on both transmitter and receiver sides, and crow filters to be able to shift the band pass filter we will need 1 channel of TIA to convert the generated current from the monitoring photodiodes in transmitter, receiver and filter side. Since it is aimed to implement 8 channel WDM we will need 8 channels of TIA for transmitter, 8 channels of receiver, 8 channels for crow filters which in this configuration there exist just 3 channels for control.

The hardware of the control board will be based on a microcontroller which is in communication with other components. Surly we need TIA for conversion of the PD's current to voltage, an analog to digital in data acquisition part. Since we need to dissipate power in micro heaters of the ring resonators we need to have digital to analog convertor to convert the digital control law. Since the power dissipation is high we need to buffer the output of DAC to make an isolation of the control signal and load.

Software structure will be based on 2 main steps. First step will be the initialization of the rings based on the comb line laser, and then in next step controlling the channels against temperature fluctuations. In next chapter, we will discuss about designed hardware and its specifications.

III. Chapter 3: Hardware

Overview

For acquiring the signals from photodiodes fabricated on silicon chips which generates a current proportional to the light power inside the micro ring resonators we will need a hardware. The photodiode as a sensor of the control cycle can be assumed. Due to hardware limitations, it is needed to convert the current into voltage to be able to digitize the acquired signal which a trans-impedance amplifier circuit is responsible for it. Digitization of the analog signals from TIAs are performed by ADC (Analog to Digital Convertor). Then, a microcontroller gathers serial data based on Serial Peripheral Interface (SPI) communication protocol to enter the processing phase.

For future purposes, microcontroller is selected from AVR-XMEGA256A3BU series to support popular communication protocols. By this availability the hardware will be able to connect the PC as a USB device under the CDC (Communication device Class) protocol. Data transmission of the hardware provides a degree of freedom to have an interface program by LABVIEW software. The microcontroller by having an accurate data needs first to initialize the rings, since by observation in experiments we cannot have very clear and organized ring resonance in spectrum of the laser output. After initialization, we need to control the ring resonator wave length which is subjected to perturbation by temperature fluctuation. Controlling the wave length of the ring resonator is made by control commands which is generated and transmitted to DAC.

The control commands generated by microcontroller are digital and should be sent to the Digital to Analog Convertor (DAC). Also, the transferring the control commands is performed by SPI. Data are accumulated in register of DAC, and according to each command DAC generates analog voltage in the output in order for heating up the related heater. As mentioned, since there exist 8 cascaded ring resonators in transmitter, receiver and also in filtering part of the optical output at least there is a need for 24 channel ADC and DAC for reaching the desired goal of project. Since there is a need for extra DAC & ADC channels in the hardware part, two 16 channel ADC (ADS1158) and one 32 channels DAC (MAX5732) are selected. To have a desirable resolution in data acquisition and command control generation both ADC and DAC are 16bit.

The converted control commands by DAC are fed to output buffers (OPA4251) which play the role of isolating load from control command. Buffers are designed based on operational amplifiers to isolate control command beside of having a high input impedance. Sinking current for heating up the integrated heaters is done by a BJT transistor which plays the role of a valve in the current flow path.

Power supply of the hardware is on board and based Buck DC/DC convertor power supply topology (TPS410172, LM3152) to have a stabilized voltage with high current support in output just by providing a DC input in range of 8 to 12 V_DC for the hardware. The main voltage of

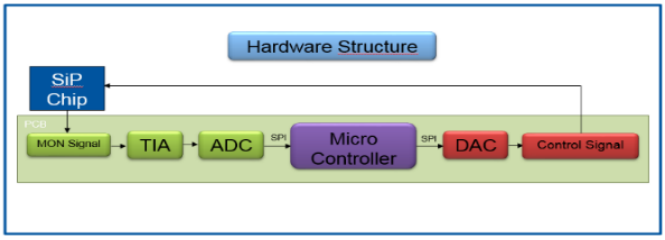

Figure 3.1- Main scheme of Hardware

the hardware based on the needs of ICs and other components is divided into +3.3V DC and +5V DC.

Based on the above descriptions about the hardware, the designed and manufactured hardware is according to block diagram as Figure 3.1.

For evaluation on the performance of the hardware every main part of it will be studied, and in the case of possibility simulation results and important considerations will be provided. It is meritorious to mention this point that the used microcontroller, ADC and DAC in the project will be reported without simulations. Since for simulation of these components we will need firstly the modeled component and secondly licensed software to be able to simulate these component. For assertion about the performance of the microcontroller the evaluation is performed on the evaluation board provided by ATMEL Company under the name of XMEGA256A3BU-XPlained. ADC and DAC components are evaluated by prototyping to test the performance under the desired conditions. Therefore, microcontroller, ADC and DAC of the designed hardware will be based on the features and performance reported by manufacturer in data sheet.

The evaluation order of the hardware will be respectively:

1. Microcontroller (Xmega256A3BU)
2. Analog to Digital Convertor (ADS1158)
3. Digital to Analog Convertor (MAX5732)
4. Power Supply (TPS40172, LM3152)
5. Trans-Impedance Amplifier – TIA (OPA380)
6. Output Buffer (OPA4251)
7. High-Current Output Buffer (OPA567)
8.

Microcontroller – Xmega256A3BU

Overview

The Atmel AVR XMEGA is a family of low power, high performance, and peripheral rich 8/16-bit microcontrollers based on the AVR enhanced RISC architecture. By executing instructions in a single clock cycle, the AVR XMEGA device achieves CPU throughput approaching one million instructions per second (MIPS) per megahertz, allowing the system designer to optimize power consumption versus processing speed.

The AVR CPU combines a rich instruction set with 32 general purpose working registers. All 32 registers are directly connected to the arithmetic logic unit (ALU), allowing two independent registers to be accessed in a single instruction, executed in one clock cycle. The resulting architecture is more code efficient while

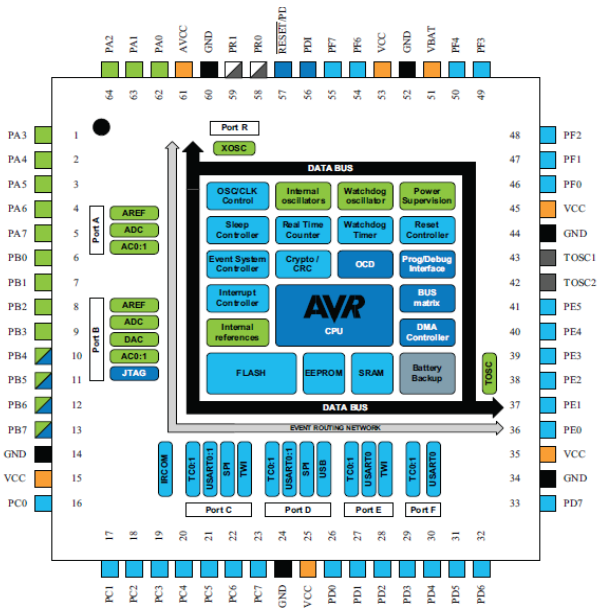

Figure III3.2 – Block Diagram and Pinout

achieving throughputs many times faster than conventional single-accumulator or CISC based microcontrollers. By combining an 8/16-bit RISC CPU with in-system, self-programmable flash, the AVR XMEGA is a powerful microcontroller family that provides a highly flexible and cost-effective solution for many embedded applications. All Atmel AVR-XMEGA devices are supported with a full suite of program and system development tools, including C compilers, macro assemblers, program Debugger/simulators, programmers, and evaluation kits**.** All Atmel AVR-XMEGA devices are supported with a full suite of program and system development tools, including C compilers, macro assemblers, program debugger/simulators, programmers, and evaluation kits**.**

Main Considerations in Microcontroller Circuit Design

- **Power supply**

  In order to have a stabilized power supply for microcontroller every power pin of the microcontroller should be grounded by a bypass capacitor. Since there is analog and digital components in the hardware design, there is a must in isolation of the analog and digital grounds. There is a consideration of redundant linear voltage regulator for power supply of the microcontroller to have ability to source the power supply by the reserved linear voltage regulator. In the final design of the power supply of the microcontroller a fuse has been considered to protect the micro controller from overloading. The allowed rang for input voltage of the power supply is 1.6 to 3.3V DC which could be selected based on the needs for CPU clock.

- **Pin Fan-out**

  Since the hardware is a prototype and the main goal is to evaluate the design then try to optimize the hardware for an optimum design in respect of size and the components, a fan out of microcontroller pins has been considered to ease the process of debugging hardware.

- **Clock Source**

  Although there exists an internal clock source for microcontroller, but an external oscillator crystal has been considered to as external clock source to be able to exploit PLL clock source of the AVR. A synchronized output clock will be used as clock source for ADCs. Because ADCs need a clock source in 16 MHz which can be Internal or external. Sourcing ADCs can be changed by a switch from external to Internal and vice versa.

- **Reset Push Button**

  Because we need to be able to reset the microcontroller manually, a push button is assigned to shoulder this responsibility.

- **Communication Ports**

  Although there is a fan out for each pin of the microcontroller, moreover there exist a JTAG port for programming and debugging and a port which contains TWI, SPI, USART protocols pins to use them separately. As mentioned in overview of the microcontroller about supporting USB protocol by it, a USB 2.0 is considered to be able to define the control board as USB device to realize the interface with LABVIEW software.

- **Controlled Impedance Layout**

  To avoid any cross talk among the lines which have sharp rise or fall signals the criteria of distance among the wires should be at least 3 times to the width of the wires. For decreasing the probability of EMI, the thickness and the width of the communication lines among the components is calculated to have impedance equal to 75[Ohm]. To have a synchronization between ADC, DAC and microcontroller clock source lines are designed such a way that to equalize the length of wires.

Summary of Microcontroller Design Summary

Supply Voltage [V]	Clock Source	Clock Frequency [MHz]	JTAG	SPI	TWI	USB	GPIO
1.6 - 3.3	Internal / External	2 - 32	✓	✓	✓	✓	✓

Table 3.1 _ Main characteristics of XMEGA256A3BU

The final layout and the 3D view of the designed microcontroller circuit is according to Figure 3.3 and 3.4.

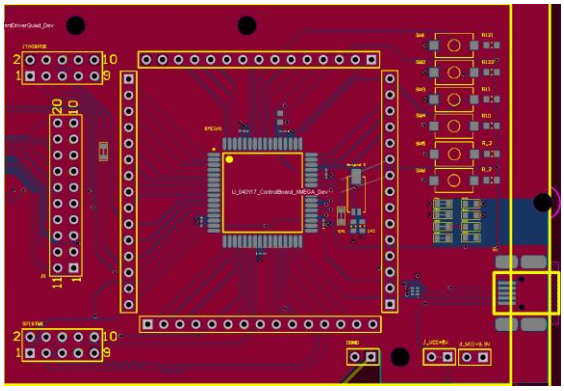

Figure 3.3 – Layout of Designed Microcontroller Circuit

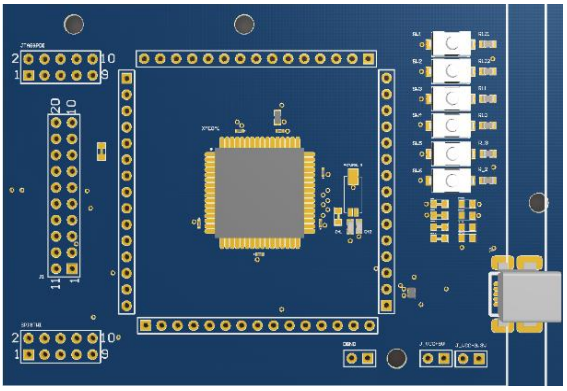

Figure 3.4 - 3D View of the designed Microcontroller Circuit

Analog to Digital Convertor (ADS1158)

The design of the ADC is very crucial in terms of accuracy and compatibility with the converted signals by TIAs. Number of the channels is second criteria in design and selection of the ADC. According to the requirement of the project ADS1158 is selected which contains 16 channel of Analog to Digital Convertor with 16 bit resolution. Total number of the needed channels based on the number of ring s is 24 but we need more channels to consider the probable developments and other needs of data conversion. Here we will briefly describe the main features of ADS1158 and the main considerations in hardware design.

Overview

Pin configuration and functional block diagram of ADS1158 shown in Figure 3.5 and 6 respectively. The main features of the ADS1158 can be summarized as:

- 16 bits, No missing Codes
- Fixed Channel (125 kSPS/Channel)
- Automatic Channel Scan (23,7 kSPS/Channel)
- 0.3 LSB (INL)
- 1 µV/°C Offset Drift, 2ppm/°C Gain Drift
- 42mW power Dissipation
- 32.768kHz Crystal Oscillator or External Clock

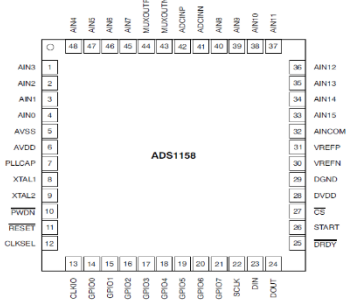

Figure 3.5- Pin Configuration

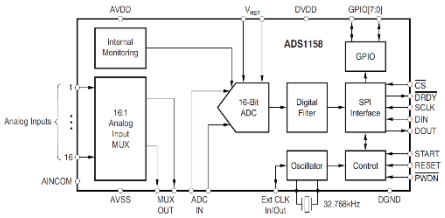

Figure 3.6- block diagram of

Main considerations in design of ADS1158 Circuit

- ***Power Supply and Reference Voltage***
  In design of the ADS1158 Circuit it has been considered to have reference voltage IC (REF5050MDREP) to ensure about the stability of the reference voltage. Supply voltage of the ADS1158 is supported by the main power supply, but for having a degree of freedom in the case of having trouble in main power supply, it is possible to supply voltage by changing the configuration of a jumper from internal power supply to external. Every power supply pin of ADS1158 is bypassed by a capacitor according to the recommendation of the producer.

- ***Internal / External Clock source***
  To be able to use the external clock source and a PLL as internal clock source, a digital switch has been considered to be able to choose the clock source. The mentioned switch can handle the control command of starting conversion, resetting ADC and observation

of the Data–Ready output of the ADC. It should be noted that external clock source is sourced by microcontroller for clock synchronization of the microcontroller and ADC. Also for exploiting the internal clock source we need to use a crystal oscillator (32.7 KHz CRYSTAL).

Summary of the main characteristics of the ADS1158

Summary of ADC in designed hardware is according to table 3.2.

	ADS1158	Unit
AVDD to AVSS	–0.3 to +5.5	V
AVSS to DGND	–2.8 to +0.3	V
DVDD to DGND	–0.3 to +5.5	V
Input current	100, momentary	mA
Input current	10, continuous	mA
Analog input voltage	AVSS – 0.3 to AVDD + 0.3	V
Digital input voltage to DGND	–0.3 to DVDD + 0.3	V
Maximum junction temperature	+150	°C
Operating temperature range	–40 to +105	°C

Table 3.2 - Main Characteristics of ADC Circuit (ADS1158)

The realized lay out and 3D view of the design of the ADS1158 is according to Figure 3.7and 3.8.

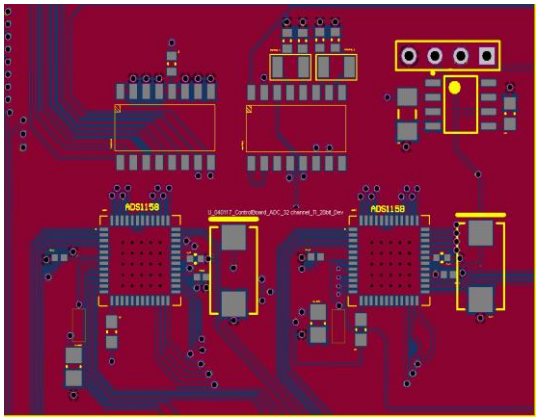

Figure 3.7 – Layout of the design of ADS1158

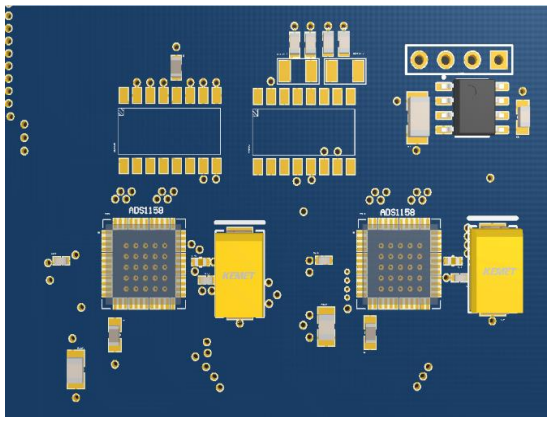

Figure 3.8 - 3D View of the Design of ADS1158

Digital to Analog Convertor (MAX5732)

Fortunately, one of the products by MAXIM Integrated Company has met our requirements and criteria of the project which is MAX5732 with input range of 0 to 5 V DC and a monotonic output by supporting SPI communication protocol. MAX5732 by supporting 32 channel DAC with resolution of 16 bit beside of supporting SPI protocol for data transmission with microcontroller is an appropriate choice in respect of accuracy and footprint. Here we briefly discuss about the main features of MAX5732 and the main consideration to take advantage of it.

Overview

The main features of the MAX5732 ca be summed up according below.

- Monotonic output up to 16 Bits
- 32 Individual DACs
- Output Voltage Ranges 0 to +5V
- Buffered Voltage Outputs Capable of Driving 10kΩ || 100pF
- SPI-/QSPI-/MICROWIRE-/DSP-Compatible 33MHz Serial Interface

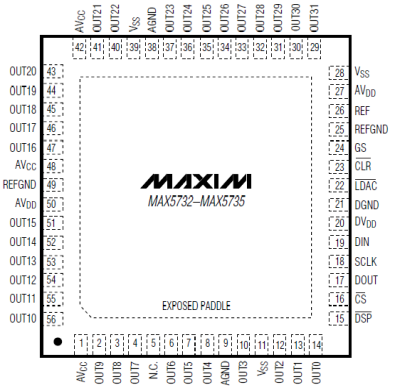

Figure 3.9- Pin configuration of DAC (MAX5732)

Main considerations in design of MAX5732 circuit

- Power Supply
  For ensuring about the reference voltage of the converter an extra reference voltage (MAX6126AASA30+) compatible to the MAX5732 is used. The same method as ADS1158 for considering a jumper for selecting external and on board power supply manually. Every power supply pin is bypassed by bypass capacitor.
- The control logic commands for starting conversion and clearing the output registers can be toggled manually by switch.

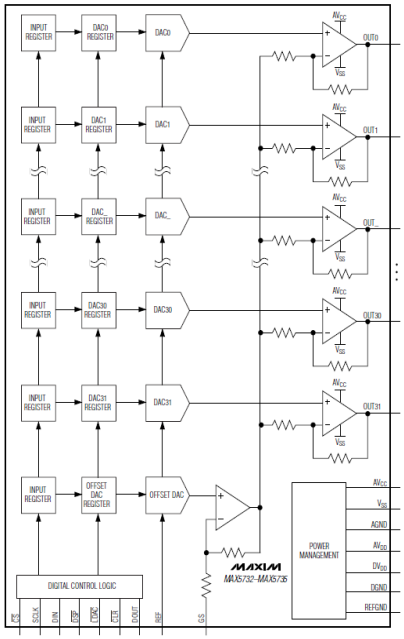

Figure 3.10 - Functional Diagram of DAC (MAX5732)

Summary of DAC (MAX5732) Design Characteristics

Summary of the main characteristics of the designed DAC circuit based on MAX5732 is according to table 3.3.

	MAX5732	Units
AVCC to VSS, AGND, DGND, REFGND	-0.3V to +12	V
VSS to AGND, DGND	-6V to +0.3	V
AVDD, DVDD to AGND, DGND, REFGND	-0.3V to +6	V
AGND to DGND, REF to AGND, DGND,	-0.3V to +0.3	V
Digital Inputs to AGND, DGND, REFGND	-0.3V to +0.3	V
DOUT to DGND	-0.3V to +6	V
OUT to VSS.	-0.3 +12V	V
Maximum Current into REF	±10	mA
Maximum Current into Any Pin	±50	mA
Continuous Power Dissipation (TA = +70°C)	2.5	W
Junction Temperature	+150	°C
Resolution	16	Bits
Integral Nonlinearity (INL)	±4	LSB

Table 3.3 – main Characteristics of DAC (MAX5732)

The realized layout and 3D of the DAC design based on MAX5732 is according to Figure 3.10.

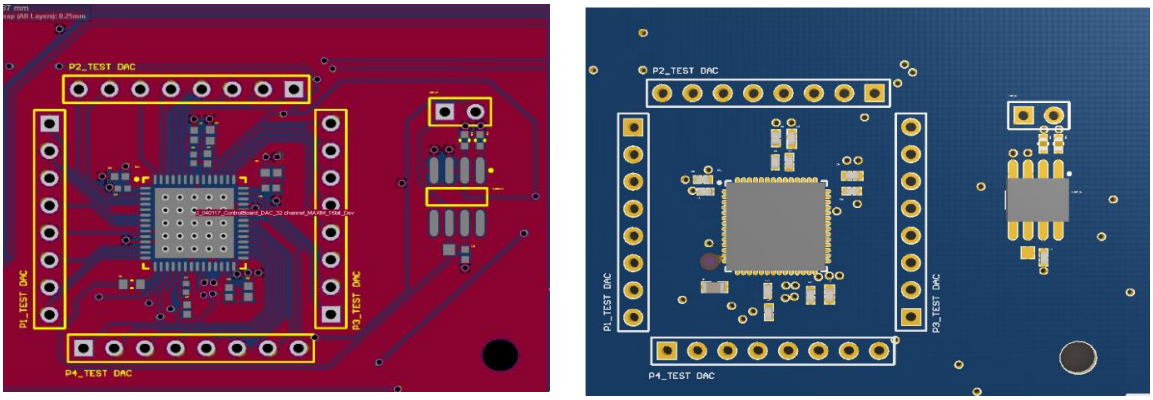

Figure 3.11 -The Layout of DAC circuit Design (MAX5732) and 3D view of the Designed DAC (Max5732

Power supply

Overview

The main part of a hardware is the power supply since it shoulders the responsibility to support the electrical power of each sections of the circuit. Output power and stability of it, are the main features of the power supply which should be satisfied in any conditions (for example unloaded, transient, max loaded, etc.). The designed power supply for the control board is based on the Buck convertor topology which is a DC/DC convertor as one of the most efficient convertors (95%). Considered range as input voltage for control board is 8 to 12 V DC which we expect to have normal behavior in the output in this area.

Since there exist a variety of ICs and components and the need for two main power supply voltage which are +3.3V and +5V DC, design of the power supply is divided into two part. Here we briefly describe the structure of the buck convertors then we will discuss about the power supply and the simulation results in the output voltage.

Buck convertor Introduction

Buck convertor is called step down which refers to stepping down the out put voltage while stepping up the current out put. It is in classification of the switched mode power supplies. The main structure of a buck convertor is based on the Figure 3.12 which includes a voltage source, a switch (transistor), a diode, and a storage element (inductance) which the current of the load is same as the current of the inductance. In order to reduce the output ripple there is filter containing a capacitor in the output which can exist a combination of two filter network for improving the output quality. Generally, there exist two states for the circuit which relates to the state of the switch to be on or off Figure 3.12 (B), (C).

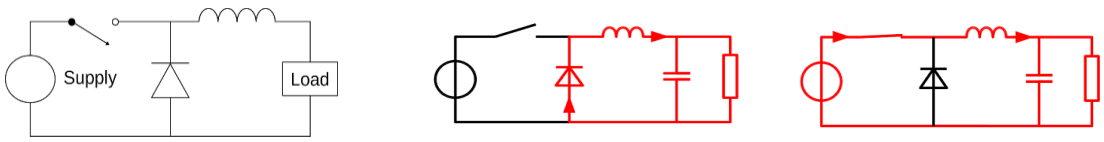

Figure 3.12 (A) Main Scheme of Buck Convertor (B) Off state Mode (C) on state Mode

Regarding the frequency switch and duty cycle, buck convertors could be categorized in two main branches which are continuous mode and discreet mode. Since we need to have continuous output current we will focus on the continuous mode.

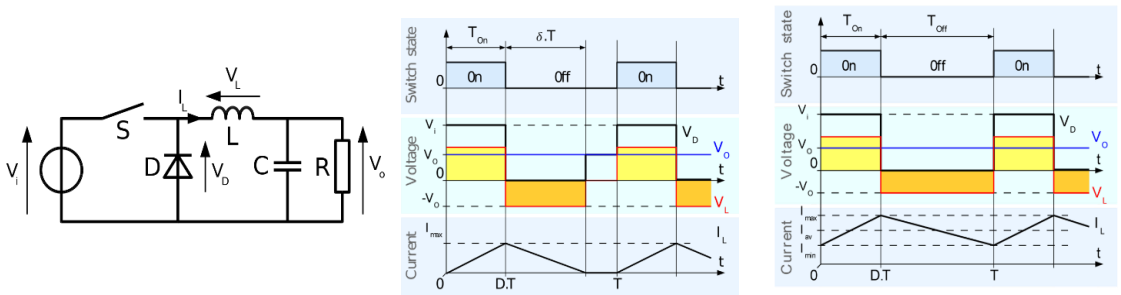

Figure 3.13 - (A) Filtered Buck Convertor (B) Discreet Mode (C) Continuous Mode

Continuous mode

A buck converter operates in continuous mode if the current through the inductor (I_L) never falls to zero during the commutation cycle. In this mode, the operating principle is described by the plots in Figure 3.13:

- When switch is on voltage across the inductance is $V_L = V_i - V_o$. The current through the inductor rises linearly and diode is revers biased by voltage source.
- When switch is off $VL = - V_O$, the diode is forward biased and the current I_L decreases.

As a summary, we have these equations for the output voltage:

$$\begin{cases} VL = Vi - Vo \quad \text{switch on} \quad , \text{Eq. 1} \\ \\ VL = -VO \quad \text{switch off} \quad , \text{Eq. 2} \end{cases}$$

The energy stored in inductor L is:

$$E = \frac{1}{2} \; L \, . \, {I_L}^2$$

And the rate of the change in I_L is:

$$V_L = L \frac{dI_L}{dt}$$

According to Eq. 1 and Eq.2 the increase in on state and of state is given by:

$$\begin{cases} \Delta I_{L_{on}} = \int_0^{t_{on}} \frac{V_L}{L} \, dt = \frac{(Vi - Vo)}{L} \; t_{on}, & t_{on} = DT \\ \Delta I_{L_{off}} = \int_{t_{on}}^{T = t_{on} + t_{off}} \frac{V_L}{L} \, dt = \frac{(Vi - Vo)}{L} \; t_{on}, & t_{on} = DT \end{cases}$$

Therefore, we can write from above equations:

$$\Delta I_{L_{on}} + \Delta I_{L_{off}} = 0 \quad \gg \quad \frac{(Vi - Vo)}{L} \; t_{on} - \frac{Vo}{L} \; t_{off} = 0$$

As we know $t_{on} = DT$ and $t_{off} = (1 - D)T$ which results:

$$Vo - DVi = 0 \;\; \gg \;\; D = \frac{Vo}{Vi}$$

From the final equation, it can be seen the output voltage varies linearly with duty cycle for a given input voltage. D as duty cycle is the ratio of the t_{on} and the period T, and it cannot be more than 1. Therefore$Vo \leq Vi$. Because of this relation this convertor is referred to step-down convertor.

Output Voltage ripple

Several factors can contribute to the voltage ripple like switching frequency, output capacitance, and inductor and load any current limiting the features of the control circuitry. At the most basic level the output voltage ripple will have an effect on the charge and discharge of the output capacitor, so:

$$d\mathrm{Vo} = \frac{idT}{C}$$

During the Off state, the current in the equation is the load current. In the On state the current is the difference between the switch current and load current. So we have:

$$\begin{cases} dT_{on} = DT = \dfrac{D}{f}\ ; & On - state \\ dT_{off} = (1-D)T = \dfrac{1-D}{f}\ ; & Of - state \end{cases}$$

Qualitatively, as the output capacitor or switching frequency increase, the magnitude of the ripple decreases. Output voltage ripple is typically a design specification for the power supply and is selected based on several factors. Capacitor selection is normally determined based on cost, physical size and non-idealities of various capacitor types. Switching frequency selection is typically determined based on efficiency requirements, which tends to decrease at higher operating frequencies, as described below in Effects of non-ideality on the efficiency. Higher switching frequency can also raise electromagnetic interference (EMI) concerns. Output voltage ripple is one of the disadvantages of a switching power supply, and can also be a measure of its quality.

Design of the power supply

The simulation of the designed power supply has been performed by WEBENCH designer application provided by Texas Instrument Company. As mentioned before, there existed the need of two main supply voltage (+3.3V, +5V). The main scheme of the designed power supply is according to the Figure 3.14.

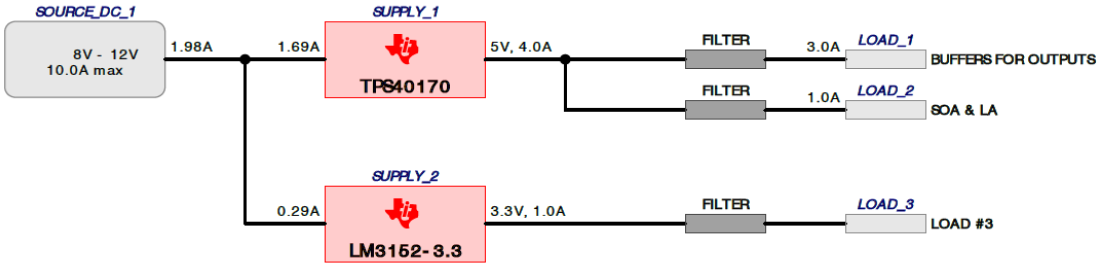

Figure 3.14 – Main scheme of the Designed Power Supply

SOURCE_DC_1 in above Figure 3.14 is the input voltage source which according to the simulation sink current from the input voltage is totally 1.98A which is sourcing two main part for sourcing the SUPPLY_1(+5VDC/ TPS40170) and SUPPLY_2 (+3.3VDC/ LM3152_3.3).

+5VDC Supply Voltage Design

The main features of the TPS40170 are:

- Wide Input Voltage Range from 4.5 V to 60 V
- 600 mV Reference Voltage with 1% Accuracy
- Programmable UVLO and Hysteresis
- Voltage Mode Control With Voltage Feed Forward
- Programmable Frequency between 100 kHz &600 kHz
- Low-side FET Sensing Overcurrent Protection
- High-Side FET Sensing Short-Circuit Protection
- Integrated Thermal Compensation
- Programmable Closed Loop Soft-Start
- Supports Pre-Biased Outputs
- Thermal Shutdown at 165°C with Hysteresis
- Voltage Tracking
- ENABLE with 1-µA Low Current Shutdown
- 8.0-V and 3.3-V LDO Output
- Integrated Bootstrap Diode
-

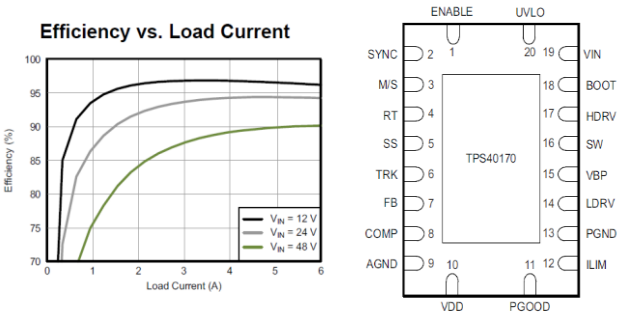

Figure 3.15 – TPS40170 PIN

For realization of the high side and the low side switch of the buck convertor the 'CSD16321Q5' from Texas Instrument Company is used. 'CSD16321Q5' is N-channel power MOSFET with the features:

- Optimized for 5-V Gate Drive
- Ultra-Low Q_g and Q_{gd}
- Low-Thermal Resistance
- Avalanche Rated

T_A = 25°C		TYPICAL VALUE	UNIT
V_{DS}	Drain-to-Source Voltage	25	V
Q_g	Gate Charge Total (4.5 V)	14	nC
Q_{gd}	Gate Charge Gate-to-Drain	2.5	nC
$R_{DS(ON)}$	Drain-to-Source On Resistance	V_{GS} =3V, 2.8	mOhm
$V_{GS(th)}$	Threshold Voltage	1.1	V

Table 3.3 – Main Characteristics of CSD16321Q5

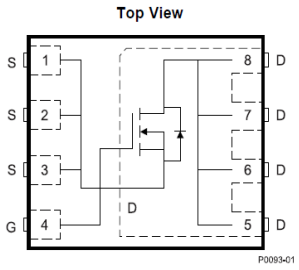

Figure 3.16 – Pin configuration of CSD16321Q5

Since the gate charge for operation of the MOSFET is very important in terms of power loss and considerations about the output power, it should be considered in final output power of the power supply. Also, the resistance of the device while operation because of voltage drop is a factor which should be studied. The characteristics of the gate charge and resistance of the drain to source of the MOSFET is according to Figure 3.17.

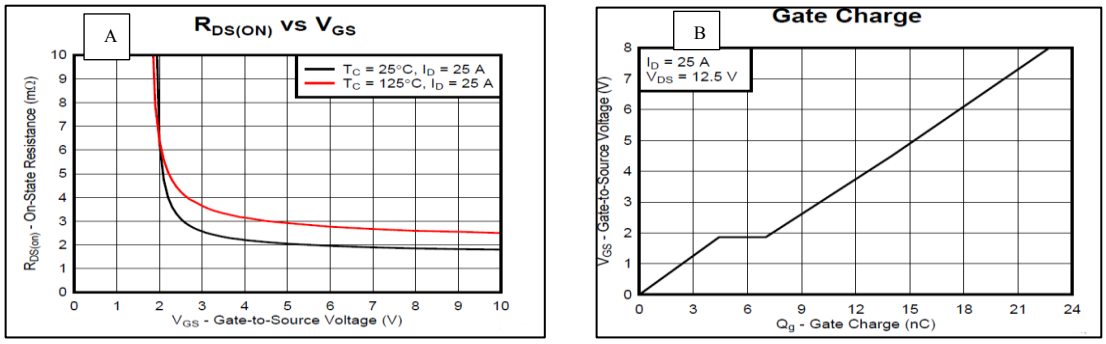

Figure 3.17 – (A) Drain Source Impedance vs. Gate source voltage (B) Gate charge vs. Gate source Voltage

Now after a brief introduction about the critical components of the +5VDC power supply, we need to introduce the the control and feedback network of the TPS40170. The simplified schematics of the design is according to figure 3.18which simulation results will be provided by WEBENCH DESIGNER & TINA software in figure 3.19.

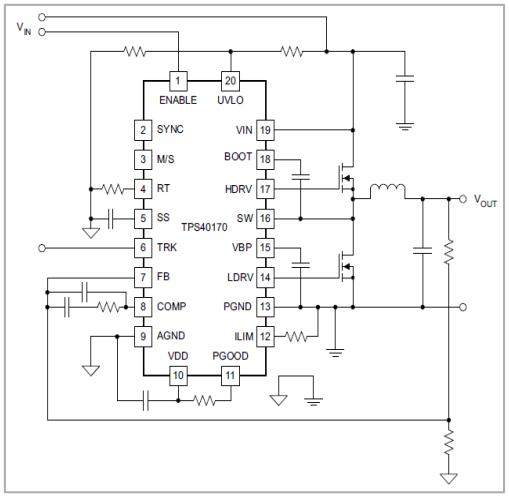

Figure 3.18 - Simplified Schematics of TPS40170

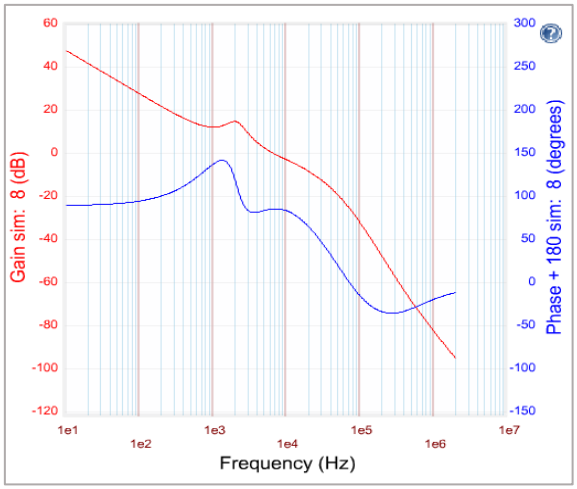

Figure 3.19 - Bode plot of the compensation Network of TPS40170

TPS40170 transient, steady state, load transient and input transient simulation results are as shown in Figures 3.20 , 3,21 , 3,22, 3.23, 3.24, 3.25, 3.26.

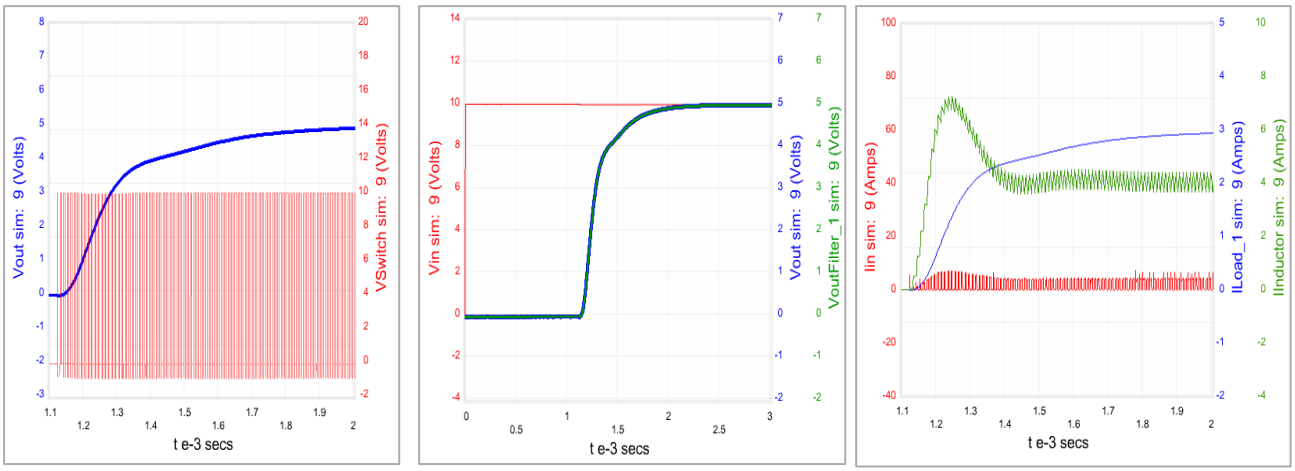

Figure 3.20- Transient Mode Simulation TPS40170

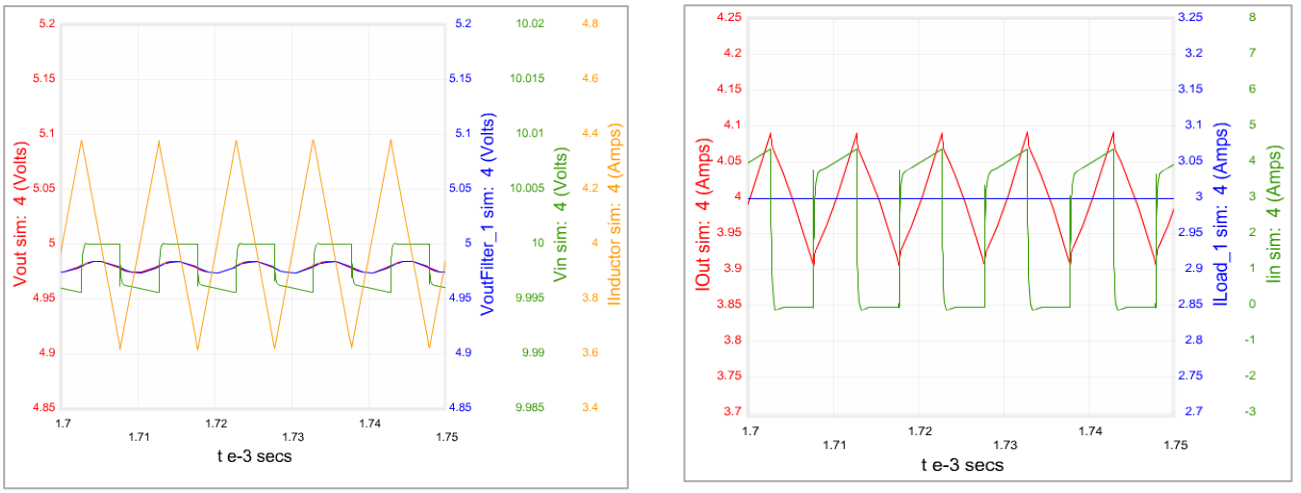

Figure 3.21- Steady State Mode TPS40170

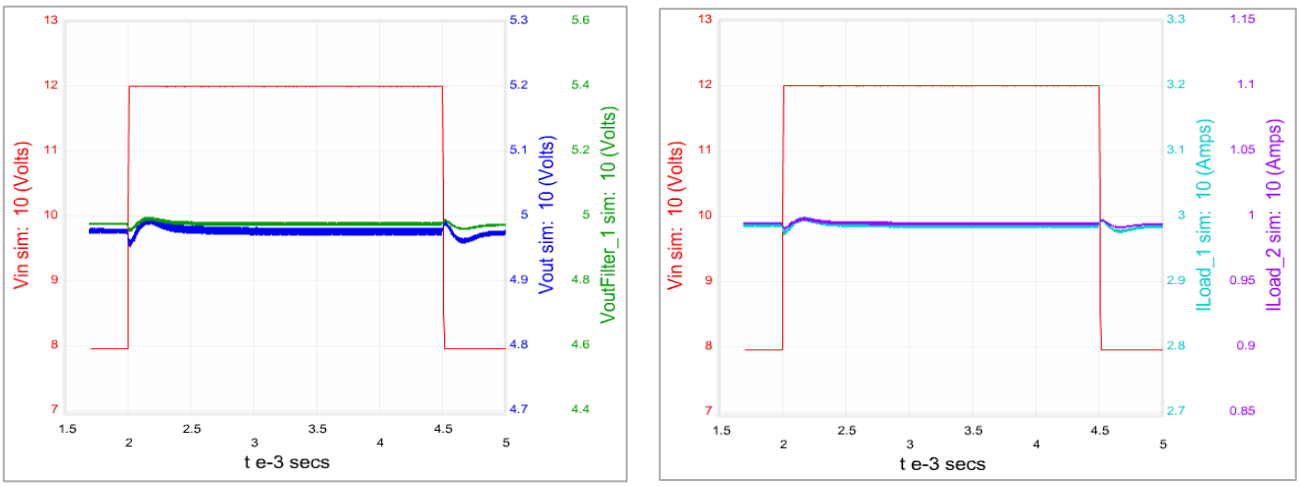

Figure 3.22 - INPUT Transient Mode Simulation TPS40170

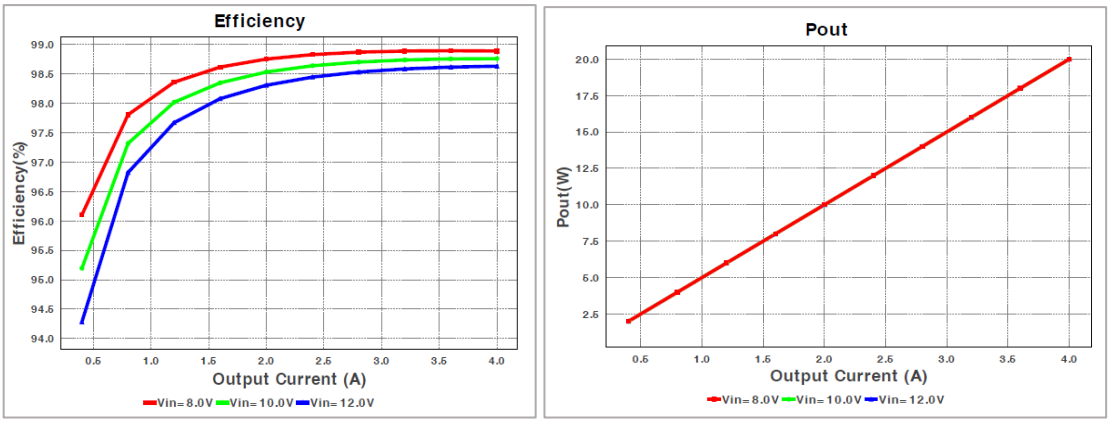

Figure 3.23 - (A) Efficiency of the Power Supply Vs. Load (B) Linear Output Power Vs. Input Voltage

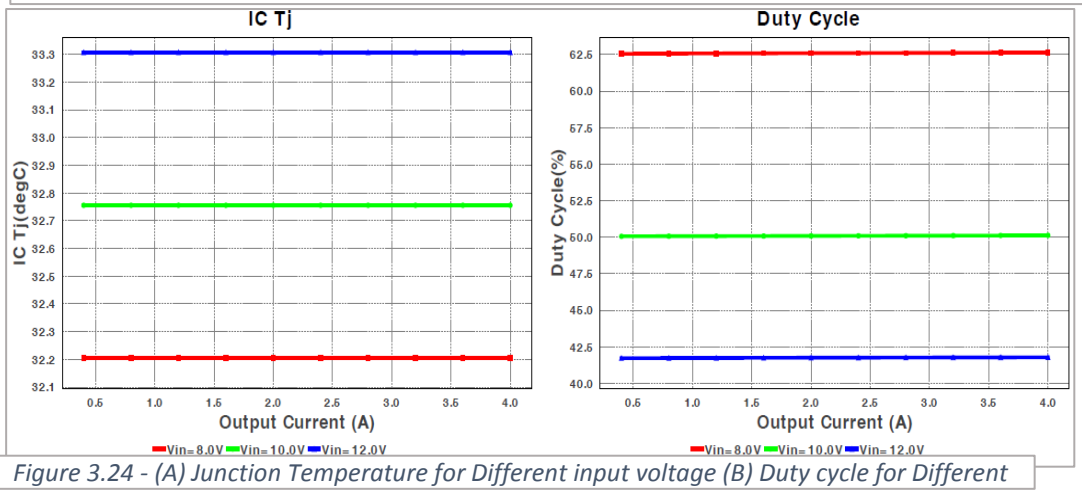

Figure 3.24 - (A) Junction Temperature for Different input voltage (B) Duty cycle for Different

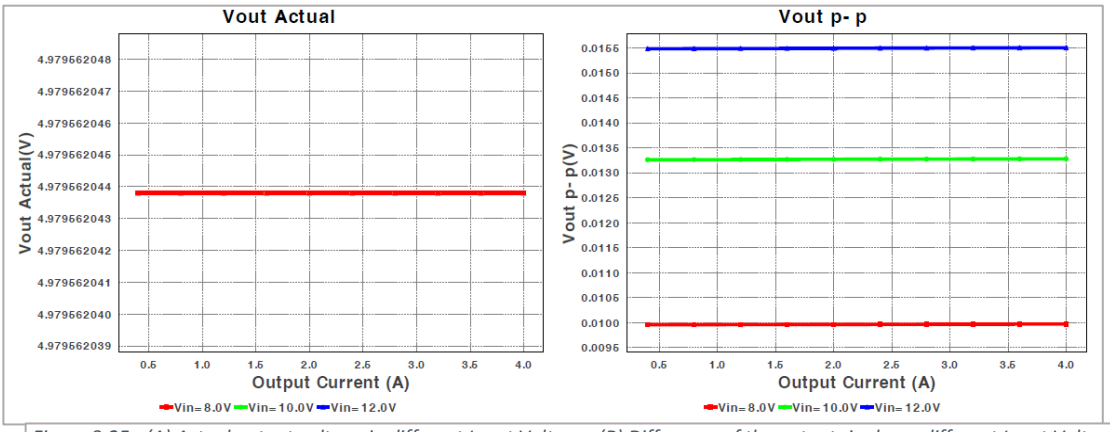

Figure 3.25 - (A) Actual output voltage in different Input Voltages (B) Difference of the output ripple vs. different Input Voltage

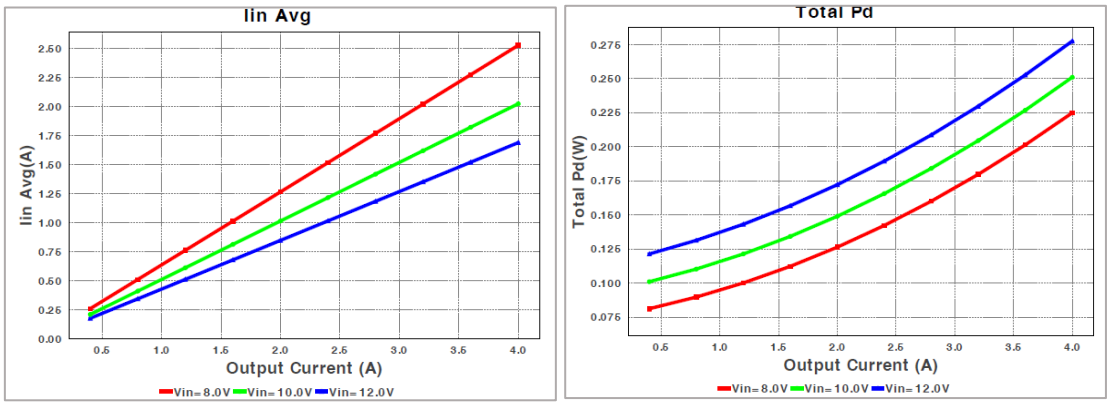

Figure 3.26- (A) Input Current vs. Output Current (B) Total Power Dissipation of the power supply TPS40172

+3.3VDC Supply Voltage Design

The LM3152_3.3 is a simple switcher controller with a wide input voltage range from the synchronous Step-down family convertors, the main features of the LM3152_3.3 are:

- 6V to 42V Input Voltage Range
- Fixed Output Voltage of 3.3v
- Fixed Switching Frequency of 250/500/750KHz
- Constant On-time Control
- Ultra-fast Transient Response
- Stable with Low ESR Capacitors
- Programmable Soft-start

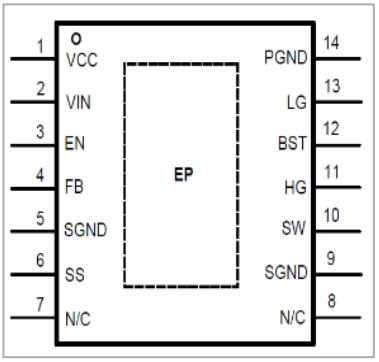

Figure 3.27 – Pin Configuration of LM3152

In order for performing switching the same switcher used in the TPS40170 is exploited (CSD16321Q5).A simplified version of the schematics for the design is according to the figure3.28 and the simulation results for transient, steady state , Input transient, and load transient mode are shown in Figure 3.29,30,31,32,33,34,35.

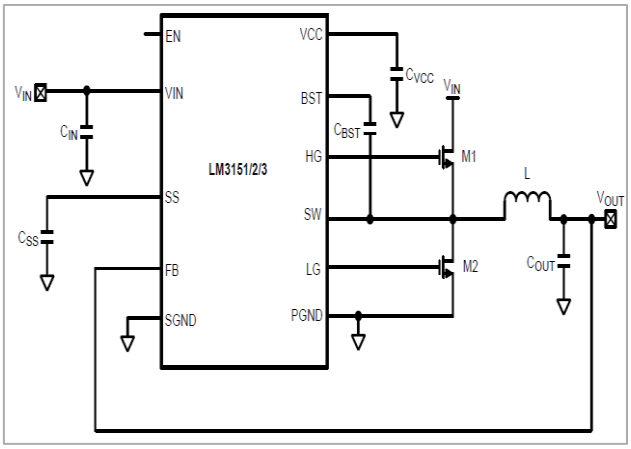

Figure 3.28- Simplified schematics of LM3152

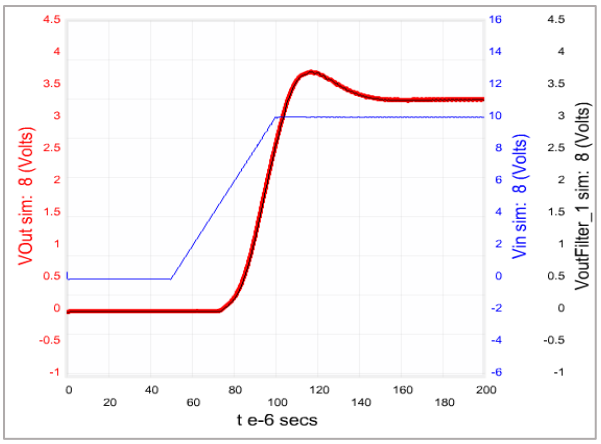

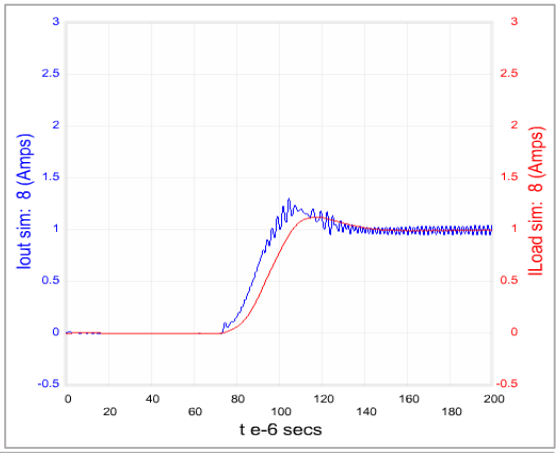

Figure 3.29- (Left picture) Transient of the Output Voltage and Settling In3.3V (Right Picture) Transient of the Output Current and Load Current

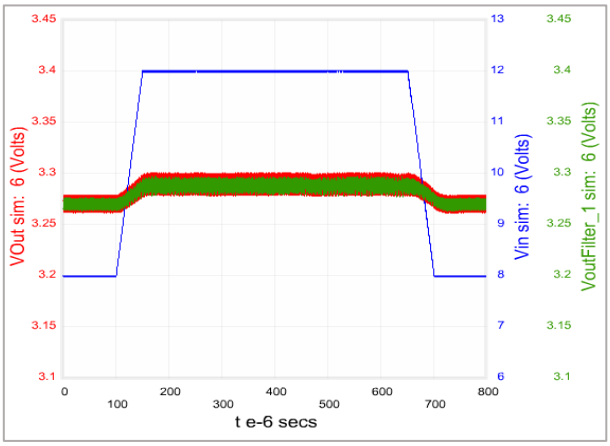

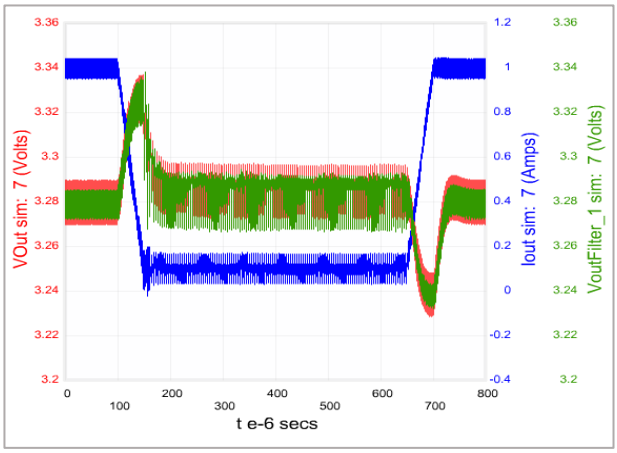

Figure 3.30 - (Left Picture) Transient of Input Voltage and Output Voltage (Right Picture) Transient of the Load form Max. To Min. and the effects On Output Voltage.

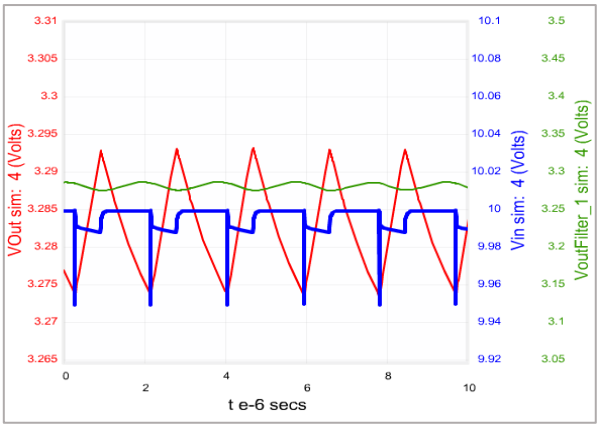

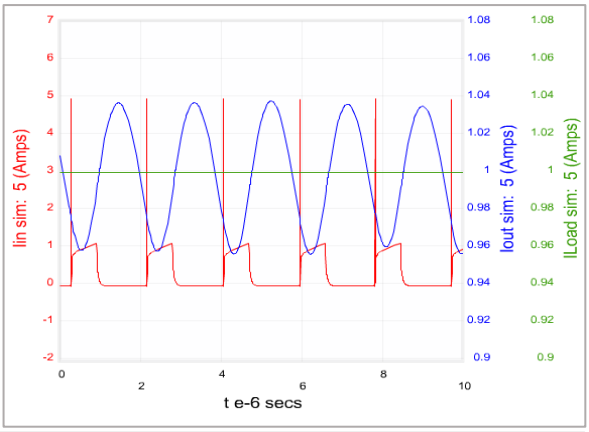

Figure 31-(Left Picture) Steady State Output Voltage, Output Filter Voltage, Input Voltage. (Right Picture) Steady state Input current, Output Current, Load Current.

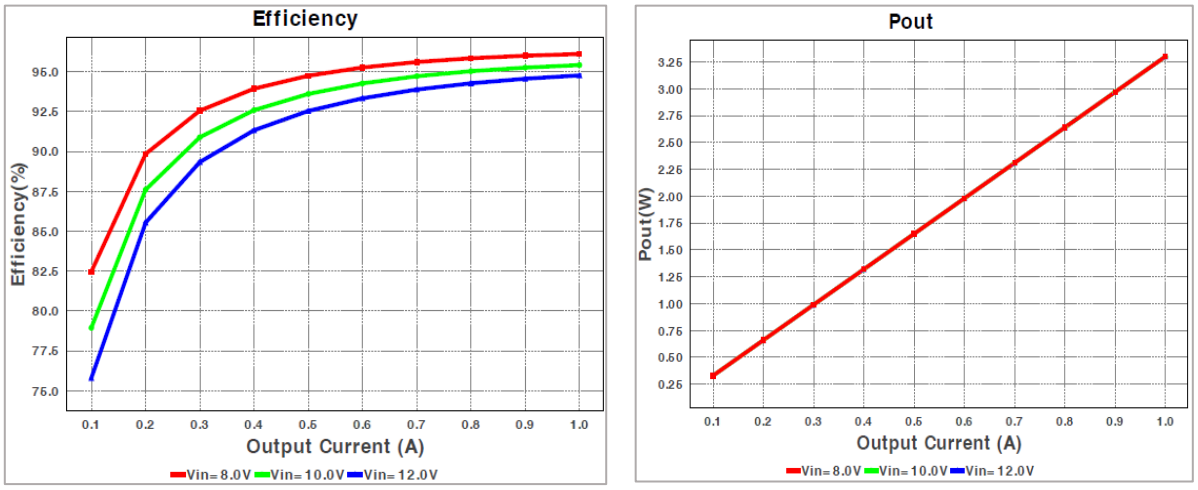

Figure 3.32 (A) Power Supply Efficiency (B) Monotonic Output Power vs. Output current

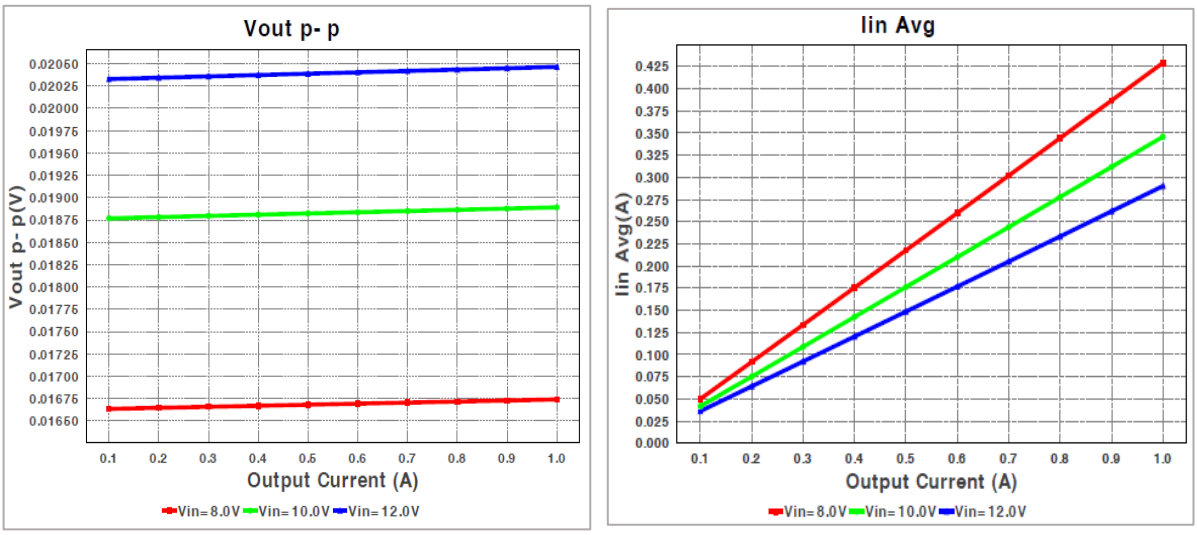

Figure 3.33 - (A) Output voltage ripple (B) Average Input current vs. output Current in different Input voltages

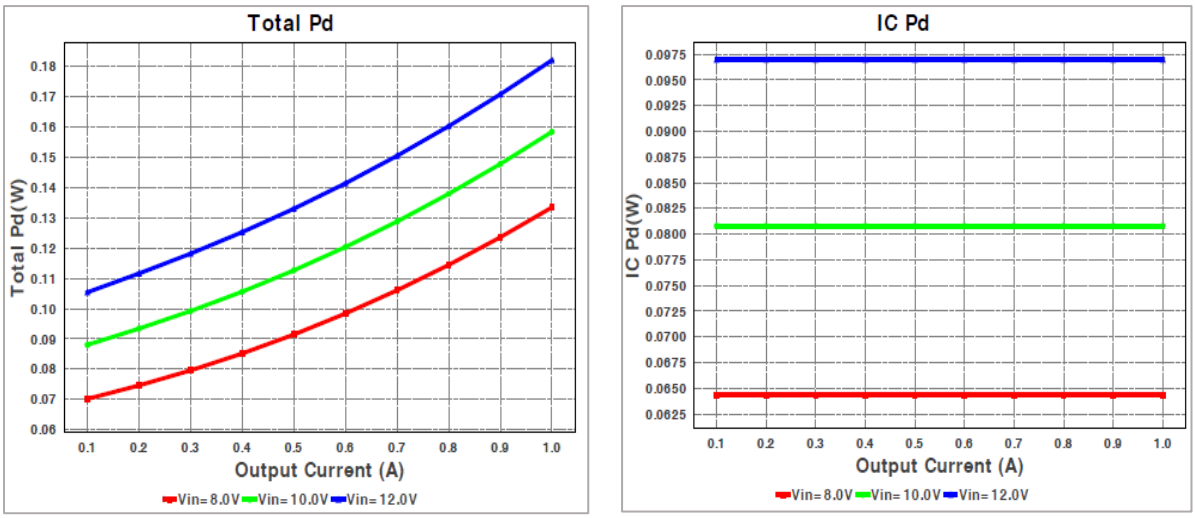

Figure 3.34 – (A) Total Power Dissipation of LM3152 (B) Power dissipation in Switcher LM3152

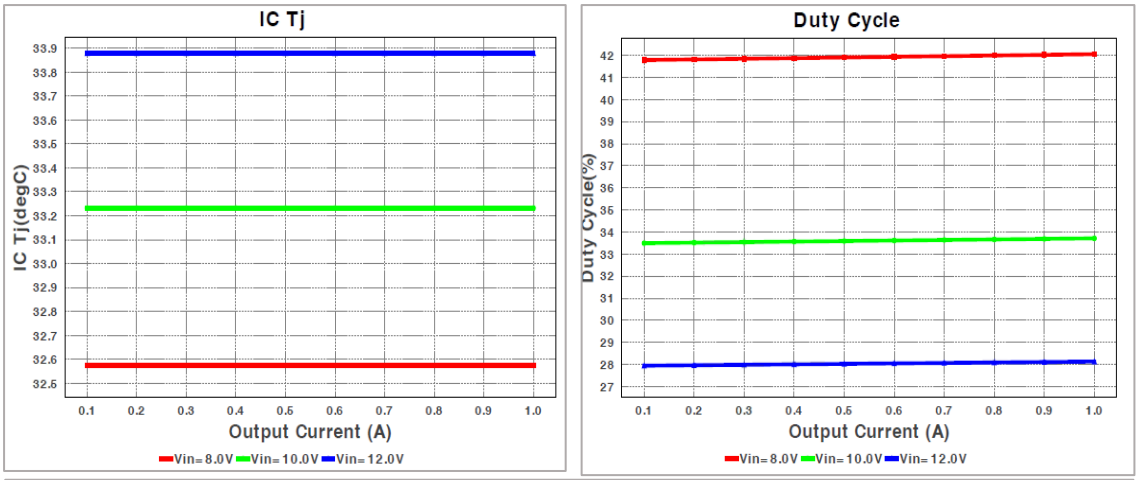

Figure 3.35 – (A) max. Junction Temperature (B) Duty Cycle Variation in Different Input Voltages

Summary of the Power Supply Design

The summary for the designed power supply is under the conditions as below:

1. Ambient tempuerature 25℃
2. V_{In_Min} = 8V and V_{In_Max} =12Vdc
3. Nominal Input voltage 10V

Power Supply	Load	Load Name	Controller	Load Voltage	Load Current	Efficiency
SUPPLY1	Load_1	Output Buffers	TPS40170	5v	3A	98.6%
SUPPLY2	Load_2	SOA & LASER	TPS40170	5v	1A	98.6%
SUPPLY3	Load_3	DIGITAL Supply Voltage	LM3152	3.3v	1A	94.6%

Table 3.4 – Summary of the Designed Power Supply Main Characteristics

The related layout and 3D view for the power supply is according to Figure 3.36

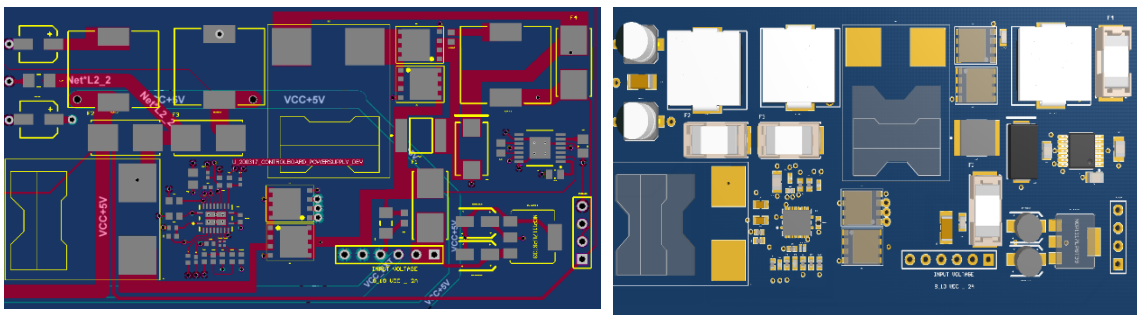

Figure 3.36 – (A) Power Supply Final Layout (B) Power Supply 3D View

Trans-Impedance Amplifier (TIA)

Since we need to convert the generated currents by photodiodes, therefore there is a need to have conversion from current to voltage in a desirable range of the ADCs. The exploited circuit to reach our goal is Trans-Impedance Amplifier (TIA). Here we briefly introduce TIA then we will discuss about the designed circuit main characteristics.

Overview

A trans-impedance amplifier (TIA) is a current-to-voltage converter, most often implemented using an operational amplifier. The TIA can be used to amplify the current output of Geiger–Müller tubes, photomultiplier tubes, accelerometers, photo detectors and other types of sensors to a usable voltage. Current-to-voltage converters are used with sensors that have a current response that is more linear than the voltage response. This is the case with photodiodes, where it is not uncommon for the current response to have better than 1% linearity over a wide range of light input. The trans-impedance amplifier presents a low impedance to the photodiode and isolates it from the output voltage of the operational amplifier. In its simplest form a trans-impedance amplifier has just a large-valued feedback resistor, Rf. The gain of the amplifier is set by this resistor and has a value of -Rf (because the amplifier is in an inverting configuration). There are several different configurations of trans-impedance amplifiers, each suited to a particular application. The one factor they all have in common is the requirement to convert the low-level current of a sensor to a voltage. The gain, bandwidth, as well as current and voltage offsets, change with different types of sensors, requiring different configurations of trans-impedance amplifiers.

Since the used configuration for our circuit is reversed bias photodiode configuration, so we will focus on this type of TIAs. The main structure of a reversed bias photodiode configuration is shown in Figure 3.37 as below:

Because of the need for changing the bias voltage of the photodiode in our configuration the positive input of the OP-AMP is connected to a voltage source pin. In order to avoid any high frequency noises in the output of the TIAs, a Low-Pass filter has been considered to pass signals in the range of the photodiodes' output and attenuate the high frequency signals. The output of the photodiodes (PD) are in the range of 1.5 kHz and it seems suitable to have low pass filter with cut-off frequency in 2 kHz. In order to have a configurable gain, instead of constant Rf, a potentiometer has been considered.

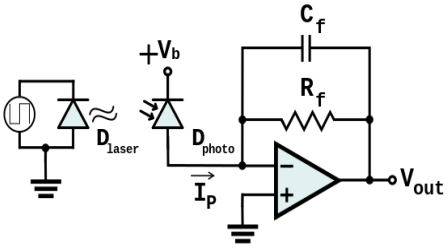

Figure 3.37 -Main scheme of Reversed Bias TIA

DC Operation

The DC and low-frequency gain of a trans-impedance amplifier is determined by the equation below:

$$-I_p = \frac{V_{out}}{R_f}$$

The C_f is used for increasing the stability of the system so now we need to discuss about the bandwidth and stability of the TIA.

Bandwidth and Stability

The frequency response of a trans-impedance amplifier is inversely proportional to the gain set by the feedback resistor. The product of the gain, Vin/Vo, is very close to being a constant for any given op-amp. The sensors that trans-impedance amplifiers are used with usually have more capacitance than an op-amp can handle. The sensor can be modeled as a current source and a capacitor Ci. This capacitance across the input terminals of the op-amp, which includes the internal capacitance of the op-amp, introduces a low-pass filter in the feedback path. The low-pass response of this filter can be characterized as the feedback factor β shown as below:

$$\beta = \frac{X_{C_i}}{R_f + X_{c_i}} = \frac{1}{1 + R_f C_i s}$$

Where X_{Ci} is reactance of capacitance C_i. This filter attenuates the feedback signal, which causes a greater demand on the amplifier gain. By considering this low pass filter effect, the circuit response equation becomes:

$$V_{out} = -\frac{I_p R_f}{1 + \frac{1}{A_{ol}\beta}}$$

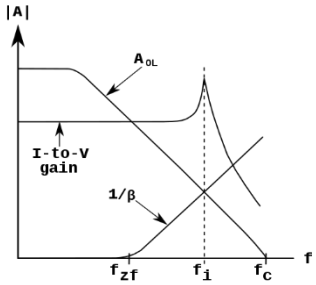

Figure 3.38– Uncompensated

Where A_{OL} is the open loop gain of op-amp. By considering C_f as a feedback capacitor of the TIA, the compensated feedback factor becomes:

$$\beta = \frac{1 + R_f C_f s}{1 + R_f (C_i + C_f) s}$$

By knowing that capacitor produces a zero at:

$$f_{C_f} = \frac{1}{2\pi R_f C_f}$$

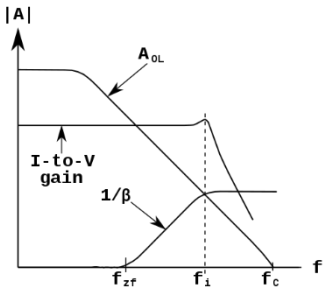

Figure 3.39– Compensated TIA

And this counteracts the pole produced by Ci at the frequency:

$$f_{zf} = \frac{1}{2\pi R_f (C_i + C_f)}$$

Noise Considerations

In most practical cases, the dominant source of noise in a trans-impedance amplifier is the feedback resistor. The output-referred voltage noise is directly the voltage noise over the feedback resistance. This Johnson–Nyquist noise has an RMS amplitude equal to:

$$v_n = \sqrt{4 K_B T R_f \Delta f}$$

Though the output noise voltage increases proportionally to $\sqrt{R_f}$, the transimpedance increases linearly with R_f, resulting in an input-referred noise current equal to:

$$i_n = \sqrt{\frac{4 K_B T \Delta f}{R_f}}$$

For a better noise performance, a high feedback resistance should thus be used. However, a larger feedback resistance increases the output voltage swing, and consequently a higher gain

from the operational amplifier is needed, demanding an operational amplifier with a high gain-bandwidth product. The feedback resistance and therefore the sensitivity are thus limited by the required operating frequency of the trans-impedance amplifier.

TIA Design

The structure of the designed TIA is according to Figure 3.40 which is simulated by TINA software, which DC characteristics, AC characteristics, step response, steady state response and noise performance simulations will be provided in figures 3.41, 42,43,44,45,46.

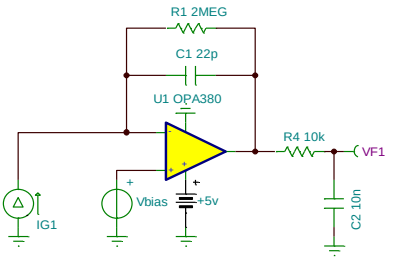

Figure 40 – Schematics of Designed TIA (OPA380)

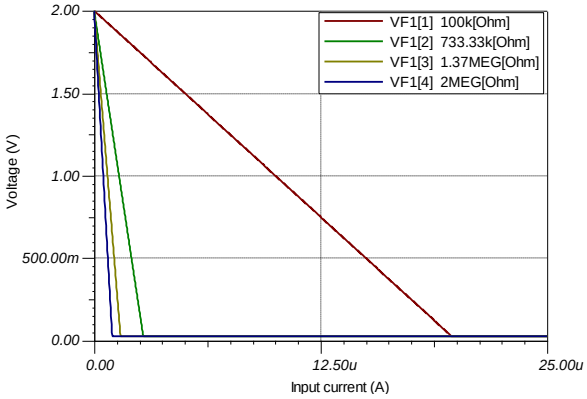

Figure 41 – DC Characteristics of TIA

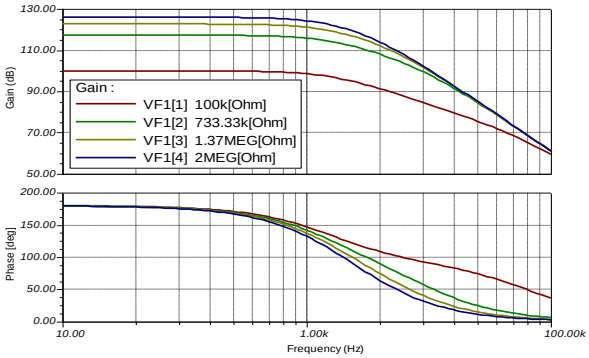

Figure 42– AC Characteristics of TIA (OPA380) by Swiping R_f from 500K to 2Meg [ohm]

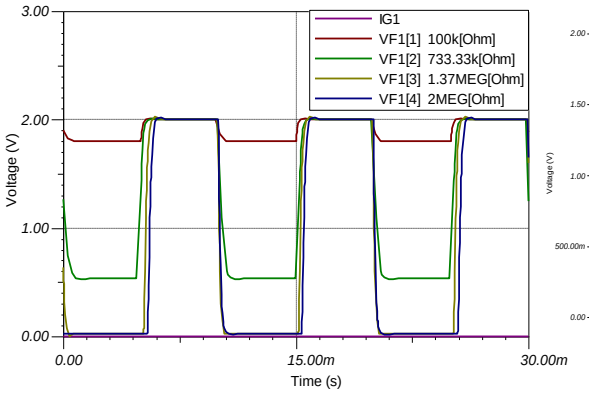

Figure 43– Step Response of TIA (OPA380) Step Input Current 1uA and Max gain 2Mohm

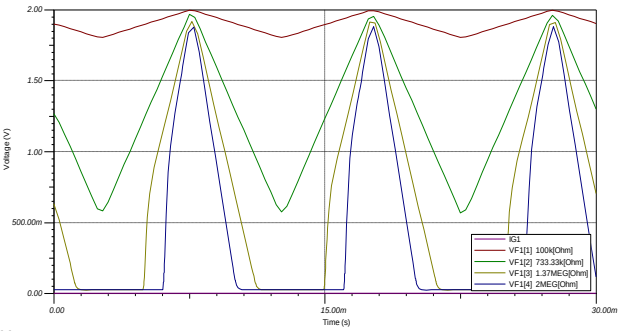

Figure 44 – TIA Response to Triangle Input (100 Hz, 1u Amplitude)

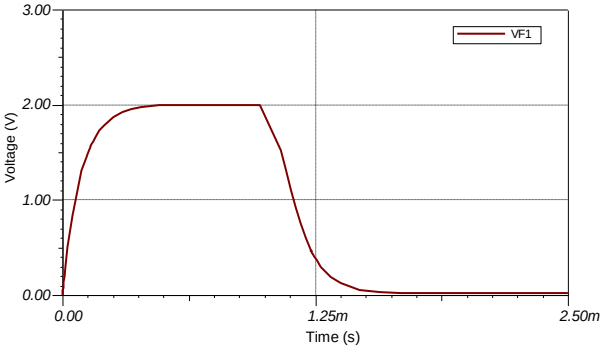

Figure 45– Steady State Response for Input Step current

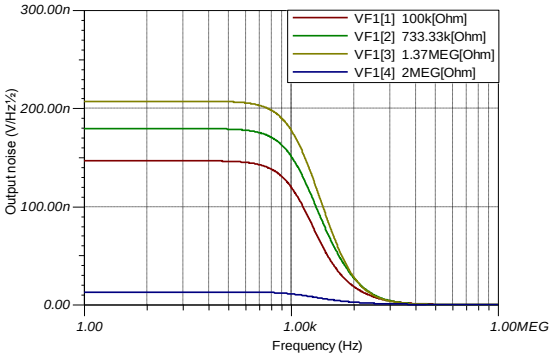

Figure 46 – Noise Analysis of TIA (OPA380) by Swiping Rf

Summary of TIA Design

The main characteristics of the designed TIA is according to Table 3.6. Then, the final layout and 3D overview of the TIA design will be provided in figures 3.47, 3.48.

Min. Supply Voltage [VDC]	Max. Supply Voltage[VDC]	Max. Gain[dB]	Max. Output Voltage[VDC]	Min. Output Voltage[VDC]	Output Filter Frequency (Low Pass)	Response Time Constant[ms]
2.7V	5.5	125	2(V_{bias})	0	1.6kHz	0.3

Table 3.5 – Summary of Main characteristics of TIA (OPA380)

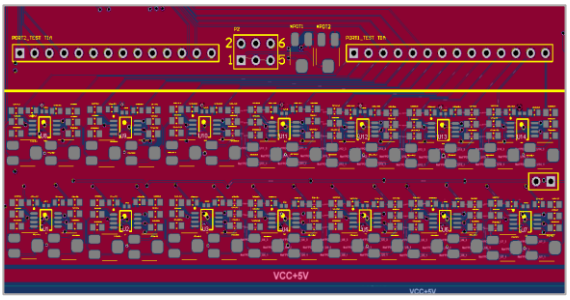

Figure 3.47– TIA Design Layout (OPA2380)

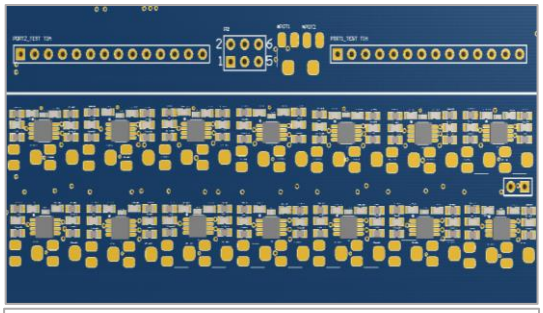

Figure 3.48– TIA Design - 3D View (OPA2380) – (14xOPA2380)

Output Buffers (OPA4251)

Overview

Since we need to be able to sink current into heaters in order for heating them up, there is a need for an appropriate output buffer respect to the needed power consumption in the heaters for controlling them, by considering this fact that the used DAC is able to generate 10mA in Max voltage 5V DC which according to our observation for a full FSR we need at least 63 [mW] and at most 80 [mW] power consumption in the heaters. On the other hand, not only for isolation of the signal and load but also for the protection of the sensitive component of the PCB form any probable overcurrent problems, a structure of combined OP-AMP and a BJT transistor for buffering is exploited.

Output Buffer Design (OPA4251)

According to the performed measurements the impedance of each heaters in TX and RX section of the silicon chips is 400 Ohm which could be considered as a resistance in our simulations. The generated output voltage by DAC MAX5732 is in range of 0 to 5 volt with a resolution of 16 bit. Therefore, it could be considered as voltage generator as input for the buffer which varies according to the generated control command of Microcontroller. The used Op-Amp for this circuit is OPA4251 which supports a wide range of supply voltage which could be an advantage which will be discussed later, and also 4 In/Out operational amplifier that reduces the footprint area. The used BJT transistor is SMBTA42 which is an NPN Silicon High–Voltage Transistor which is show as figure 49.

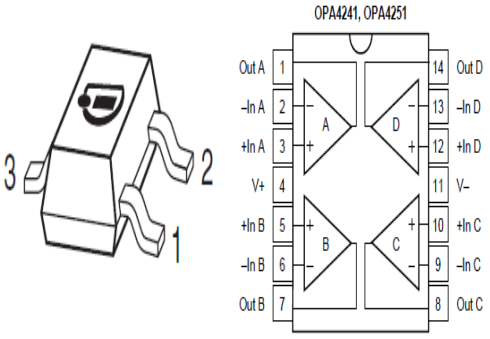

Figure 3.49 – Pin configuration of SMBTA42

The circuit under the evaluation is acording the figure 57 which is simulated by TINA Software provided by Texas Instrument company.In order to have linear and monotonic relation between input voltage and output voltage we need to impose higher supply voltage for the Op-Amp since in the case of providing the 5VDC for the OPA4251 we will have a linear but non-monotonic relation of the input and output, which is shown n figure 4.to have ability on the gain of the output instead of R2 we considered a potentiometer in range of 1k to 120k.The reason for selection of low range potentiometer is the ratio of the highest voltage as supply voltage of the Op-Amp [2.7 to 36 V] and the input voltage [0 to 5Vdc] which defines the gain of the circuit that at most would be 7.

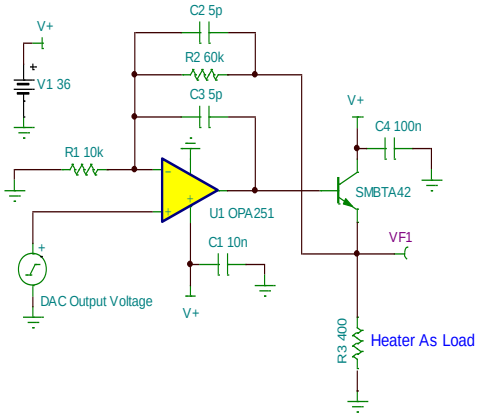

Figure 3.50 - Output Buffer Schematics

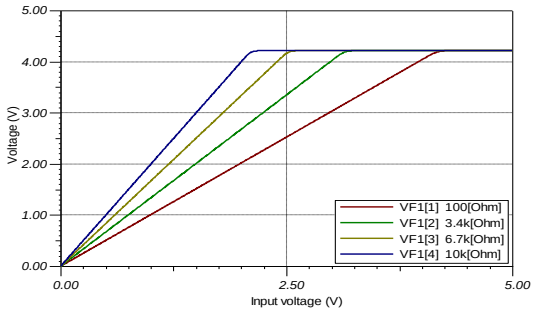

Figure 3.51– DC Characteristics with 5V DC power

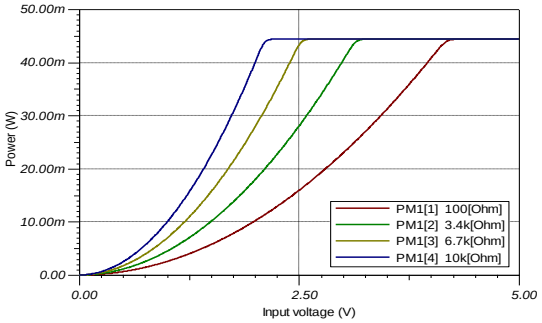

Figure 3.52 – Power Dissipation in the Load (400 Ohm Resistance Micro-Heater)

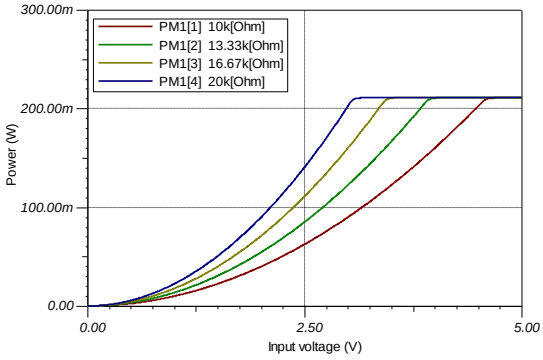

Figure 3.53 - Power Dissipation in the Load (400 Ohm)

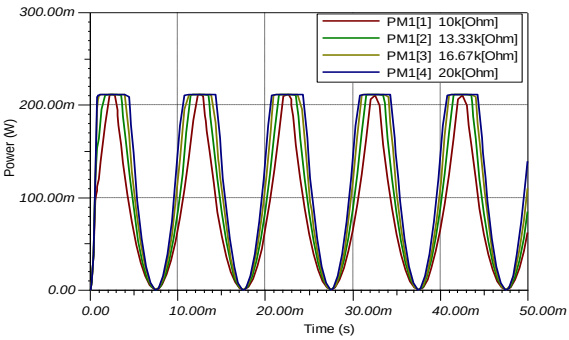

Figure 3.54- Response of the Buffer to Triangular wave

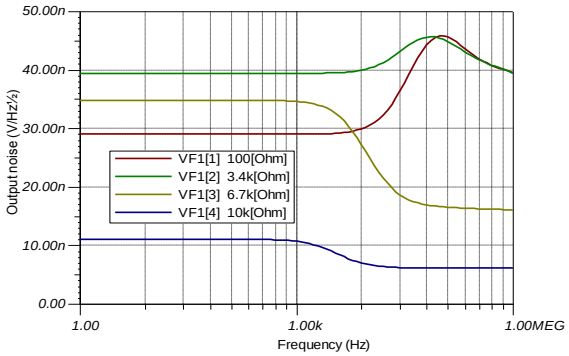

Figure 3.55 - Noise Analysis

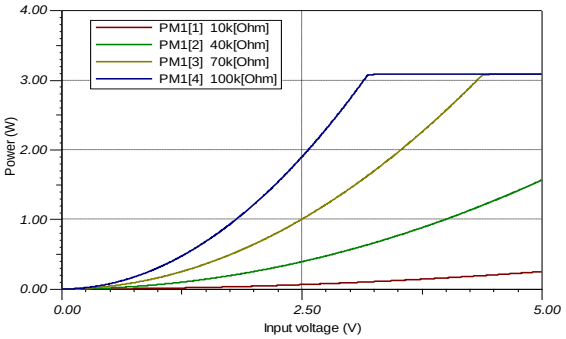

Figure 3.56 - Nominal Maximum Power Dissipation

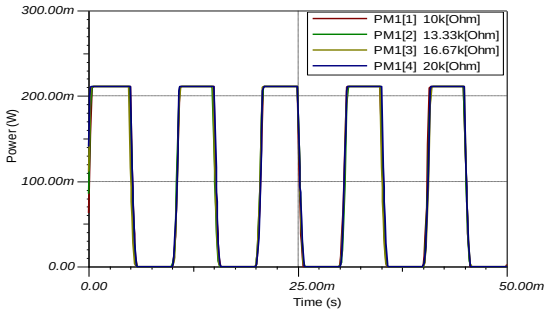

Figure 3.57 - Response of the Buffer to Square wave Input with 100Hz Frequency 5V amplitude

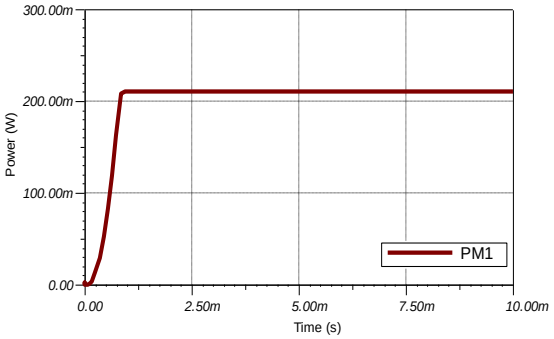

Figure 3.58 – Steady state response to Step Input (5V Amplitude)

It should be mentioned non-monotonic output voltage does not have any effect on the control procedure because we are interested in the amount of power dissipation in the Micro-Heaters not the voltage applied on them. Just for clarification of the idea the out current simulation is provided in figure 5. As shown in the figure with +5VDC power supply we cannot reach the power more than 45 [mW]. So, we need to supply a higher voltage for the circuit which is considered by jumpers to change the power supply of the output buffers. The following simulations will be provided by +10 VDC as supply voltage.

Summary of Output Buffer Design

Min. Supply Vol. [V]	Max. Supply Vol. [V]	Min. Input Vol. [V]	Max. Output Vol. [V]	Max. Power Dissipation [W]	Response Time Constant [ms]	Max. Noise [V/Hz$^{1/2}$]
2.7	36	0	5	3	1	45n

Table 3.6 – Summary of designed Output buffer (OPA4251)

The designed output buffer has been realized according to the figure 3.59, 3.60 as layout and 3D view.

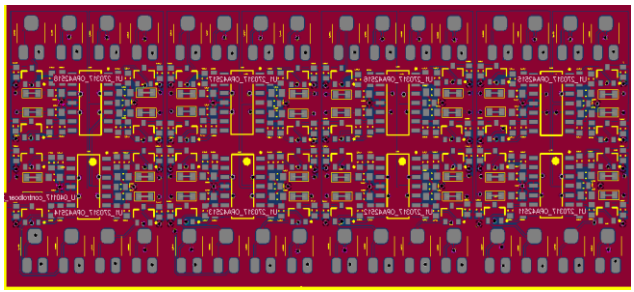

Figure 3.59 – Lay out of Output Buffer

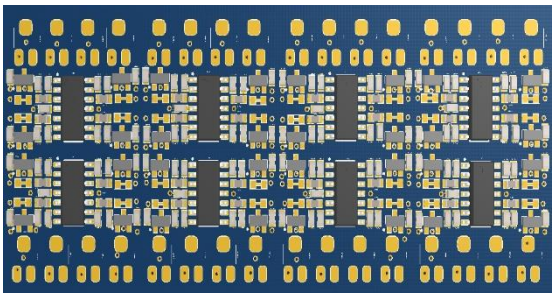

Figure 3.60 – 3D View of Designed Output

High Current Output Buffer (OPA567)

Overview

Since there is a need for high current output buffer for controlling laser and the SOA components of the silicon chips a high current output buffer is designed to realize our goals. The main component of this buffer is OPA567. Here we will briefly study the characteristics of designed buffer and simulation results.

OPA567

The top view of OPA567 is according to Figure 3.61 and the main features of OPA567 are:

- HIGH OUTPUT CURRENT: 2A
- OUTPUT SWINGS TO: 150mV of Rails with IO = 2A
- THERMAL PROTECTION
- ADJUSTABLE CURRENT LIMIT
- TWO FLAGS: Current Limit and Temperature warning
- LOW SUPPLY VOLTAGE OPERATION: 2.7V to 5.5V
- SHUTDOWN FUNCTION WITH OUTPUT DISABLE

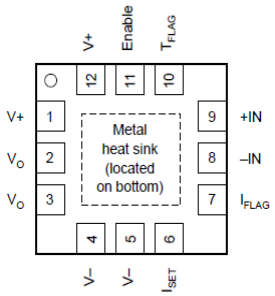

Figure 61– Pin Configuration of OPA567

Since there exists a high current sink from the output of the IC, therefore the proper layout and thermal protection is highly crucial. For thermal protection, the temperature flag is directly connected to the shutdown input of the IC. In the case of overloading or rising temperature of the IC over the allowed limit automatically output will be disabled.

OPA567 Design

The designed circuit schematics beside of the provided simulations for OPA567 by TINA Software in structure of the output buffer is reported as below. Considered input voltage in simulation is the output of DAC MAX5732 which is under the control of the microcontroller.

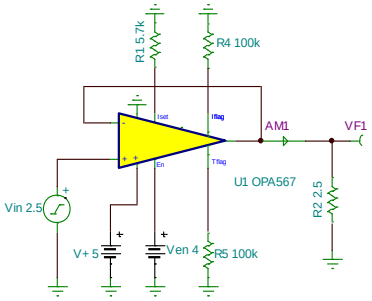

Figure 3.62 – Designed OPA567 High Current

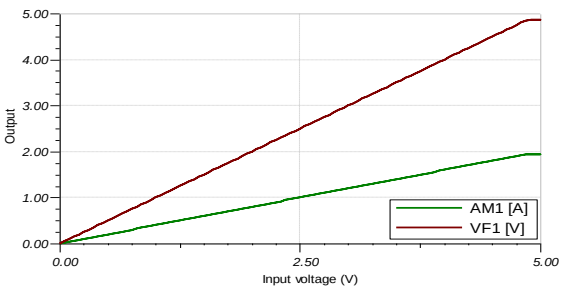

Figure 3.63 – DC Characteristics of OPA567

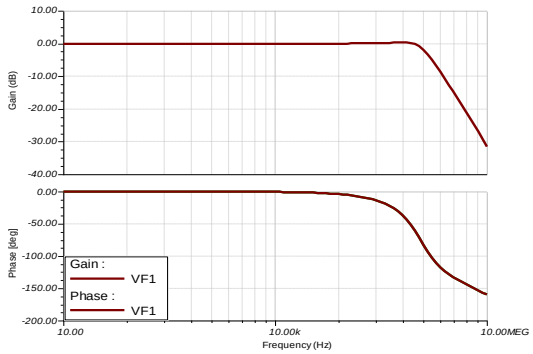

Figure 3.64 – AC Characteristics of OPA567

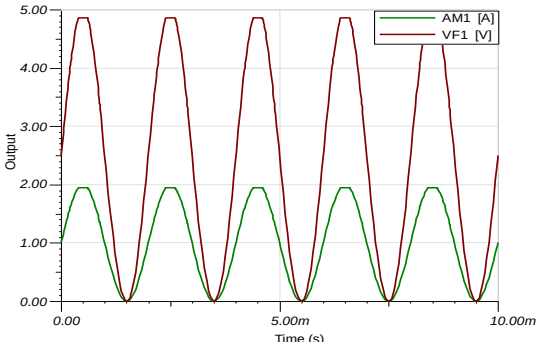

Figure 3.65 – OPA567 Response to Sinusoidal Wave (500Hz, Amplitude 5V)

Summary of OPA567 Design

Summary of the design characteristics is according to table 3.8.

Supply voltage range [V]	Output Voltage Range [V]	Output Max. Current [A]	Thermal Shutdown	Thermal Flag	Tunable Max. Output Current
2.7 – 5.5	0 - 5	2	✓	✓	✓

Table 3.7 - Main Characteristics of Designed High-Current Output Buffer (opa567)

The layout and 3D view of the designed OPA567 output buffer is according to Figure 3.66 and 3.67.

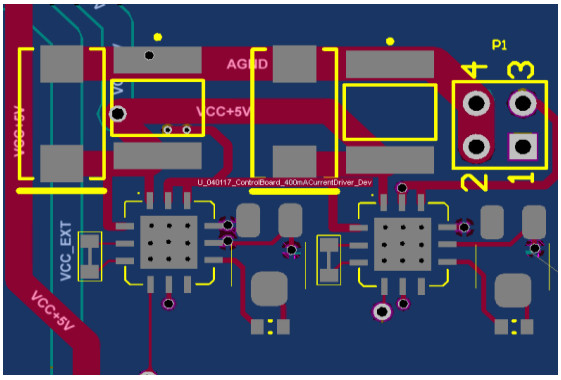

Figure 3.66 - OPA567 Layout

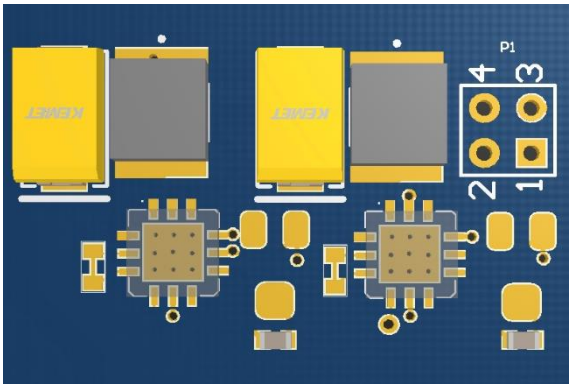

Figure 3.67 - OPA567 3D View

Now by completing the design of hardware, and by knowing he all features of it, we can start to design and evaluate our system in view of implementing a software which will run the data acquisition and control generation. Next section we will discuss about the control plant and implemented software for our hardware.

IV. Chapter 4: Software

Overview

Digital control offers distinct advantages over analog control that explain its popularity.

Here are some of its many advantages:

Accuracy: ability to represent analog signals in 12 bits or more 0s and 1s digital signals.

Implementation errors: The errors that result from digital representation and arithmetic are negligible

Flexibility: A digital controller is implemented in firmware or software and its modification is possible without a complete replacement of the original controller

Speed: high speed sampling and processing data is possible and it is increasing by developing and improvements in computer area.

Cost: very large-scale integration (VLSI) technology have made it possible to manufacture better, faster, and more reliable integrated circuits and to offer them to the consumer at a lower price. This has made the use of digital controllers more economical even for small, low-cost applications

Definition of hardware based on microcontroller leads us to have digital view in our control system. Since based on the designed hardware, the measurements are analog and converted to digital, also control commands are digital and are converted to analog. Obviously, the control system is a digital control system which is controlling an analog system. As an overview, we can describe our digital control system configuration according to the Figure 4.1.

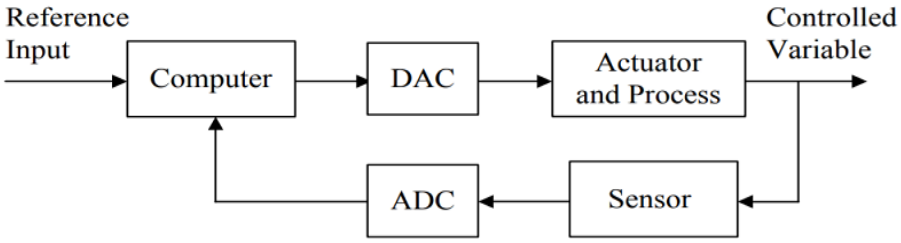

Figure 4.1- Configuration of a digital control system.

Next sections are allocated to the definition of the controlled system in view of the control theory and characterization and modeling of the relations of the inputs and outputs of the system. Then there will be a discussion about the most popular controllers as PI and PID and their simulations in MATLAB. Moreover, we will discuss about the approaches to define a set point for our control system which is called “initialization process” for our control system. By known set points for our system and by modelled system, implementation of the simulated controllers by hardware and realization of them will be discussed.

System Under control

To tune the ring resonators there is a fabricated thermal heater to dissipate power for shifting the resonance wave length of the ring resonators. Therefore, these micro heaters are playing the role of actuator in our control system. As a measurement device in our control system we have photodiodes which have a proportional generated current to the light power inside the ring resonators. As we know each ring resonator has a specific resonance wave length, and if we have a laser line exactly according to the resonance wave length of the ring resonator, we will a coupling of laser at the same wave length of the ring resonator. Thus, when there is coupling of light among the wave guide and the ring resonator which can be in transmitter or receiver side, we will have generated current in monitoring photodiodes which are in category of Ge photodiodes. These components are fabricated inside the silicon chip which is wire bounded to RF interface board and we have access to them by interface pins.

The other components like ADC and DAC we will have some assumptions in modelling the system. List of the assumptions for ADC and DAC are reported as below.

ADC model assumptions

- ADC outputs are exactly equal in magnitude to their inputs (i.e., quantization Errors are negligible).
- The ADC yields a digital output instantaneously
- Sampling is perfectly uniform (i.e., occurs at a fixed rate)

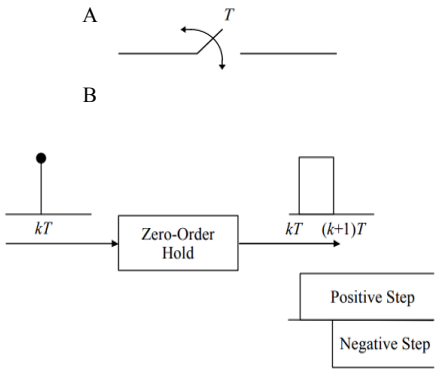

Figure 4.2 - (A) Ideal sampler model of an ADC (B) Model of a DAC as a zero-order hold

Then the ADC can be modeled as an ideal sampler with sampling period T as shown in Figure 4.2. Clearly, the preceding assumptions are idealizations that can only be approximately true in practice. Quantization errors are typically small but nonzero; variations in sampling rate occur but are negligible, and physical ADCs have a finite conversion time. Nevertheless, the ideal sampler model is acceptable for most engineering applications.

DAC model assumptions

- DAC outputs are exactly equal in magnitude to their inputs
- The DAC yields an analog output instantaneously
- DAC outputs are constant over each sampling period

Then the input-output relation of the DAC is given by

$$\{U(k)\} \xrightarrow{ZOH} U(t), kT \leq t \leq (K+1)T, \qquad K = 0,1,2,\ldots$$

Where $\{U(k)\}$ is the input sequence. This equation describes a zero-order hold (ZOH), shown in figure 2(B). In practice, the DAC requires a short but nonzero interval to yield an output; its output is not exactly equal in magnitude to its input and may vary slightly over a sampling period. But the model of Figure 2(A) is sufficiently accurate for most engineering applications.

The zero-order hold is the most commonly used DAC model and is adopted in most digital control texts. Analyses involving other hold
Circuits are similar.

Zero-order hold (ZOH) Transfer Function

By using the Laplace transform of a unit step and the time delay theorem for Laplace transforms we have:

$$L\{1(t)\} = \frac{1}{s}$$

$$L\{1(t-T)\} = \frac{e^{-sT}}{s}$$

Where 1(t) denotes the unit step. Therefore, the transfer function of the ZOH is:

$$G_{ZOH} = \frac{1 - e^{-sT}}{s}$$

By considering the frequency response of the ZOH we will have pattern shown in Figure 4.3.

In the frequency range of interest where the sinc function is positive, the angle of frequency response of the ZOH hold is seen to decrease linearly with frequency, whereas the magnitude is proportional to the sinc function. As shown in Figure 3.4, the magnitude is oscillatory with its peak magnitude equal to the sampling period and occurring at the zero frequency.

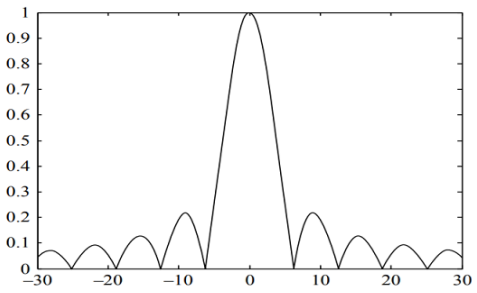

Figure 4.3 - Magnitude of the frequency response of the zero-order hold with T = 1 s.

DAC, analog subsystem, and ADC combination transfer function
The cascade of a DAC, analog subsystem, and ADC, shown in Figure 4, appears in our digital control system.

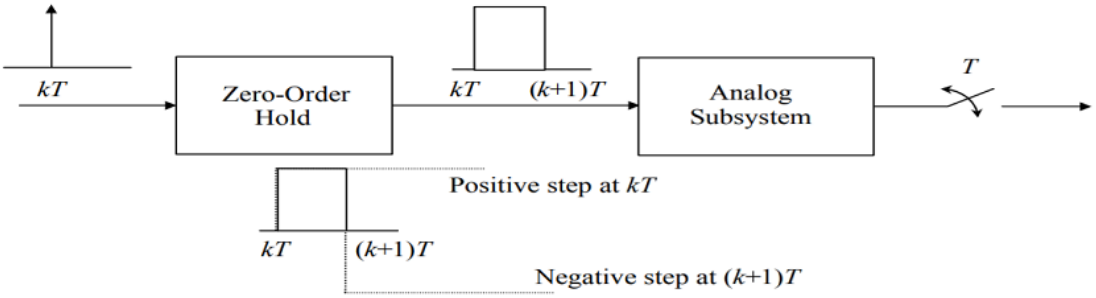

Figure 4.4- Cascade of DAC, analog subsystem, and ADC

Because both the input and the output of the cascade are sampled, it is possible to obtain its z-domain transfer function in terms of the transfer functions of the individual subsystems.
Using the DAC model, and assuming that the transfer function of the analog subsystem is G(s), the transfer function of the DAC and analog subsystem cascade is

$$G_{ZA}(s) = G(s)G_{ZOH}(s) = (1 - e^{-sT})\frac{G(s)}{s}$$

The impulse response of a cascaded system which is combination of an ADC, DAC and an analog sub system is the analog system step response minus a second step response delayed by one sampling period. This response is shown in Figure 4.5 for a second-order underdamped analog subsystem. The analog response of this system is sampled to give the sampled impulse response

$$g_{ZA}(kT) = g_s(kT) - g_{s(kT-T)}$$

By z-transforming, we obtain the z-transfer function of the DAC (zero-order hold), analog subsystem, and ADC (ideal sampler) cascade according to the equation below. The impulse response of mentioned cascaded system is shown in the Figure 4.5.

$$G_{ZAS(z)} = (1 - z^{-1})L\left\{\frac{G(s)}{s}\right\}$$

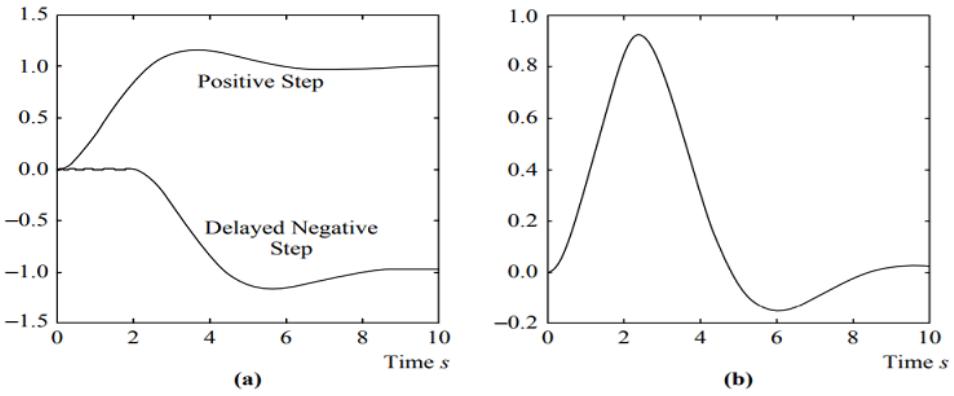

Figure 11- Impulse response of a DAC and analog subsystem. (a) Response of an analog system to Step inputs. (b) Response of an analog system to a unit pulse input.

The closed-loop transfer function

The block diagram shown in Figure 4.6 includes a comparator, a digital controller with transfer function C(z), and the ADC-analog subsystem DAC transfer function $G_{ZAS}(z)$. The controller and comparator are microcontroller programs. The block diagram is identical to those commonly encountered in s-domain analysis of analog systems, with the variable s replaced by z. Hence, the closed-loop transfer function for the system is given by

$$G_{cl}(z) = \frac{C(z)G_{ZAS}(z)}{1 + C(z)G_{ZAS}(z)}$$

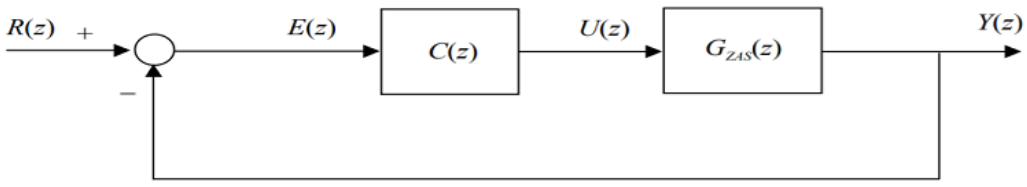

Figure 4.6 - Block diagram of a single-loop digital control system

Analog disturbances in a digital system

Disturbances are variables that are not included in the system model but affect its response. They can be deterministic, such as load torque in a position control system, or stochastic, such as sensor or actuator noise. However, almost all disturbances are analog and are inputs to the analog subsystem in a digital control loop. Since in our hardware we use TIA to convert the current of the photodiodes to voltage we have a noise in the acquired data. A block diagram view for a system in exposure of disturbance is shown in the Figure 4.7. The transfer function of such system will be defined as below.

$$Y(z) = \frac{(GG_dD)(z)}{1 + G_{zas}(z)C(z)}$$

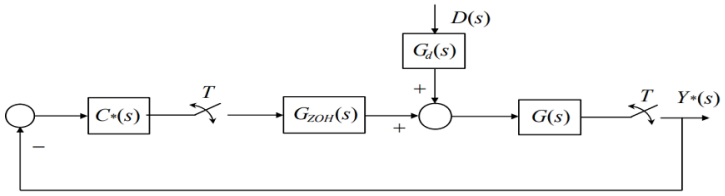

Figure 4.7 - Block diagram of a digital system with an analog disturbance

Analog sub system evaluation

Overview

As we described, our measurements are performed by fabricated photodiodes inside the silicon chip, and actuator is the micro heaters on top of ring resonator, Therefore, we need to evaluate the 3 main components and their characteristics which are ring resonators, micro heaters, monitoring photodiodes. In this section, static behavior of each components will be studied and their mathematical formulation will be provided as the measurements of monitoring photodiodes, micro heaters.

m) Ring resonator

The basic configuration, which consists of unidirectional coupling between a ring resonator with radius r and a waveguide, is described in Fig. 8, based on Yariv (2002a, b). Defining that a single unidirectional mode of the resonator is excited, the coupling is lossless, single polarization is considered, none of the waveguide segments and coupler elements couple waves of different polarization, the various kinds of losses occurring along the propagation of light in the ring resonator filter are incorporated in the attenuation constant, the interaction can be described by the matrix relation:

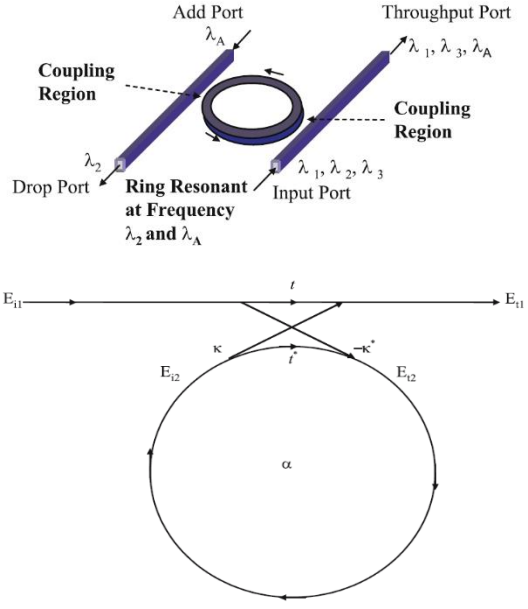

Figure 12 – (A) (B)

$$\begin{pmatrix} E_{t1} \\ E_{t2} \end{pmatrix} = \begin{pmatrix} t & k \\ -k^* & t^* \end{pmatrix} \begin{pmatrix} E_{i1} \\ E_{i2} \end{pmatrix}$$

Where E is complex mode amplitude, t and k coupler parameters, and * denotes the complex value of t and k.

$$|k^2| + |t^2| = 1$$

In order to further simplify the model, E_{i1} is chosen to be equal to 1. Then the round trip in the ring is given by

$$E_{i2} = \alpha \, . \, e^{j\theta} \, E_{t2}$$

where α is the loss coefficient of the ring (zero loss: $\alpha = 1$) and $\theta = \omega L/c$, L being the circumference of the ring which is given by $L = 2\pi r$, r being the radius of the ring measured from the center of the ring to the center of the waveguide, c the phase velocity of the ring mode ($c = c_0/n_{eff}$) and the fixed angular frequency $\omega = kc_0$, c_0 refers to the vacuum speed of light. The vacuum wavenumber k is related to the wavelength λ through: $k = 2\pi/\lambda$. Using the vacuum wavenumber, the effective refractive index n_{eff} can be introduced easily into the ring coupling relations by

$$\beta = k \,.\, n_{eff} = \frac{2\pi \,.\, n_{eff}}{\lambda}$$

From the equation above we can derive these relations as

$$E_{t1} = \frac{-\alpha + t.e^{-j\theta}}{-\alpha\, t^* + e^{-j\theta}},$$

$$E_{i2} = \frac{-\alpha\, k^*}{-\alpha\, t^* + e^{-j\theta}},$$

$$E_{t2} = \frac{-k^*}{1 - \alpha t^* e^{j\theta}}\ .$$

This leads to the transmission power *Pt*1 in the output waveguide, which is

$$P_{t1} = |E_{t1}|^2 = \frac{\alpha^2 + |t|^2 - 2\alpha|t|\cos(\theta + \varphi_t)}{1 + \alpha^2|t|^2 - 2\alpha|t|\cos(\theta + \varphi_t)}$$

Where t =$|t|$ exp(jφ_t), $|t|$ representing the coupling losses and φ_t the phase of the coupler. The circulating power P_{i2} ring is given by

$$P_{i2} = |E_{i2}|^2 = \frac{\alpha^2(1 - |t|^2)}{1 + \alpha^2|t|^2 - 2\alpha|t|\cos(\theta + \varphi_t)}$$

On resonance, $(\theta + \varphi_t) = 2\pi m$, where *m* is an integer, the following is obtained:

$$P_{t1} = |E_{t1}|^2 = \frac{(\alpha - |t|)^2}{(1 - \alpha|t|)^2}$$

and

$$P_{i2} = |E_{i2}|^2 = \frac{\alpha^2(1 - |t|^2)}{(1 - \alpha|t|)^2}$$

A special case happens when $\alpha = |t|$, when the internal losses are equal to the coupling losses. The transmitted power becomes 0. This is known in literature as critical coupling, which is due to destructive interference.

The next configuration which is discussed is the basic ring resonator add‑drop configuration, consisting of one input, one output waveguide and the ring resonator. The four ports of the ring resonator are referred to in the following as input port, throughput port, drop port and add port according to Figure 4.9 (A). The ring resonator simulation model has been updated according to Figure 9. For simplification E_{i1} is as defined before equal to 1. At resonance, the output power from the drop port is given by:

$$P_{t2_{Resonance}} = \frac{(1 - |t_1|^2)(1 - |t_2|^2).\alpha}{(1 - |t_1 t_2|^2)}$$

The throughput port mode amplitude E*t*1 will be zero at resonance for identical symmetrical couplers *t*1 = *t*2 if $\alpha = 1$, which indicates that the wavelength on resonance is fully extracted by the resonato

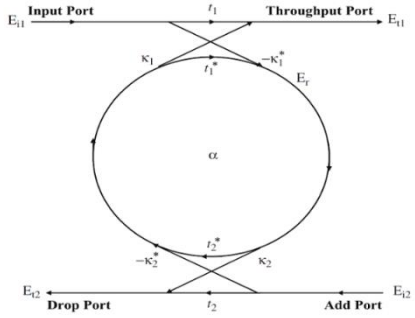

Figure 4.8 - Model of a basic add‑drop single ring resonator filter

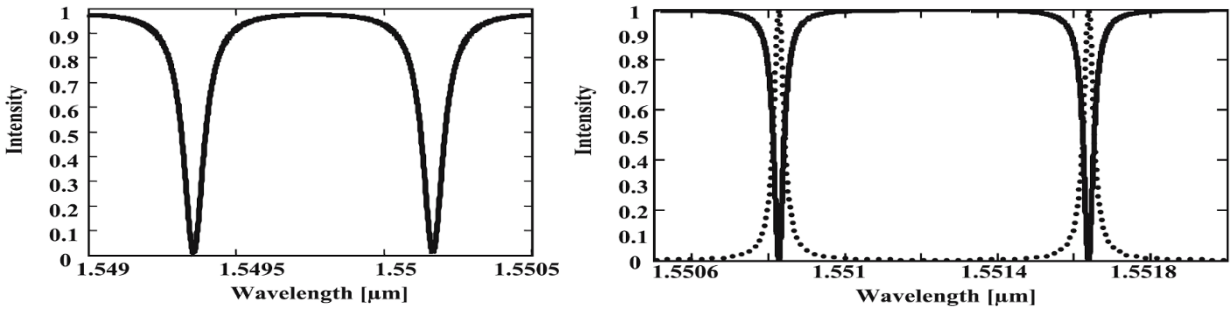

Figure 4.9 -(A) Notch type ring resonator filter characteristic (B) Add –drop ring resonator filter characteristic

The ring is regarded as an oscillator of energy amplitude $e(t)$, normalized so that $p(t)$ represents the total energy stored in the ring. Energy and power in the ring are related through

$$p(t) = |e(t)|^2 = P(t)\frac{2\pi r}{v_g}$$

Where vg is the group velocity. The ring resonator has a resonant frequency of ω_R and amplitude decay time-constant of $1/\tau$. The decay rate and the power exciting the ring resonator are related to each other. The decay rate includes the power coupled to the transmitted wave $1/\tau_{tr}$, the power lost due to intrinsic effects $1/\tau_{ie,}$ and power coupled to the output waveguide $1/\tau_{t2}$. This leads to

$$\frac{1}{\tau} = \frac{1}{\tau_{tr}} + \frac{1}{\tau_{ie}} + \frac{1}{\tau_{t2}}.$$

The time rate of change in ring energy can then be written as

$$\frac{d}{dt}e = \left(j\omega_R - \frac{1}{\tau}\right)e - k^*.E_{i1}$$

The relation between the coupling parameter k^* and the decay rates of the transmitted wave $1/\tau_{tr}$ and the output waveguide $1/\tau_{t2}$, is determined by power conservation.

n) Thermal effects on micro ring resonator based devices

Most optical devices exhibit some vulnerability to temperature changes. However, the high thermo-optic coefficient of silicon ($1.86 \cdot 10^{-4}$ K $^{-1}$) and the wavelength selectivity of microring resonators make them especially susceptible to fluctuations in temperature. The shift in the resonant wavelength of a microring with respect to temperature is given by

$$\frac{d\lambda}{dT} = \left(n_{eff}\,\alpha_{sub} + \frac{\partial n_{eff}}{\partial T}\right)\frac{\lambda_0}{n_g}$$

where λ_0 is the resonant wavelength, n_{eff} is the effective index, α_{sub} is the substrate expansion coefficient, and n_g *is* the group index. Because the optical mode is tightly confined in the silicon

core, and because the thermo-optic coefficient of SiO_2 (1×10^{-5} K^{-1}) is a magnitude lower than that of Si, the corresponding contribution is omitted from above equation. Additionally, because α_{sub} (2.6×10^{-6} K^{-1} for a Si substrate) is two orders of magnitude smaller than the thermo-optic coefficient for silicon, it can be omitted as well, leaving the commonly reduced expression,

$$\frac{d\lambda}{dT} = \frac{\partial n_{eff}}{\partial T}\frac{\lambda_0}{n_g}$$

The repercussions of resonance shift on microring functionality will be dependent on the quality factor (Q) of the resonance. However, for typical applications, deviations in temperature > 1 K will render the microring-based device inoperable. This susceptibility of microring based devices is not compatible with the temperature ranges typical of microelectronic environments. It should be clarified that it is not the absolute temperature that is hazardous for microring-functionality; rather, it is the relative changes in temperature during active operation of the optical link.

Resolutions to this problem can be classified into two categories: 1) solutions that reduce the thermal dependence of the microring resonator (denoted as "athermal" solutions), and 2) solutions that actively maintain the local temperature of the microring resonator (denoted as "control- based" solutions). In general, a significant advantage of athermal solutions is that they require no active power consumption to implement. The disadvantages of athermal solutions is their difficult fabrication, either though the incorporation of non-CMOS materials, or additional photonic structures. In contrast, the only additional structures that control-based systems typically require are integrated heaters and photodetectors, elements that are readily available in a typical silicon photonic platform. However, the main disadvantage of control-based systems is their active power consumption.

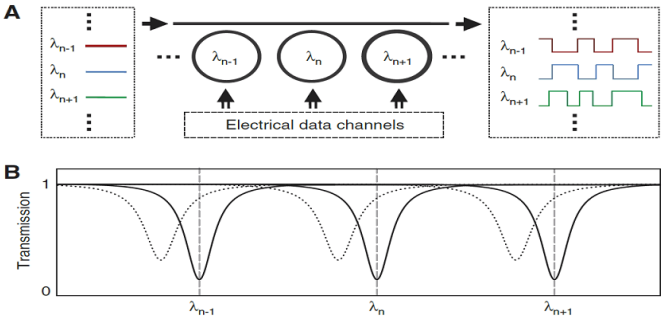

Figure 4.10 - (A) Microring modulators of varying radii can be cascaded along a waveguide bus to generate WDM optical modulation. (B) Transmission spectrum for densely spaced WDM microring modulators.

o) Micro heater effect on shift resonance

Heat power generated by the micro heaters is: $P = V^2/R$ where R is the resistance of the micro heater and V is the applied voltage. The temperature rise in the wave guide, due to heat, is: $\Delta T = \frac{P}{K}$, where K is the effective thermal conductance. Combining the above two expressions we have: $T = \frac{V^2}{KR}$. Also, from the thermos-optic effect, the resonance wave length shift is related to the temperature change as: $\Delta\lambda = A_T\Delta T$, where A_T is the effective thermos-optic resonance shift coefficient. So, we will have:

$$\Delta\lambda = A_T\frac{V^2}{KR}$$

This equation shows the quadratic variation of the resonance wavelength versus applied voltage. Also, by knowing the that the resonance shift of the resonator is $\Delta\omega = 2\,\frac{\sin\theta'}{\tau_c}$ which can be approximated as $\Delta\omega = 2\,\frac{\theta'}{\tau_c}$ where θ' is near zero or a multiple integer factor ofπ. By using the relation of $\frac{\Delta\omega}{\omega_0} = -\frac{\Delta\lambda}{\lambda}$ we can find the variation of the resonance wavelength as:

$$\Delta\lambda = 2\,\frac{\theta'}{\tau_c}\,\frac{\lambda_0}{\omega_0} = \frac{\theta'\,\lambda_0}{Q_c}$$

Where $Q_c = \frac{\omega_0\,\tau_c}{2}$ is the coupling quality factor between the resonator and the waveguide. Also, variation of θ' due to the change in the refractive index of the waveguide because of temperature change is obtained as $\theta' = \frac{2\pi L\Delta n_{eff}}{\lambda_0}$, in which L is the length of the heater on the waveguide. Because, most of the mode energy density is concentrated in the core of the silicon waveguide and the thermos-optic coefficient of silicon is much stronger than that of surrounding oxide then with a very good approximation we can say $\Delta n_{eff} = \alpha_T\,\Delta T$. As a result, we can have:

$$\Delta\lambda = \frac{2\pi\,\alpha_T\,\Delta T}{Q_c} = \frac{2\pi\,\alpha_T\,L}{Q_c}\,\frac{V^2}{KR}$$

Characterization of the micro heaters

As expected from the previous section the behavior of the ring resonator wave length shift versus applied power dissipation in the micro heaters are quadratic, which can be measured by sweeping the current or voltage (dependent to the source) and measuring the laser spectrum and we can see the shift in the wave length of the ring resonator is according to the Figure 4.11 for transmitter tuners and Figure 4.12 for receiver side. As we can see for tuning a full FSR in transmitter side we need approximately 55.5mW power dissipation and 43.6mW for receiver side.

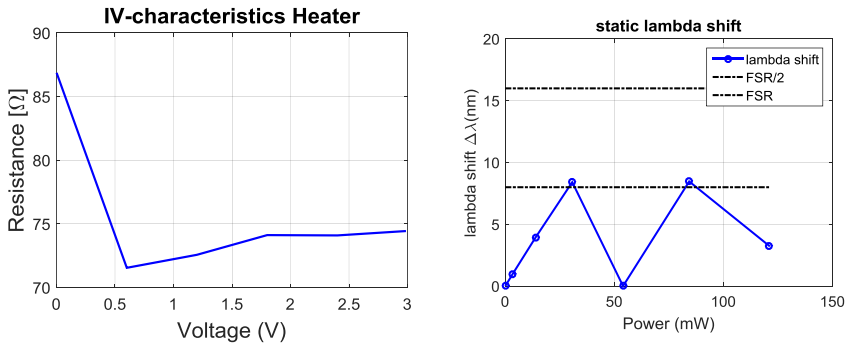

Figure 4.11- (A) current Voltage characterization of the micro heaters in Tx (B) Ring resonator wavelength shift versus dissipated power

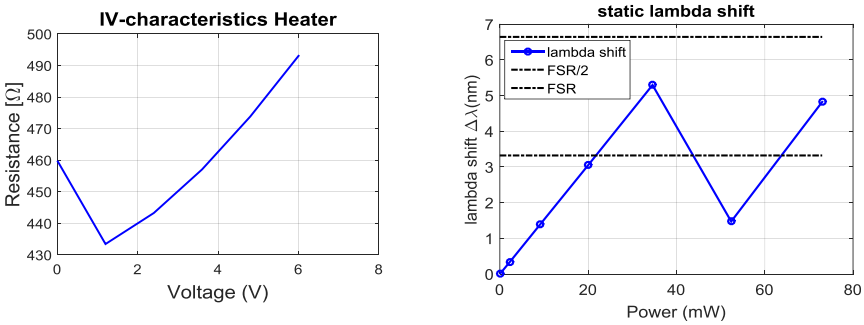

Figure 4.12- (A) current Voltage characterization of the micro heaters in Rx (B) Ring resonator wavelength shift versus dissipated power

Monitoring photodiodes (Ge PDs)

Output Impedances(Ohm)	Transmitter PDs	Receiver PDs
100	1.1184E-05	4.7379E-06
220	2.70579E-05	2.70579E-05
1k	3.657E-05	3.6893E-05
2k	3.55278E-05	3.56889E-05
10k	2.3188E-05	2.3188E-05
120k	3.72909E-06	3.72103E-06
200k	2.30997E-06	2.30675E-06
500k	9.55574E-07	9.55574E-07
1.1M	4.8456E-07	4.8294E-07

Table 4.1

The PDs used to monitor the ring resonators is kind of Ge photodiodes which their electromagnetic wavelength is in range of 400–1700 nm. Main features of a photodiode could be responsivity, dark current, and response time. Based on performed measurements dark current for monitoring photodiodes is according to the table 4.1 which shows the photodiode dark current versus different output impedances.

Based on the performed measurements on monitoring photodiode responsivity of these components are 0.3 A/W. Response time for the Ge photodiodes fabricated on silicon could be defined by equation $t_r = \sqrt{t_{drift}^2 + t_{driftused}^2 + t_{RC}^2}$. The response time can be approximated by equation $t_r = \frac{0.35}{f_{3db}}$. Generally, in photovoltaic mode of operation (no bias), rise time is dominated by the diffusion time for diffused areas less than 5 mm^2 and by RC time constant for larger diffused areas for all wavelengths. When operated in photoconductive mode (applied reverse bias), if the photodiode is fully depleted, such as high-speed series, the dominant factor is the drift time. In non-fully depleted photodiodes, however, all three factors contribute to the response time. Cut-off frequency of the monitoring photodiodes based on the design are 2 GHz so the response time of a Ge photodiode is calculated equal to 1.75×10^{-10} which in our case is very fast and negligible. Responsivity, dark current, and bandwidth of the monitoring photodiodes are shown in Figure 4.13. Since the structure of the all photodiodes in both transmitter and receiver side is identical we present just one of the characterizations for receiver side.

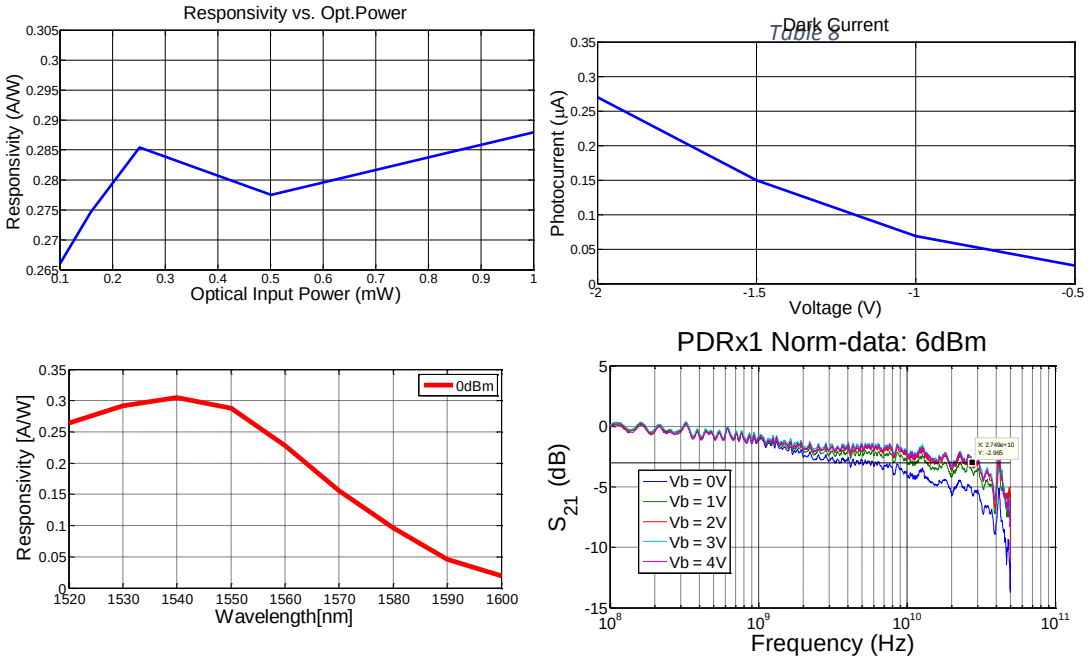

Figure 4.13– (A) Responsivity of photodiode to the optical power (B)Generated Dark Current for different Bias voltages (C) Responsivity of the PD in 9dBm (D) bandwidth of monitoring photodiodes with 2 GHz cut off frequency

As we see there is a lot of degrees of freedom to define a total transfer function for the cascaded system of DAC, analog subsystem and ADC. Therefore, it seems identification of the system under control is very rational to define the lag of system and relation of the input and out of the system. In order to apply identification methods, we will need data which a reasonable protocol should be defined for data acquisition to record the input and output data. Next section we will discuss about the method of data acquisition and modeling the system by identification methods. We will try to model system as SISO and MIMO system and the motivations will be provided.

Data Acquisition and Identification

Data Acquisition

Data acquisition of this system will be different from other usual devices or systems. Since at first, we need to initialize the system. Initialization of the system is performed by sweeping the current in the micro heaters for a full FSR for each ring resonator which initialization idea will be discussed later. However, Converted current from the photodiodes are dependent to the value of the gain in TIAs. This calibration will be very challenging in transmitter photodiodes. Because we have optical power losses in two main optical components which is directly affecting the value of the generated current. The optical components are grating couplers and crow filters which cause around 12 dBm losses of the light power. And, the difference of the resonance wavelength of the ring resonators and different responsivity to optical power by photodiodes causes a different current generation.

In receiver side, we have less power loss in optical components, however, the different power of the laser lines is impacting the output of the TIAs. Also, difference in power of the laser lines have the same effect on the transmitter side. Thus, data acquisition is dependent to calibration of the output of the TIAs to have almost the same behavior in all channels. Based on the design of the TIAs we will have mainly two situation which should be considered in data acquisition and data identification. These situations are the saturation of the TIA outputs because of the high or low amplification gain. According to the design we need to have decrease trend in the output of the TIA from the bias voltage in exposure of the optical power and it will be in minimum voltage which is around zero in maximum value of the optical power feasible in the system. As mentioned, we have different laser lines in MLL[3] laser and we should select a laser spectrum which has approximately same power level in laser lines. It is obvious a known laser spectrum is a reference for us to identify and lock on the laser lines to initialize and start the controlling the ring resonators.

Based on the defined protocol for data acquisition we measured the TIA outputs by transferring them by USB port of the microcontroller to the PC to be recorded for identification by MATLAB identification toolbox. Before data acquisition, it is crucial to initialize the system, which is offsetting the outputs of the DAC to put ring resonators in the resonance edge. Otherwise, we will have problem of dead zone in the relation of the output and input. Also, it can induce confusions and mistakes in different laser lines which should be consequent and indeed lower need of energy consumption in the micro heaters. Data acquisition will perform in a situation shown in the Figure 4.14 which the photodiodes are absorbing light inside the ring and there is current generation to be detected by TIAs. As mentioned, we will have wavelength shift to higher wave lengths so initialization should be performed such a way to be able to decrease and increase the microheaters current to see the output response. Obviously, since signal modulation is performed in left side of the ring resonators so we need to identify system in this region (Figure 4.14 – Modulation Area).

Data acquisition after the discussed procedure is performed like arbitrary inputs in range of 0.1mA and the output variation against input is gathered. Modeling the relation of the input and output is realized by MATLAB identification toolbox by state space estimation of the data for all 8 transmitter and receiver side of the system. All the transfer functions are estimated and

[3] Mode locked laser

fitted in high percentage (>99%) as a 5-order discreet system. the reason of identification of the system as discreet is using the DAC output as data acquisition in data rate of 23.7ksps per channel which will cause $4e^{-5}$ sampling time of the system.

The result of the identification of the system will be provided in appendix for each data set with the state space matrices but conversion of the state space to transfer function model will be in table 4.2 and 4.3 by criteria of finial prediction error (FPE) and mean squared error (MSE). Since the acquired data have mean value, removing the mean value is very important to identify in higher accuracy. Another challenge for data acquisition is the output of TIAs which are susceptible to noise in higher frequency which filtering the acquired data before identification could contribute in higher accuracy of fitting.

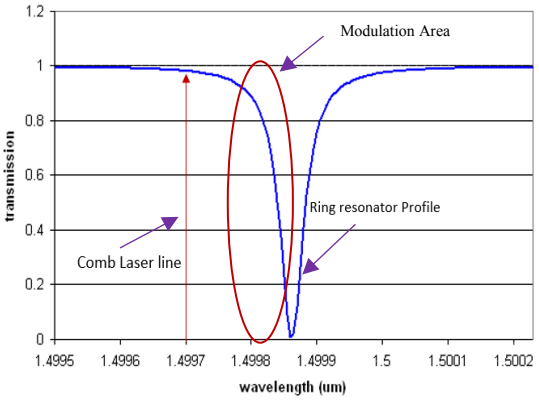

Figure 4.14 – Desired situation for the ring resonators and comb laser lines to start Data Acquisition

The identification method used in this modelling is Subspace algorithms for the identification of combined deterministic-stochastic systems. (N4SID) which is suitable for identifying mixed deterministic-stochastic systems. The N4SID algorithms are always convergent (non-iterative) and numerically stable since they only make use of QR and Singular Value Decompositions. By a very concise look at the Nyquist diagram and by considering the BIBO[4] system all the identified transfer functions are stable.

By introducing the identified model for each channel, the evaluation of the models by the step plot, bode diagram and Nyquist diagram will be provided for each channel in both transmitter and receiver side. As we know by increasing the current the response of the TIA against photodiode current tends to decrease and all the step plots show a decrement profile instead of usual step responses. By achieving the transfer functions of each channel, we can provide a simulation for tuning a PID controller and evaluating the response of system against probable disturbances which is affecting directly to wavelength of ring resonator. Next section will be about the design of PID controller and exposure of closed loop system against disturbances to study performance of the controller and output of the system.

Please note that first table is related to transfer functions of the transmitter side and second table is related to receiver side. In step plot, bode diagrams and Nyquist diagrams red labeled diagrams are for transmitter side and blue labeled diagrams are for receiver side.

[4] Bounded Input Bounded Output

Transmitter channels	Transfer Function	FPE	MSE	Fit %
Tx1	$\frac{0.0002346\ z^{-1} - 0.0009521\ z^{-2} + 0.001449\ z^{-3} - 0.0009797\ z^{-4} + 0.0002484\ z^{-5}}{1 - 4.95\ z^{-1} + 9.802\ z^{-2} - 9.708\ z^{-3} + 4.808\ z^{-4} - 0.9528\ z^{-5}}$	$5.26e^{-13}$	$5.25e^{-13}$	99.8
Tx2	$\frac{-0.006809\ z^{-1} + 0.0273\ z^{-2} - 0.04108\ z^{-3} + 0.02748\ z^{-4} - 0.006897\ z^{-5}}{1 - 4.944\ z^{-1} + 9.785\ z^{-2} - 9.689\ z^{-3} + 4.801\ z^{-4} - 0.952\ z^{-5}}$	$3.6e^{-13}$	$3.59e^{-13}$	99.9
Tx3	$\frac{0.00172\ z^{-1} - 0.006811\ z^{-2} + 0.01012\ z^{-3} - 0.006682\ z^{-4} + 0.001655\ z^{-5}}{1 - 4.902\ z^{-1} + 9.615\ z^{-2} - 9.43\ z^{-3} + 4.626\ z^{-4} - 0.9077\ z^{-5}}$	$1.06e^{-13}$	$1.06e^{-13}$	99.9
Tx4	$\frac{-0.003232\ z^{-1} + 0.01278\ z^{-2} - 0.01896\ z\text{-}3 + 0.0125\ z^{-4} - 0.003092\ z^{-5}}{1 - 4.899\ z^{-1} + 9.599\ z^{-2} - 9.406\ z^{-3} + 4.609\ z^{-4} - 0.9033\ z^{-5}}$	$1.06e^{-11}$	$1.06e^{-11}$	99.7
Tx5	$\frac{-0.0002117\ z^{-1} + 0.0008492\ z^{-2} - 0.001278\ z^{-3} + 0.0008551\ z^{-4} - 0.0002146\ z^{-5}}{1 - 4.896\ z^{-1} + 9.591\ z^{-2} - 9.395\ z^{-3} + 4.602\ z^{-4} - 0.9016\ z^{-5}}$	$5.15e^{-14}$	$5.15e^{-14}$	100
Tx6	$\frac{-0.0002505\ z^{-1} + 0.0009817\ z^{-2} - 0.001443\ z^{-3} + 0.0009432\ z^{-4} - 0.0002312\ z^{-5}}{1 - 4.969\ z^{-1} + 9.881\ z^{-2} - 9.825\ z^{-3} + 4.886\ z^{-4} - 0.9723\ z^{-5}}$	$6.18e^{-11}$	$6.17e^{-11}$	99.7
Tx7	$\frac{-0.001668\ z^{-1} + 0.006619\ z^{-2} - 0.009853\ z^{-3} + 0.00652\ z^{-4} - 0.001618\ z^{-5}}{1 - 4.971\ z^{-1} + 9.888\ z^{-2} - 9.836\ z^{-3} + 4.893\ z^{-4} - 0.9741\ z^{-5}}$	$3.06e^{-11}$	$3.05e^{-11}$	99.7
Tx8	$\frac{-0.0008246\ z^{-1} + 0.003277\ z^{-2} - 0.004884\ z^{-3} + 0.003237\ z^{-4} - 0.0008046\ z^{-5}}{1 - 4.963\ z^{-1} + 9.857\ z^{-2} - 9.79\ z^{-3} + 4.863\ z^{-4} - 0.9664\ z^{-5}}$	$1.17e^{-13}$	$1.18e^{-13}$	99.9

Table 4.2 – TX tuning control system transfer Functions

Receiver channels	Transfer Function	FPE	MSE	Fit %
Rx1	$\frac{-0.001288\,z^{-1} + 0.005115\,z^{-2} - 0.007617\,z^{-3} + 0.005043\,z^{-4} - 0.001253\,z^{-5}}{1 - 4.969\,z^{-1} + 9.878\,z^{-2} - 9.821\,z^{-3} + 4.884\,z^{-4} - 0.9717\,z^{-5}}$	$1.47e^{-12}$	$1.45e^{-12}$	99.9
Rx2	$\frac{0.0002557\,z^{-1} - 0.001037\,z^{-2} + 0.001575\,z^{-3} - 0.001064\,z^{-4} + 0.0002694\,z^{-5}}{1 - 4.95\,z^{-1} + 9.802\,z^{-2} - 9.708\,z^{-3} + 4.808\,z^{-4} - 0.9528\,z^{-5}}$	$3.52e^{-12}$	$3.52e^{-12}$	99.8
Rx3	$\frac{-0.0009294\,z^{-1} + 0.003657\,z^{-2} - 0.005396\,z^{-3} + 0.003539\,z^{-4} - 0.0008706\,z^{-5}}{1 - 4.961\,z^{-1} + 9.847\,z^{-2} - 9.775\,z^{-3} + 4.853\,z^{-4} - 0.9641\,z^{-5}}$	$9.23e^{-12}$	$9.22e^{-12}$	99.8
Rx4	$\frac{0.001268\,z^{-1} - 0.005065\,z^{-2} + 0.00759\,z^{-3} - 0.005056\,z^{-4} + 0.001263\,z^{-5}}{1 - 4.942\,z^{-1} + 9.772\,z^{-2} - 9.664\,z^{-3} + 4.78\,z^{-4} - 0.9459\,z^{-5}}$	$3e^{-12}$	$2.99e^{-12}$	99.8
Rx5	$\frac{-0.0028\,z^{-1} + 0.01113\,z^{-2} - 0.0166\,z^{-3} + 0.011\,z^{-4} - 0.002735\,z^{-5}}{1 - 4.917\,z^{-1} + 9.672\,z^{-2} - 9.513\,z^{-3} + 4.679\,z^{-4} - 0.9206\,z^{-5}}$	$5.09e^{-12}$	$5.09e^{-12}$	99.7
Rx6	$\frac{-0.0002625\,z^{-1} + 0.001047\,z^{-2} - 0.001567\,z^{-3} + 0.001042\,z^{-4} - 0.0002601\,z^{-5}}{1 - 4.896\,z^{-1} + 9.593\,z^{-2} - 9.401\,z^{-3} + 4.608\,z^{-4} - 0.904\,z^{-5}}$	$6.8e^{-15}$	$6.79e^{-15}$	100
Rx7	$\frac{-0.0002541\,z^{-1} + 0.0009958\,z^{-2} - 0.001464\,z^{-3} + 0.0009568\,z^{-4} - 0.0002346\,z^{-5}}{1 - 4.969\,z^{-1} + 9.881\,z^{-2} - 9.825\,z^{-3} + 4.886\,z^{-4} - 0.9723\,z^{-5}}$	$2.18e^{-11}$	$2.17e^{-11}$	99.97
Rx8	$\frac{-0.001355\,z^{-1} + 0.005367\,z^{-2} - 0.007971\,z^{-3} + 0.005262\,z^{-4} - 0.001303\,z^{-5}}{1 - 4.972\,z^{-1} + 9.892\,z^{-2} - 9.842\,z\text{-}3 + 4.898\,z^{-4} - 0.9751\,z^{-5}}$	$1.06e^{-12}$	$1.06e^{-12}$	99.98

Table 4.3 – RX tuning control system transfer Functions

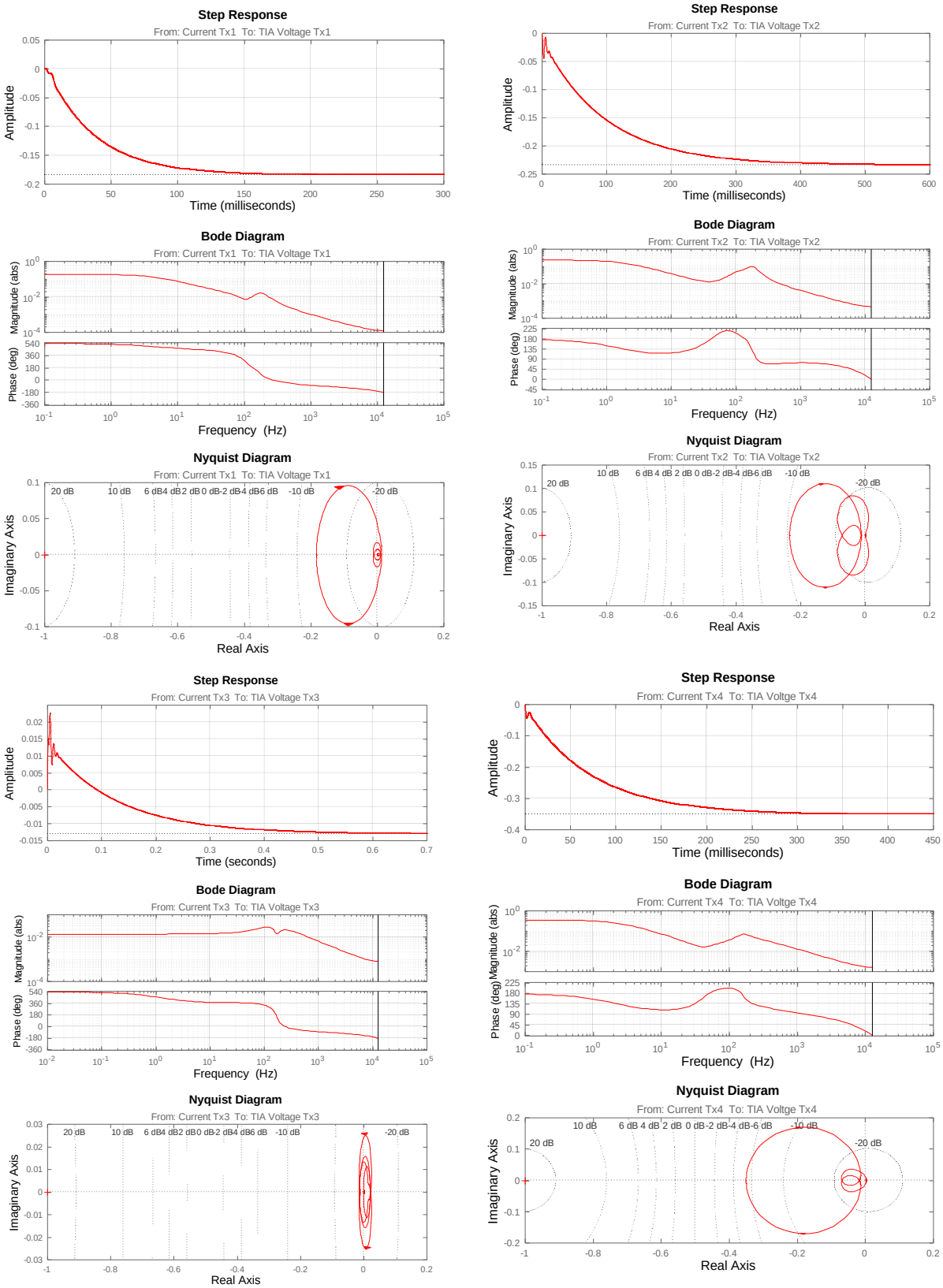

Figure 13- Step plot, Bode diagram and Nyquist diagrams of Tx1/Tx2/Tx3/Tx4

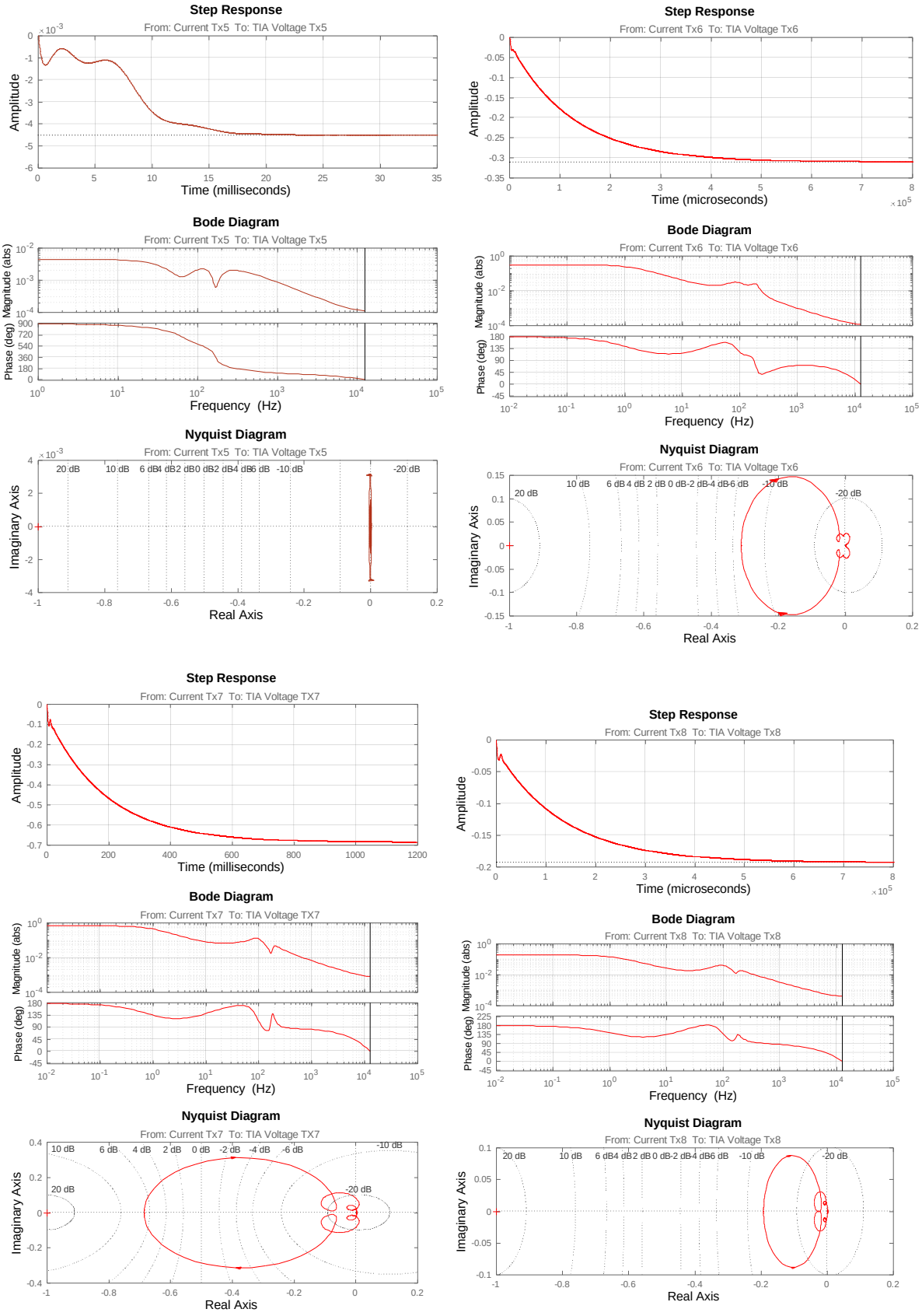

Figure 14 - Step plot, Bode diagram and Nyquist diagrams of Tx5/Tx6/Tx7/Tx8

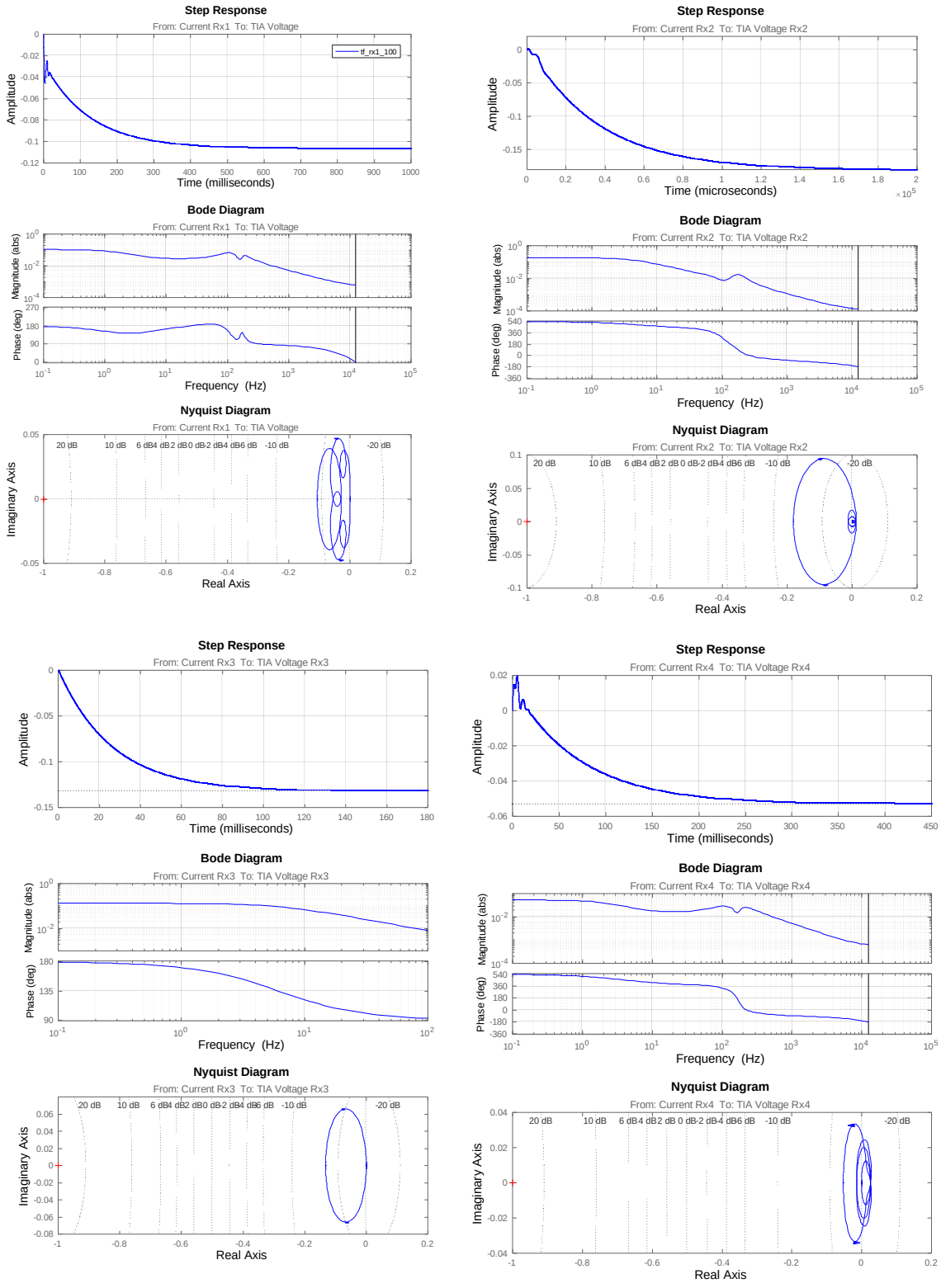

Figure 15 - Step plot, Bode diagram and Nyquist diagrams of Rx1/Rx2/Rx3/Rx4

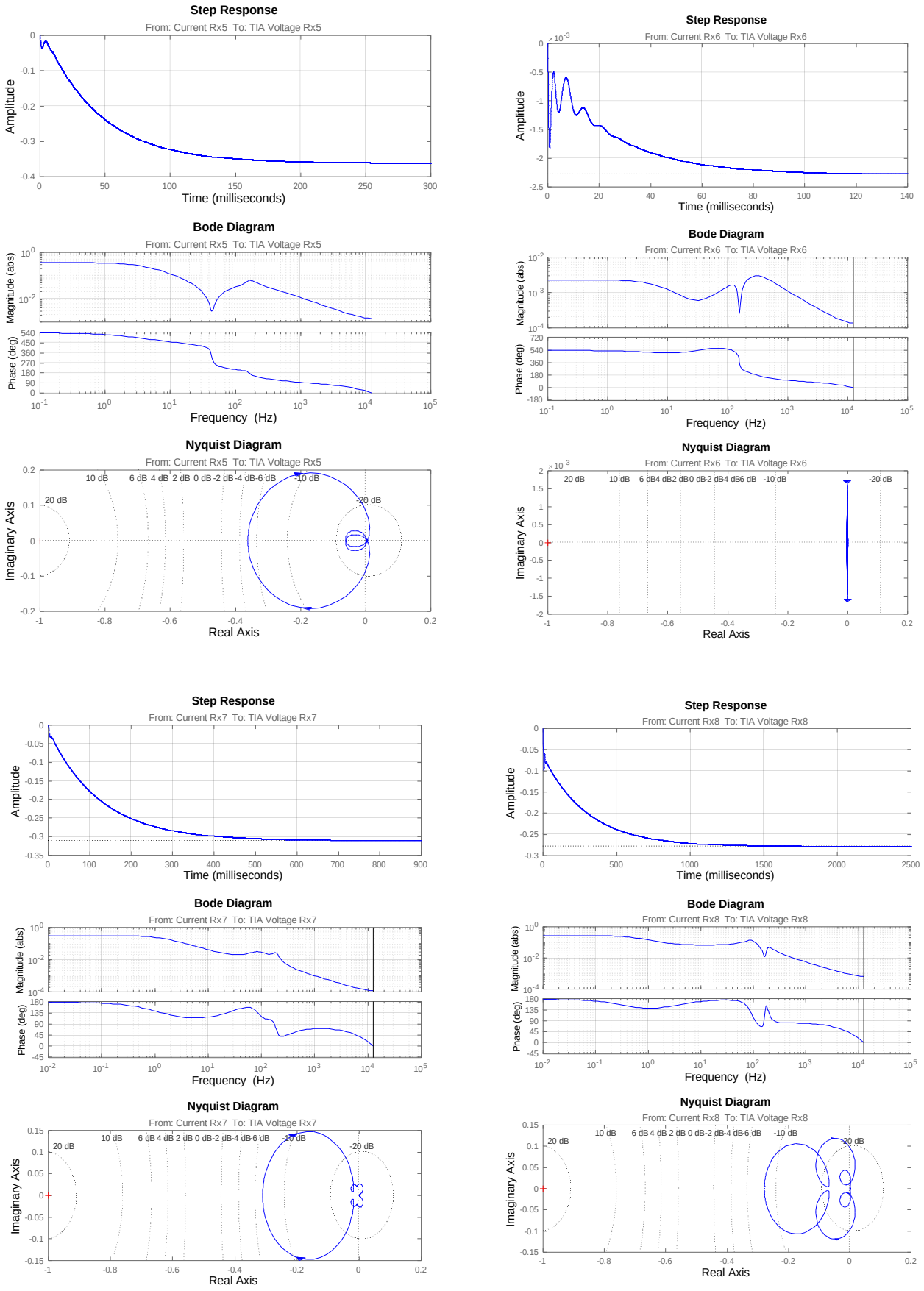

Figure 16 - Step plot, Bode diagram and Nyquist diagrams of Rx4/Rx5/Rx7/Rx8

PID Controller Simulation

In the design of the controller we should consider some challenges of the controller in some cases. First challenge is susceptibility of the output of the TIAs to noise. Therefore, we need to consider a noisy output of the system by considering a noisy output which is sampled by ADC. In 4 main methods, we can face this problem which can be categorized as 1) decreasing the gain of TIAs which cause losing the output range of the TIAs. 2) Averaging the channels of the ADCs which in selected component averaging is possible by setting the averaging value. 3) Averaging the data inside the microcontroller which is a reason of a lag in processing data by averaging loop during the control process. 4) Using two degree of freedom PID controller which is very suitable for noisy output systems. Thus, using a PIDF controller structure could help us to overcome this problem, so a noisy output which is added to output of the analog subsystems disturbance will be simulated.

Moreover, during the experiments we have lots of components which we need to turn on and off, for example, optical drivers or data generator etc. Thus, we need to evaluate the performance of the controller and system against a disturbance which are like impulse and cause deviation of the temperature stability in the analog subsystem. The variation of the ambient temperature is evaluated by a ramp disturbance in worst case which cause a full FSR wavelength shift in analog subsystem which in real is impossible to have such variation in experimental atmosphere. At most ambient temperature can affect 0.1 up to 0.3 of FSR in experimental labs which temperature is under control. Since there is tendency to adaptivity of the controller outside the lab atmosphere, this simulation is performed to observe the controller efficiency against these disturbances.

Furthermore, we aim to stabilize the ring resonator in a specific wave length which is the wavelength of the comb laser line. As mentioned before we have problems in stability of the lasers in photonics and these instabilities cause a disturbance for tuning the ring resonators in a wavelength. By initializing the ring resonators, we can set a reference value for each ring resonator which deviation from that reference point is a sign of wavelength shift to either right or left in wavelength axes. Another crucial point is to have a degree of freedom to cool down the ring resonator and according to the design we know we are not able to cool down it, so starting in reference point which is greater than zero is very important. For example, setting a reference point at 3mA as input for control reference is very suitable than 0mA since we can decrease and increase to cool down and heat up the ring resonator.

The simulation is performed in Simulink in 2 main configurations. First configuration is about the impulse disturbance plus noise as output of the analog subsystem which noise is a uniform noise with amplitude of 20mV and impulse disturbance is an impulse signal with amplitude of 1V and frequency of 2Hz suitable to on/off disturbance od the system which is added to uniform noise, and second configuration has the same noise added to a ramp signal which is saturated in 2V as continuous and finite disturbance of the system. The result of simulations for each channel of transmitter and receiver side are individually reported. Also saturation of the PID output value is considered since in reality we cannot apply more than maximum 12mA to each micro heater.

Please note that simulation is performed for a situation which we start from a zero state and the difference of the step response in identification and simulation is due to detrending the data for increasing the accuracy of the identification procedure. However, by inversion of the relation of the output and input to have monotonic and linear relation between the output and input, a negative unit gain is considered.

Simulation Configurations and Simulation results of PID controller of Transmitter side

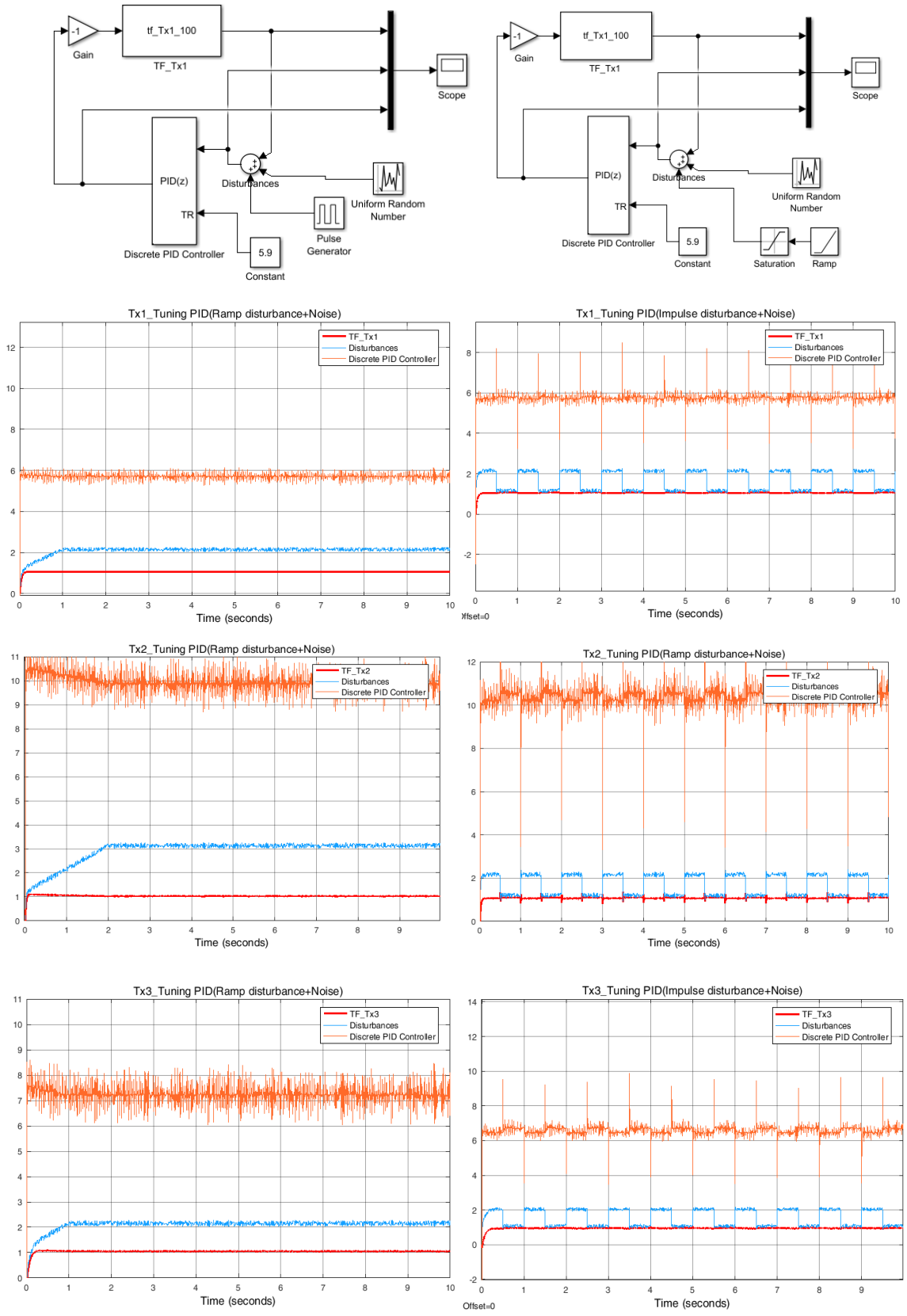

Figure 4.17 – Simulation configuration and results TX controller for Ramp + uniform Noise and Impulse + uniform Noise

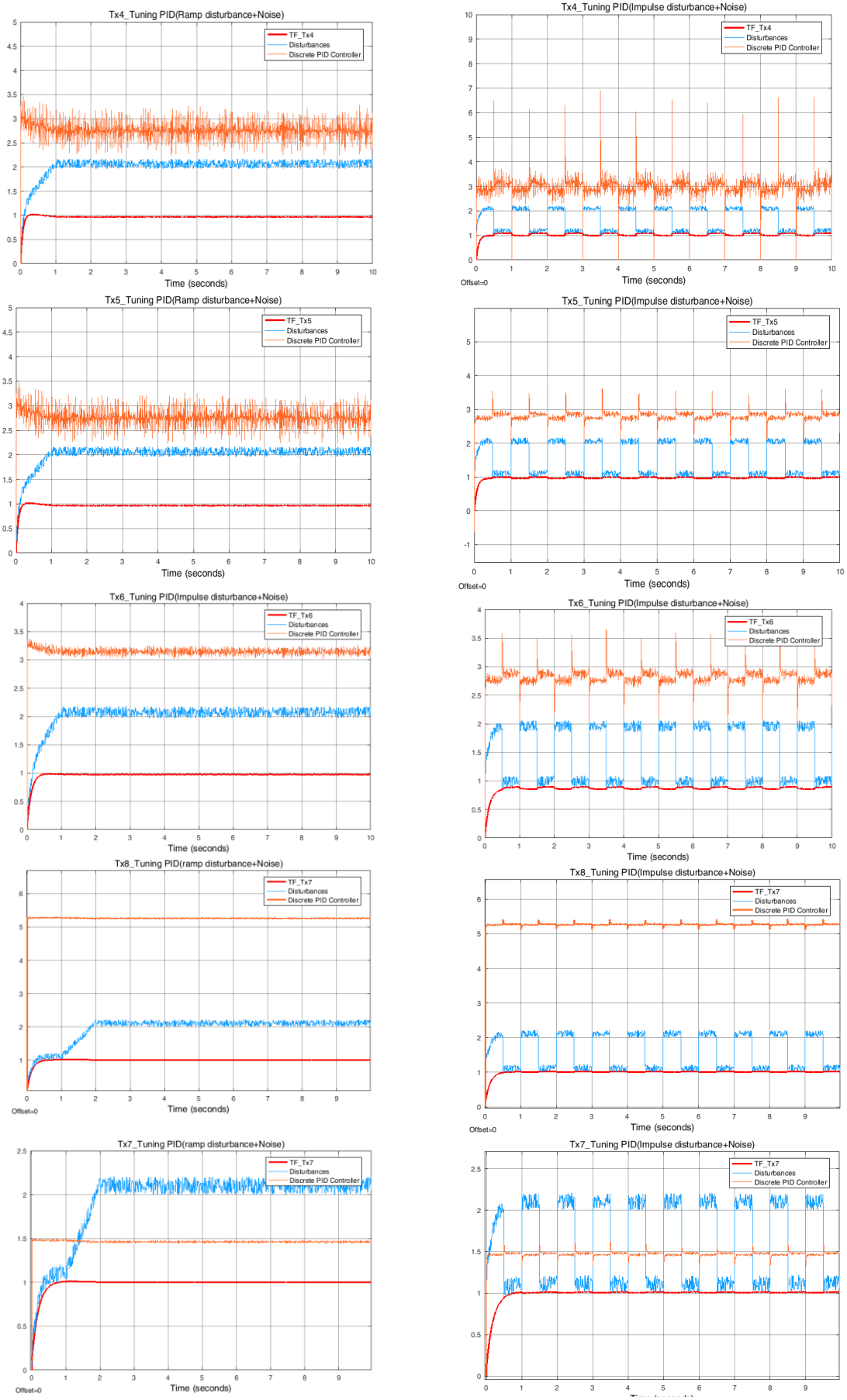

Figure 4.18– Simulation results of TX controller for Ramp + uniform Noise and Impulse + uniform Noise

Simulation of PID for receiver side

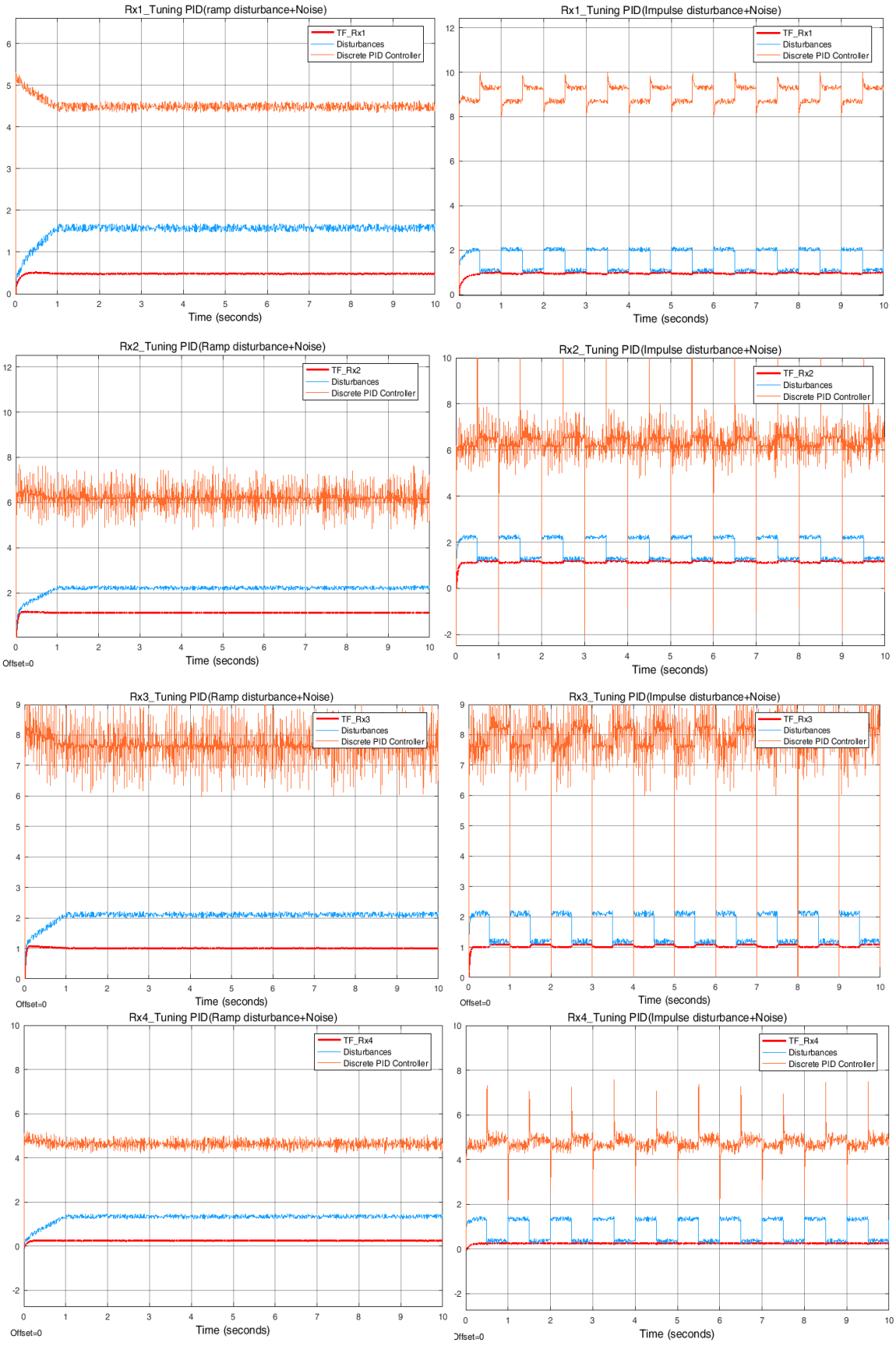

Figure 4.19 – Simulation results of Receiver tuning controller for Ramp + uniform Noise and Impulse + uniform Noise

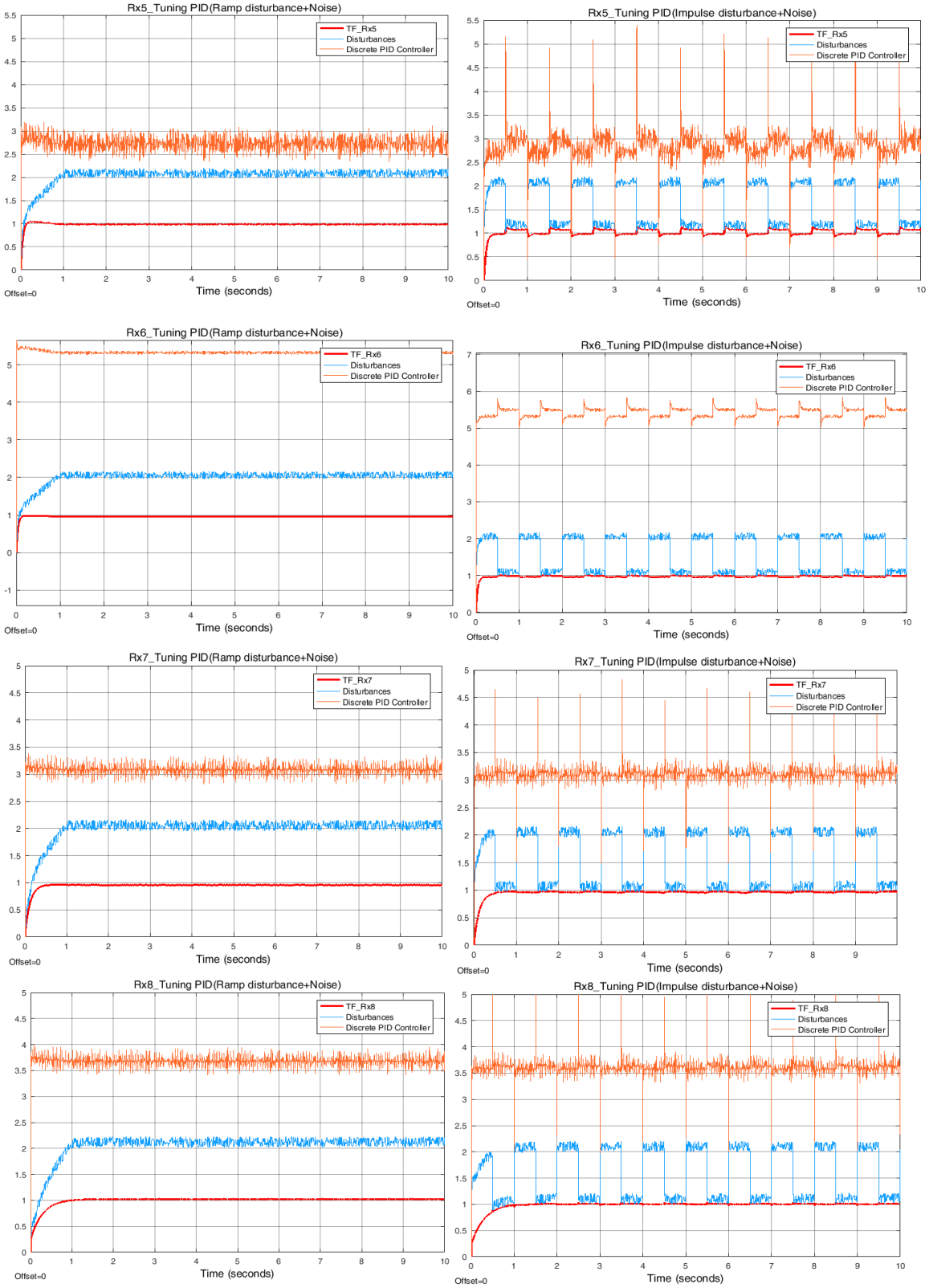

Figure 4.20 Simulation results of Receiver tuning controller for Ramp + uniform Noise and Impulse + uniform Noise

Approaches to control System

Initialization of controller

According to described analog subsystem, we would like to tune each ring resonator in the consequent lines of the comb laser. Therefore, a laser with known spectrum is a reference and known for us. As mentioned before, the laser is filtered before entering to transmitter side so we will have attenuation in the rejection band of the filter for the laser spectrum. This procedure is shown in the Figure 4.22 below which contains the laser spectrum before and after the crow filter.

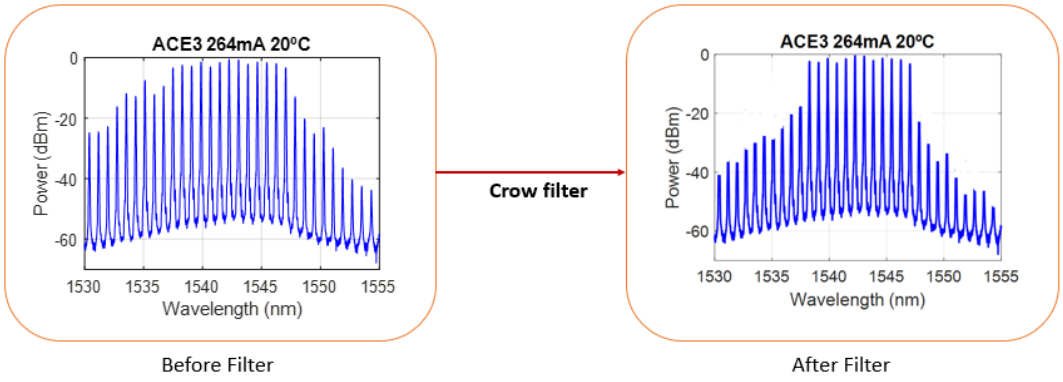

Figure 4.22 (A) Laser spectrum before crow filter (B) laser Spectrum after crow filter

Thus, by a known laser spectrum we know how many laser lines we have in the system and initialization can be based on this reference. As we know, by sweeping we can shift all the ring resonators full FSR. It means we can detect how many laser lines we have in passband of the filter. We know by passing the laser line at each wave length output of TIAs will saturate in zero and by shifting more the ring resonator TIA output voltage will increase to reach 2V. Therefore, according to the descending and ascending of the TIA in a full FSR our control system can detect and count the laser lines. The same procedure is operable for receiver side too.

By evaluation of the number of the laser lines to tune the ring resonators by sweeping current in all channels by the software implemented inside the microcontroller and saving the number of the saturations and the value of the applied current for each laser line, program enters to second phase to initialize each ring resonator. By this assumption which we do not have order in the wave length of the ring resonators, program starts from the first channel of transmitter to tune it in the nearest laser line. Since there is probability of tuning the other channels at the same wavelength we need to compare every time in tuning of the channels with previous channels to ensure we do not have any overlap in the rings resonance. It is very important to start tuning the channels first in transmitter side to have a local reference to set receiver channels according to them. Because we would like to modulate signal in the transmitter at a specific wavelength and we expect to receive it at the same wavelength too.

We can define a criterion for software to ensure that there is no overlap in the channels. This criterion is performed after tuning the first channel. Second channel starts to increase to find the point after first channel so if there is no overlap in channels there should not exist any change in the first channel TIA output. Because by overlapping the ring resonators we have double coupling of light inside the rings at that wave length, so for a constant amount of laser

power we will have half of optical power in ring resonators. Therefore, the first channel output voltage varies from the set point and increases from the previous point. It means we are at the same resonance so program should skip this point and should approach to the next or previous laser line beside the first channel. Procedure of comparison is performed by program and based on TIAs voltage up to tuning the 8 channels of the transmitter. Then according to the order of the tuned channels in transmitter side and by attention to the order of the channels in transmitter side, program arranges the ring resonators in receiver side based on laser lines.

The best point for initialization of the ring resonators is the midpoint of the TIAs' voltage to observe descending and ascending trend, otherwise the saturation of the TIAs in high or low level do not allow us to perform a good controlling on the rings. Saturation zones can deviate the whole system from the set point and initialization process will be needed to repeat. Another constrain which should be considered is to limit the output of the DAC in order not to apply more than 12mA in the case of saturation or initialization. Lower energy consumption for tuning the ring resonators is an additional goal which can be considered in initialization process. However, sometimes because of the arrangement of the rings, software needs to put channel ring in desired wave length by applying more currents. The expected outcome of the initialization process is presented in Figure 4.16.

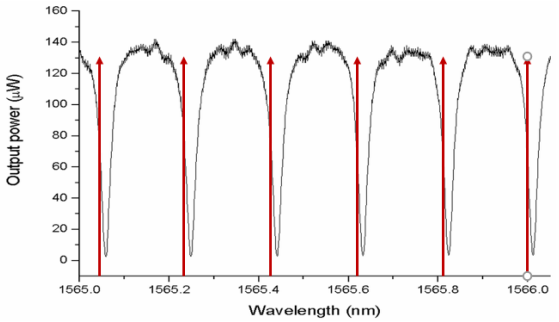

Figure 4.16– Expected initialization outcome for TX & RX

By initialization procedure, software is able to store the reference points to enter the control phase which is performed by PID controller. The flow of the program for initialization will be shown in Figure 4.17 to clarify this procedure.

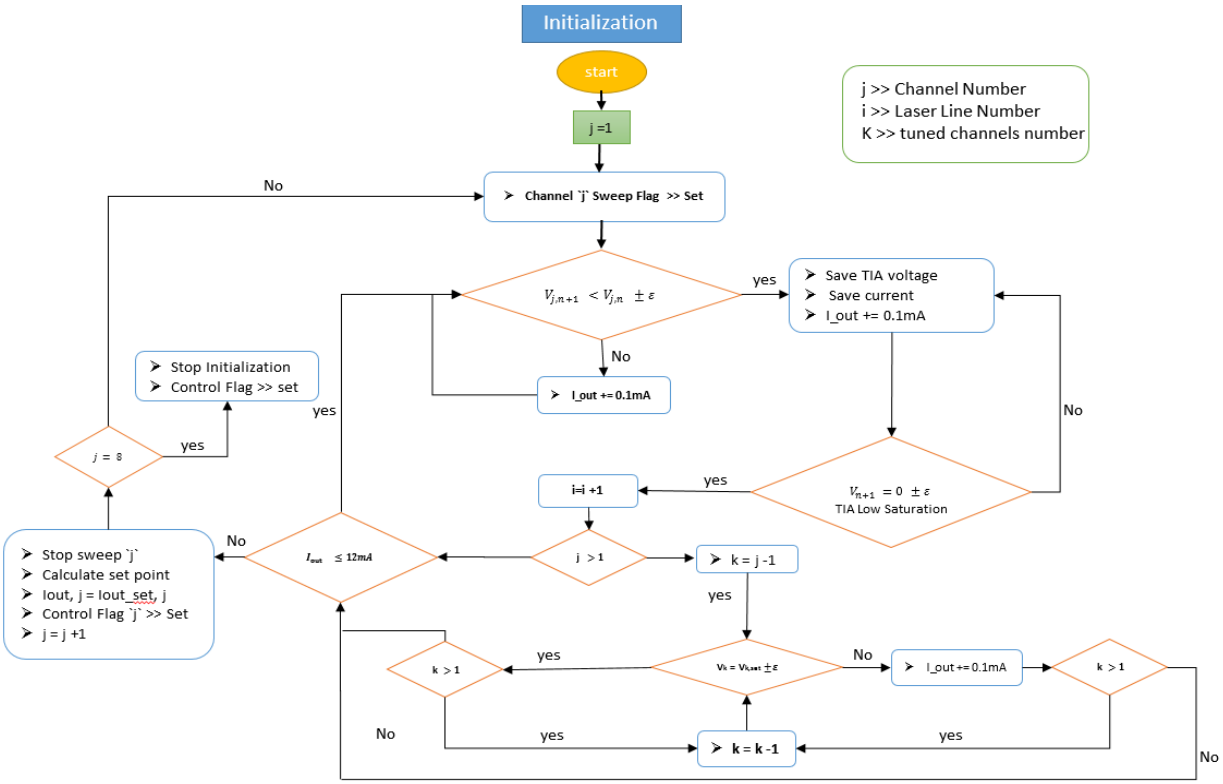

Figure 4.17– Initialization Program Structure

PID Controller

For the continuous-time PID, we start with the so-called parallel form

$$u(t) = k_p e(t) + k_i \int_0^t e(\tau)d\tau + k_d \frac{de(t)}{dt}$$

By exploiting Laplace transformation, we have:

$$C(s) = k_p + \frac{k_i}{s} + k_d s$$

For practical implementation, it is quite common to modify the derivative term to an LPF filter, to make it less noisy, so we will have:

$$C(s) = k_p + \frac{k_i}{s} + \frac{N k_d s}{1 + \frac{N}{s}}$$

A straightforward way to discretize this controller is to convert the integral and derivative terms to their discrete-time counterpart. There are commonly 3 variations to do so, by means of forward Euler, backward Euler, and trapezoidal methods. Below we give representation for each. Given a sampling period T_s, the integral term Ki/s can be represented in discrete-from by

Forward Euler: $\frac{K_i T_s}{z-1}$

Backward Euler: $\frac{K_i T_s z}{z-1}$

Trapezoidal: $\frac{K_i T_s}{2} \frac{z+1}{z-1}$

As we know, we are dealing with a digitized control system. Therefore, we need to define difference equation as control law inside the microcontroller. According to the identified model for the inputs and outputs, we know we have 5 order discreet system. Generally for a system with n-pole and m-zero we can have a transfer function as:

$$\frac{U(z)}{E(z)} = \frac{\beta_0 z^m + \beta_1 z^{m-1} + \cdots + \beta_{m-1} z + \beta_m}{\alpha_0 z^n + \alpha_1 z^{n-1} + \cdots + \alpha_{n-1} z + \alpha_n}$$

Based on this transfer function we can define the control law by applying shifting property of Z-transform term by term which is implementable inside the microcontroller is according to:

$$u(k) = b_0 e(k-n+m) + b_1 e(k-n+m+1) + \ldots + b_{m-1} e(k-n+1) + b_m e(k-n) - a_1 u(k-1) - \ldots - a_{n-1} u(k-2) - a_n u(k-n)$$

Therefore, as 5 order discreet system we will have a control law according to the equation below:

$$u(k) = b_0 e(k) + b_1 e(k-1) + b_2 e(k-2) + b_3 e(k-3) + b_4 e(k-4) - a_1 u(k-4) - a_2 u(k-3) - a_3 u(k-2) - a_4 u(k-5) - a_5 u(k)$$

In order for feasibility of implementation of the PID controller in the microcontroller we need to take advantage of model order reduction in our identified model. Aim is to achieve a structure of second order transfer function of the system without violation of the main features of the system which can affect the controller performance [1]. Thus, at first we need to reduce the order of the transfer functions to second order and then try to optimize our PID controller for this structure. In order to implement on a microcontroller, a discrete-time controller in the Z-domain must be transformed to its difference equation from as explained before. Only now the process becomes more involved because the sampling time is embedded in the gains. Also, our controller now has the filter in its derivative term. It is straightforward for the reader to verify that the discrete-time PID controller can be manipulated into the form:

$$C(z) = \frac{U(z)}{E(z)} = \frac{b_0 + b_1 z^{-1} + b_2 z^{-2}}{a_0 + a_1 z^{-1} + a_2 z^{-2}}$$

Where U (z) and E (z) are controller output and input, respectively, and the coefficients are described by

$$b_0 = k_p(1 + NT_s) + k_i T_s(1 + NT_s) + k_d N$$

$$b_1 = -(k_p(2 + NT_s) + k_i T_s + 2k_d N)$$

$$b_2 = k_p + k_d N$$

$$a_0 = (1 + NT_s)$$

$$a_1 = -(2 + NT_s)$$

$$a_2 = 1$$

To yield the difference equation for controller output

$$u(k) = -\frac{a_1}{a_0}u(k-1) - \frac{a_2}{a_0}u(k-2) + \frac{b_0}{a_0}e(k) + \frac{b_1}{a_0}e(k-1) + \frac{b_2}{a_0}e(k-2)$$

For model order reducrion we used the MATLAB model order reducer application by method of balanced truncation. Now by having the description of the controller, the way of implementation and method for model order reduction we represent the step reponse,impulse response which a uniform distribution with 0.2V is added to the original model transfer functions and reduced order models. This simulation can be shown as Figure 4.18 and the results in Figure 4.20 and 4.21.

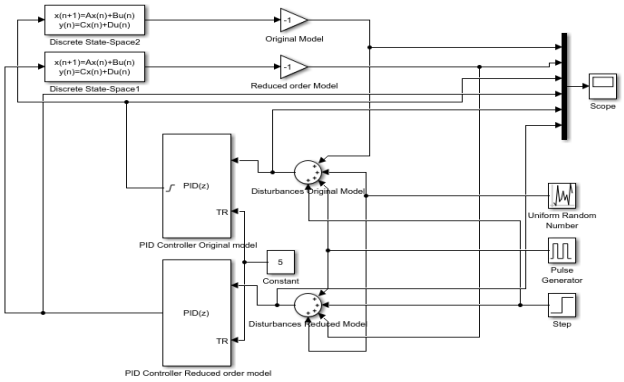

Figure 4.18– Simulation Configuration for Original and Reduced Order Models of TX & RX

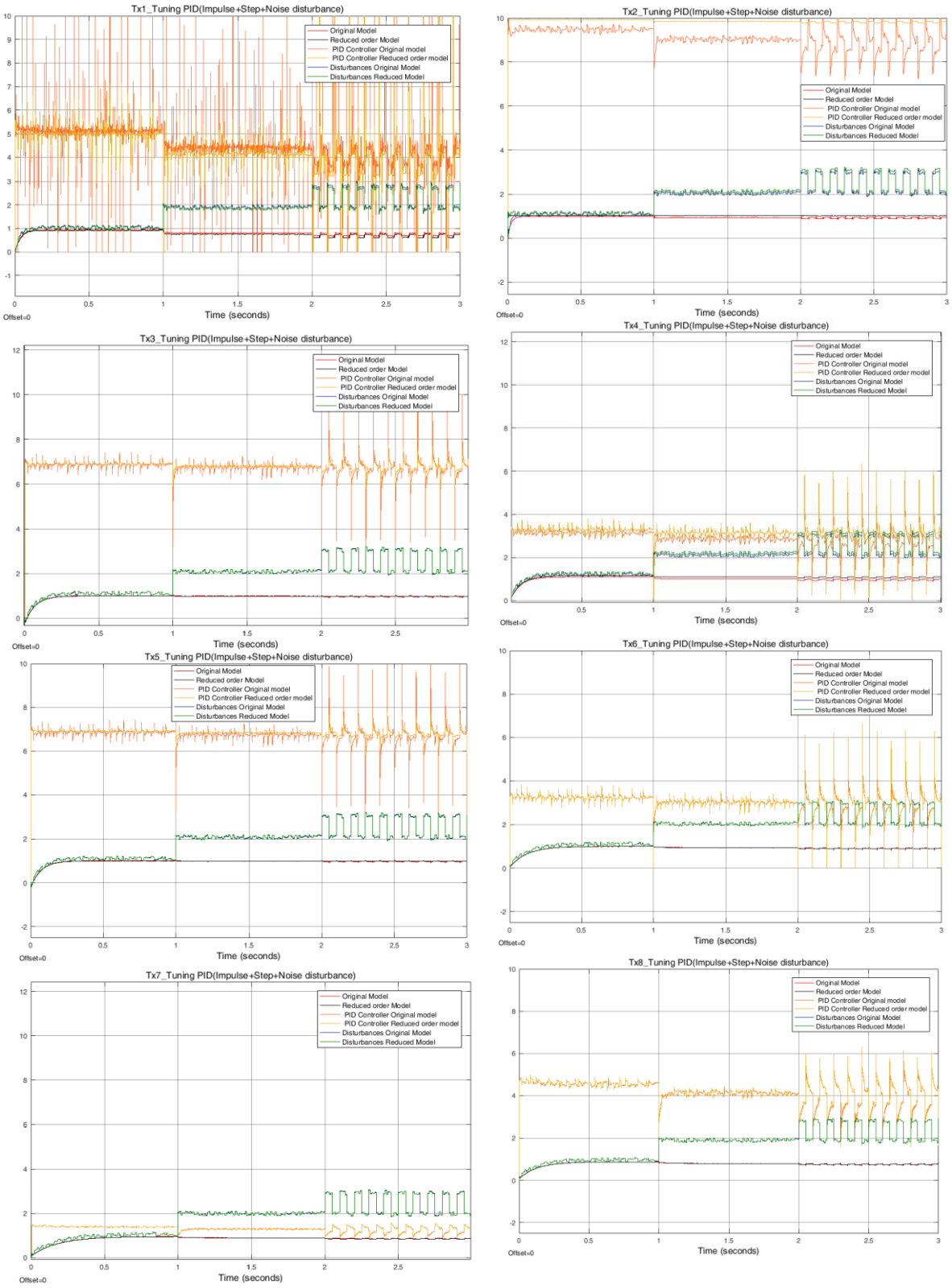

Figure 4.19 – Original and reduced order model response to Step / Impulse / Uniform Noise

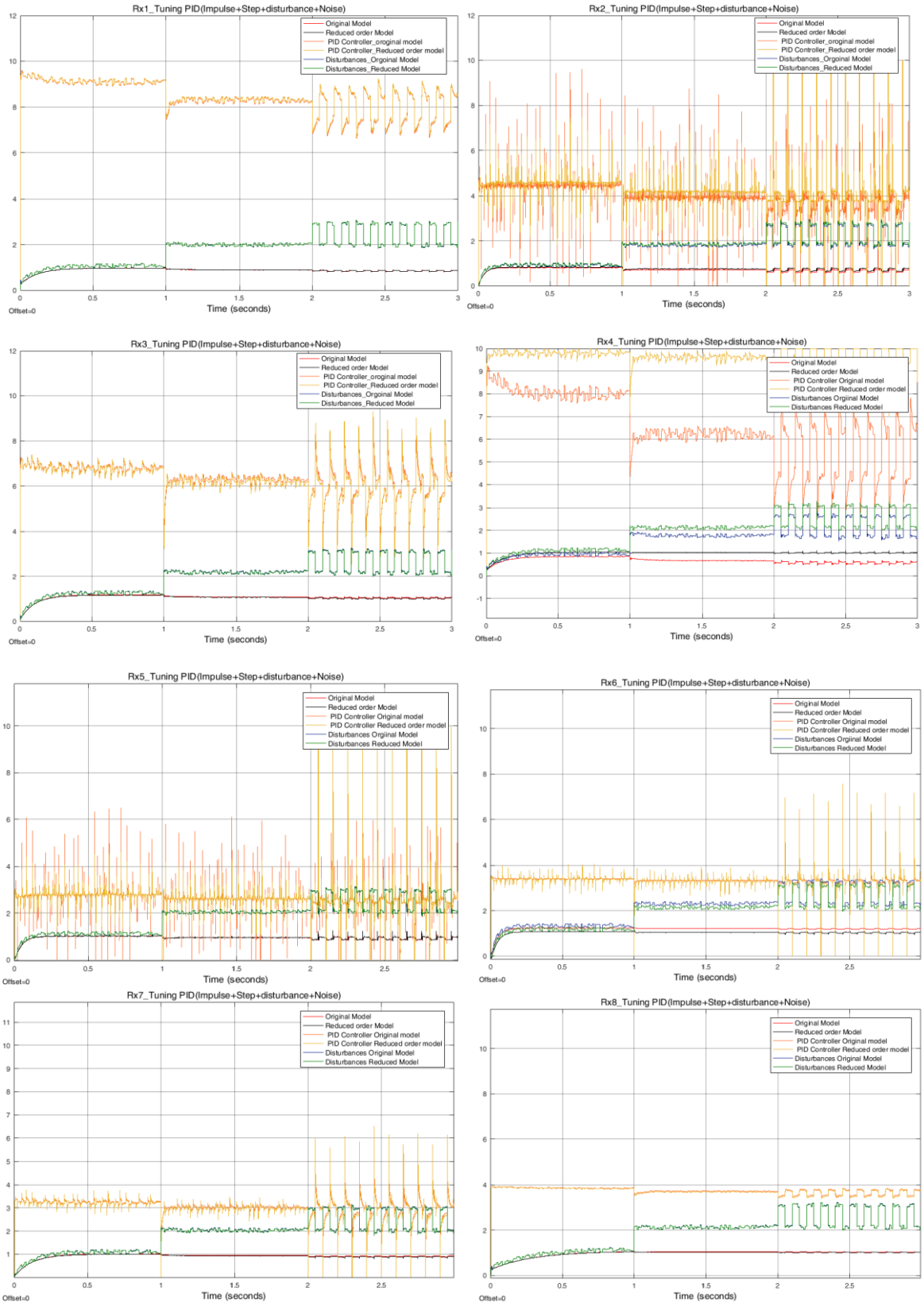

Figure 4.20- – Original and reduced order model response to Step / Impulse / Uniform Noise

Also, table of comparison of the PID values for original model and reduced order model is reported as below in table 4.4 and 4.55.

Tx1 – (A)Original Model (B)Reduced Order Model

Controller Parameters	A	Controller Parameters	B
	Tuned		Tuned
Kp	-7.4876	Kp	-9.0733
Ki	-363.8106	Ki	-274.4873
Kd	0.023815	Kd	0.078412
Tf	0.0036906	Tf	0.011609

Performance and Robustness	Tuned	Performance and Robustness	Tuned
Rise time	0.0259 seconds	Rise time	0.027 seconds
Settling time	0.106 seconds	Settling time	0.0693 seconds
Overshoot	6.87 %	Overshoot	3.8 %
Peak	1.07	Peak	1.04
Gain margin	19.7 dB @ 320 rad/s	Gain margin	30.5 dB @ 515 rad/s
Phase margin	65 deg @ 50 rad/s	Phase margin	65 deg @ 50.2 rad/s
Closed-loop stability	Stable	Closed-loop stability	Stable

Tx2 – (A)Original Model (B)Reduced Order Model

Controller Parameters	A	Controller Parameters	B
	Tuned		Tuned
Kp	-11.1431	Kp	-11.0816
Ki	-382.5637	Ki	-337.7525
Kd	0.12219	Kd	0.026266
Tf	0.010995	Tf	0.0030608

Performance and Robustness	Tuned	Performance and Robustness	Tuned
Rise time	0.0345 seconds	Rise time	0.0254 seconds
Settling time	0.138 seconds	Settling time	0.0462 seconds
Overshoot	0 %	Overshoot	0.0449 %
Peak	1	Peak	1
Gain margin	19.6 dB @ 1.12e+03 rad/s	Gain margin	21.7 dB @ 452 rad/s
Phase margin	76.6 deg @ 53 rad/s	Phase margin	75 deg @ 60.3 rad/s
Closed-loop stability	Stable	Closed-loop stability	Stable

Tx3 – (A)Original Model (B)Reduced Order Model

Controller Parameters	A	Controller Parameters	B
	Tuned		Tuned
Kp	-7.0084	Kp	-9.8407
Ki	-99.7133	Ki	-109.7409
Kd	0.10822	Kd	0.083383
Tf	0.016585	Tf	0.0084951

Performance and Robustness	Tuned	Performance and Robustness	Tuned
Rise time	0.068 seconds	Rise time	0.0518 seconds
Settling time	NaN seconds	Settling time	0.287 seconds
Overshoot	0 %	Overshoot	0 %
Peak	0.979	Peak	0.999
Gain margin	11.8 dB @ 66.8 rad/s	Gain margin	9.26 dB @ 86.5 rad/s
Phase margin	67 deg @ 16.6 rad/s	Phase margin	69.3 deg @ 21.6 rad/s
Closed-loop stability	Stable	Closed-loop stability	Stable

Tx4 – (A)Original Model (B)Reduced Order Model

Controller Parameters	A	Controller Parameters	B
	Tuned		Tuned
Kp	-15.5518	Kp	-16.1871
Ki	-362.1112	Ki	-395.6535
Kd	0.07523	Kd	0.035025
Tf	0.0048596	Tf	0.0021848

Performance and Robustness	Tuned	Performance and Robustness	Tuned
Rise time	0.0219 seconds	Rise time	0.0219 seconds
Settling time	0.09 seconds	Settling time	0.101 seconds
Overshoot	5.84 %	Overshoot	4.31 %
Peak	1.06	Peak	1.04
Gain margin	48.7 dB @ 8.94e+03 rad/s	Gain margin	47.9 dB @ 3.93e+04 rad/s
Phase margin	75 deg @ 76.3 rad/s	Phase margin	85.5 deg @ 84.7 rad/s
Closed-loop stability	Stable	Closed-loop stability	Stable

Tx5 – (A)Original Model (B)Reduced Order Model

Controller Parameters	A	Controller Parameters	B
	Tuned		Tuned
Kp	-271.7154	Kp	-286.7259
Ki	-22677.7961	Ki	-18945.4835
Kd	0.1071	Kd	0.10647
Tf	0.00057511	Tf	0.00056562

Performance and Robustness	Tuned	Performance and Robustness	Tuned
Rise time	0.0107 seconds	Rise time	0.0112 seconds
Settling time	0.0525 seconds	Settling time	0.0734 seconds
Overshoot	4.63 %	Overshoot	0 %
Peak	1.05	Peak	1
Gain margin	7.32 dB @ 328 rad/s	Gain margin	7.92 dB @ 351 rad/s
Phase margin	76 deg @ 172 rad/s	Phase margin	80 deg @ 175 rad/s
Closed-loop stability	Stable	Closed-loop stability	Stable

Tx6 – (A)Original Model (B)Reduced Order Model

Controller Parameters	A	Controller Parameters	B
	Tuned		Tuned
Kp	-11.6691	Kp	-16.5141
Ki	-163.6927	Ki	-221.4977
Kd	0.12014	Kd	0.08606
Tf	0.01117	Tf	0.0060204

Performance and Robustness	Tuned	Performance and Robustness	Tuned
Rise time	0.0495 seconds	Rise time	0.0422 seconds
Settling time	0.207 seconds	Settling time	0.174 seconds
Overshoot	5.02 %	Overshoot	3.55 %
Peak	1.05	Peak	1.04
Gain margin	35 dB @ 1.37e+03 rad/s	Gain margin	27.2 dB @ 7.85e+04 rad/s
Phase margin	76 deg @ 33.1 rad/s	Phase margin	87 deg @ 45.7 rad/s
Closed-loop stability	Stable	Closed-loop stability	Stable

Tx7 – (A)Original Model (B)Reduced Order Model

Controller Parameters	A	Controller Parameters	B
	Tuned		Tuned
Kp	-1.9634	Kp	-3.0989
Ki	-18.4002	Ki	-27.6451
Kd	0.036135	Kd	0.041421
Tf	0.019324	Tf	0.013389

Performance and Robustness	Tuned	Performance and Robustness	Tuned
Rise time	0.18 seconds	Rise time	0.133 seconds
Settling time	0.579 seconds	Settling time	0.458 seconds
Overshoot	3.83 %	Overshoot	3.62 %
Peak	1.04	Peak	1.04
Gain margin	82.4 dB @ 7.85e+04 rad/s	Gain margin	44.8 dB @ 3.21e+03 rad/s
Phase margin	78 deg @ 9.5 rad/s	Phase margin	83.4 deg @ 13.7 rad/s
Closed-loop stability	Stable	Closed-loop stability	Stable

Tx8 – (A)Original Model (B)Reduced Order Model

Controller Parameters	A	Controller Parameters	B
	Tuned		Tuned
Kp	-9.1486	Kp	-14.2545
Ki	-90.2252	Ki	-271.2237
Kd	0.11061	Kd	0.14194
Tf	0.012113	Tf	0.0099811

Performance and Robustness	Tuned	Performance and Robustness	Tuned
Rise time	0.13 seconds	Rise time	0.059 seconds
Settling time	0.197 seconds	Settling time	0.257 seconds
Overshoot	1.09 %	Overshoot	7.89 %
Peak	1.01	Peak	1.08
Gain margin	59.5 dB @ 4.12e+03 rad/s	Gain margin	44.3 dB @ 5.74e+03 rad/s
Phase margin	85.6 deg @ 15.2 rad/s	Phase margin	77.7 deg @ 27.5 rad/s
Closed-loop stability	Stable	Closed-loop stability	Stable

Table 4.4 – Controller Parameters and Performance Criteria for Original and Reduced Order Model of TX

Rx1 – (A)Original Model (B)Reduced Order Model

Controller Parameters	
A	Tuned
Kp	-21.9838
Ki	-1046.2045
Kd	0.4106
Tf	0.018715

Controller Parameters	
B	Tuned
Kp	-20.9899
Ki	-950.4675
Kd	0.41205
Tf	0.019669

Performance and Robustness	Tuned
Rise time	0.035 seconds
Settling time	0.182 seconds
Overshoot	6.59 %
Peak	1.07
Gain margin	37.4 dB @ 2.45e+03 rad/s
Phase margin	90.4 deg @ 53.5 rad/s
Closed-loop stability	Stable

Performance and Robustness	Tuned
Rise time	0.0356 seconds
Settling time	0.188 seconds
Overshoot	6.41 %
Peak	1.06
Gain margin	39.6 dB @ 6.33e+03 rad/s
Phase margin	86.9 deg @ 50.9 rad/s
Closed-loop stability	Stable

Rx2 – (A)Original Model (B)Reduced Order Model

Controller Parameters	
A	Tuned
Kp	-9.0006
Ki	-289.2458
Kd	0.028307
Tf	0.0036746

Controller Parameters	
B	Tuned
Kp	-8.894
Ki	-329.7826
Kd	0.011087
Tf	0.0019119

Performance and Robustness	Tuned
Rise time	0.0305 seconds
Settling time	0.0548 seconds
Overshoot	0.256 %
Peak	1
Gain margin	18.8 dB @ 329 rad/s
Phase margin	75 deg @ 50.2 rad/s
Closed-loop stability	Stable

Performance and Robustness	Tuned
Rise time	0.0308 seconds
Settling time	0.0909 seconds
Overshoot	2.33 %
Peak	1.02
Gain margin	23.3 dB @ 532 rad/s
Phase margin	75 deg @ 50.4 rad/s
Closed-loop stability	Stable

Rx3 – (A)Original Model (B)Reduced Order Model

Controller Parameters	
A	Tuned
Kp	-31.5805
Ki	-559.1265
Kd	0.26439
Tf	0.0083948

Controller Parameters	
B	Tuned
Kp	-25.2183
Ki	-730.5261
Kd	0.12898
Tf	0.0051374

Performance and Robustness	Tuned
Rise time	0.0316 seconds
Settling time	0.138 seconds
Overshoot	4.81 %
Peak	1.05
Gain margin	16.2 dB @ 1.4e+03 rad/s
Phase margin	82.3 deg @ 56.2 rad/s
Closed-loop stability	Stable

Performance and Robustness	Tuned
Rise time	0.031 seconds
Settling time	0.15 seconds
Overshoot	8.8 %
Peak	1.09
Gain margin	35.9 dB @ 1.08e+04 rad/s
Phase margin	81.4 deg @ 53.6 rad/s
Closed-loop stability	Stable

Rx4 – (A)Original Model (B)Reduced Order Model

Controller Parameters	
A	Tuned
Kp	-28.4074
Ki	-222.7504
Kd	0.13223
Tf	0.0046753

Controller Parameters	
B	Tuned
Kp	-35.9555
Ki	-183.6277
Kd	0.07224
Tf	0.013428

Performance and Robustness	Tuned
Rise time	0.178 seconds
Settling time	0.422 seconds
Overshoot	0 %
Peak	0.997
Gain margin	7.53 dB @ 126 rad/s
Phase margin	77.3 deg @ 20.5 rad/s
Closed-loop stability	Stable

Performance and Robustness	Tuned
Rise time	0.4 seconds
Settling time	0.573 seconds
Overshoot	0 %
Peak	0.997
Gain margin	6.77 dB @ 351 rad/s
Phase margin	75 deg @ 27.6 rad/s
Closed-loop stability	Stable

Rx5 – (A)Original Model (B)Reduced Order Model

Controller Parameters	
A	Tuned
Kp	-12.7541
Ki	-217.396
Kd	0.0052513
Tf	0.0010524

Controller Parameters	
B	Tuned
Kp	-14.1242
Ki	-137.0439
Kd	0.011705
Tf	0.00096401

Performance and Robustness	Tuned
Rise time	0.0196 seconds
Settling time	0.0782 seconds
Overshoot	0 %
Peak	0.999
Gain margin	26.2 dB @ 261 rad/s
Phase margin	75 deg @ 92.3 rad/s
Closed-loop stability	Stable

Performance and Robustness	Tuned
Rise time	0.0188 seconds
Settling time	0.212 seconds
Overshoot	0 %
Peak	1
Gain margin	18.5 dB @ 263 rad/s
Phase margin	75 deg @ 101 rad/s
Closed-loop stability	Stable

Rx6 – (A)Original Model (B)Reduced Order Model

Controller Parameters	
A	Tuned
Kp	-561.568
Ki	-38703.1952
Kd	5.6159
Tf	0.010034

Controller Parameters	
B	Tuned
Kp	-0.052823
Ki	-2641.138
Kd	0
Tf	0

Performance and Robustness	Tuned
Rise time	0.0257 seconds
Settling time	0.0645 seconds
Overshoot	3.25 %
Peak	1.03
Gain margin	26.4 dB @ 951 rad/s
Phase margin	78.2 deg @ 70.2 rad/s
Closed-loop stability	Stable

Performance and Robustness	Tuned
Rise time	0.365 seconds
Settling time	0.649 seconds
Overshoot	0 %
Peak	0.999
Gain margin	Inf dB @ NaN rad/s
Phase margin	90 deg @ 6.03 rad/s
Closed-loop stability	Stable

Rx7 – (A)Original Model (B)Reduced Order Model

Controller Parameters	
A	Tuned
Kp	-14.8309
Ki	-277.1703
Kd	0.12537
Tf	0.0084767

Controller Parameters	
B	Tuned
Kp	-15.034
Ki	-282.7004
Kd	0.12805
Tf	0.010812

Performance and Robustness	Tuned
Rise time	0.0358 seconds
Settling time	0.178 seconds
Overshoot	7.64 %
Peak	1.08
Gain margin	26.4 dB @ 1.13e+03 rad/s
Phase margin	75 deg @ 43.7 rad/s
Closed-loop stability	Stable

Performance and Robustness	Tuned
Rise time	0.0378 seconds
Settling time	0.173 seconds
Overshoot	7.92 %
Peak	1.08
Gain margin	23.9 dB @ 7.85e+04 rad/s
Phase margin	75 deg @ 43.7 rad/s
Closed-loop stability	Stable

Rx8 – (A)Original Model (B)Reduced Order Model

Controller Parameters	
A	Tuned
Kp	-8.6936
Ki	-168.0142
Kd	0.40028
Tf	0.046081

Controller Parameters	
B	Tuned
Kp	-8.6077
Ki	-166.1797
Kd	0.39675
Tf	0.04613

Performance and Robustness	Tuned
Rise time	0.0812 seconds
Settling time	0.43 seconds
Overshoot	7.15 %
Peak	1.07
Gain margin	26.1 dB @ 689 rad/s
Phase margin	85.6 deg @ 21.7 rad/s
Closed-loop stability	Stable

Performance and Robustness	Tuned
Rise time	0.0806 seconds
Settling time	0.432 seconds
Overshoot	7.1 %
Peak	1.07
Gain margin	40.1 dB @ 2.66e+03 rad/s
Phase margin	85.1 deg @ 21.7 rad/s
Closed-loop stability	Stable

Table 4.5 – Controller Parameters and Performance Criteria for Original and Reduced Order Model of RX

Approaches for Realization of Control Methods by Hardware

Overview

Translation of control theory and its realization depends on an optimized software which is able to process data in an efficient way in terms of time and performance. Aimed software to reach the desires of this project is based on C programming for microcontrollers under Atmel Studio software. An efficient structure of software needs to have complete view about the performance of the components in the hardware. As we know we are dealing with a microcontroller which is in interaction with ADC and DAC. We need to define a setting for our components by software which is contributing the control cycle. For example, the average rate of the ADC will be set by microcontroller and of course the method of data acquisition and generation of control law to have less time consumption is a responsibility of software.

In this section, we would like to have an overview about the software structure and the methods of the communication among the components will be discussed. As mentioned before the basic of the communication protocol among ADC and DAC with microcontroller is based on SPI which needs to have especial setting and drivers which will be discussed briefly and then the structure of the software in the shape of flow chart diagram will be presented.

Hardware Component Drivers

Serial Peripheral Interface SPI

Serial Peripheral Interface (SPI) is an interface bus commonly used to send data between microcontrollers and small peripherals such as shift registers, sensors, and SD cards. It uses separate clock and data lines, along with a select line to choose the device you wish to talk to. A common serial port, the kind with TX and RX lines, is called “asynchronous” (not synchronous) because there is no control over when data is sent or any guarantee that both sides are running at precisely the same rate. Since computers normally rely on everything being synchronized to a single “clock” (the main crystal attached to a computer that drives everything), this can be a problem when two systems with slightly different clocks try to communicate with each other.

To work around this problem, asynchronous serial connections add extra start and stop bits to each byte help the receiver sync up to data as it arrives. Both sides must also agree on the transmission speed (such as 9600 bits per second) in advance. Slight differences in the transmission rate aren’t a problem because the receiver re-syncs at the start of each byte.

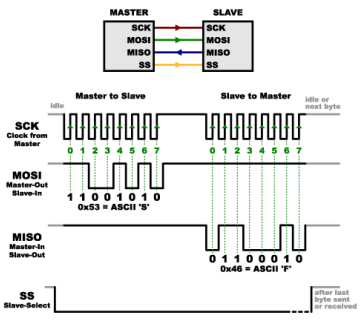

Figure 4.22 – SPI Protocol

SPI works in a slightly different manner. It’s a “synchronous” data bus, which means that it uses separate lines for data and a “clock” that keeps both sides in perfect sync. The clock is an oscillating signal that tells the receiver exactly when to sample the bits on the data line. This could be the rising (low to high) or falling (high to low) edge of

the clock signal; the datasheet will specify which one to use. When the receiver detects that edge, it will immediately look at the data line to read the next bit (see the arrows in the below diagram). Because the clock is sent along with the data, specifying the speed isn't important, although devices will have a top speed at which they can operate.

In SPI, only one side generates the clock signal (usually called CLK or SCK for Serial Clock). The side that generates the clock is called the "master", and the other side is called the "slave". There is always only one master (which is almost always your microcontroller), but there can be multiple slaves (more on this in a bit). When data is sent from the master to a slave, it's sent on a data line called MOSI, for "Master Out / Slave In". If the slave needs to send a response back to the master, the master will continue to generate a prearranged number of clock cycles, and the slave will put the data onto a third data line called MISO, for "Master In / Slave Out". Structure of a master and a slave component is shown in Figure 30. One last line which is called SS is used for Slave Select. This tells the slave that it should wake up and receive / send data and is also used when multiple slaves are present to select the one you'd like to talk to. To sum up SPI protocol we can categorize the advantage and disadvantage of it according to below.

Advantage	Disadvantage
• Faster than asynchronous serial • Receiver hardware can be a simple shift register • support multiple slaves	• Require more signal lines • The communications must be pre-arranged • master controls all communications • requires separate SS lines to each slave

ADC and DAC drivers

According to the introduction about SPI protocol, we need to shift a set of bits into the ADC and DAC in our hardware which the configuration of the bits will define the mode of operation in our components. According to data sheet ADS1158 as used ADC of the hardware, it will accept 3 bytes of data, and DAC will accept 4 bytes of data. We will briefly describe the responsibility of each byte of data in ADC and DAC and the features which could be exploited from these availabilities.

ADS1158 as ADC in designed hardware can operate in 2 main mode for data measurement which is 1) Channel Data Read Direct mode and 2) Channel data register read mode. In first case pin of DIN for ADC will be hold low or high which after 3 clocks, component automatically will enter to first mode. Indeed, entering this mode needs to drive the SS pin low

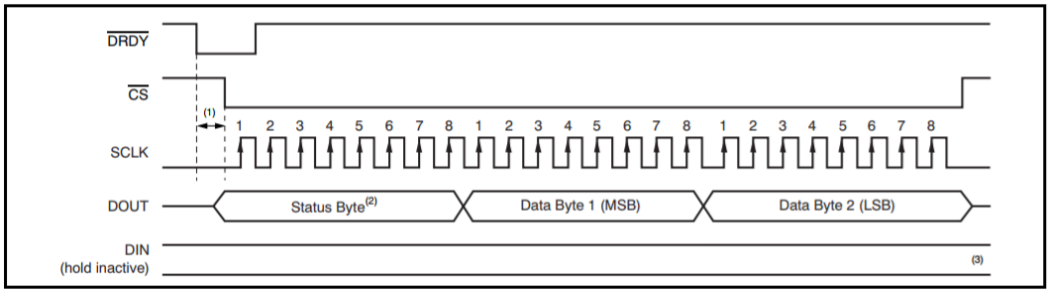

Figure 4.23 – SPI protocol communication setting for Data Read direct mode of ADS1158

by master which is controller to select the ADC to be in interaction mode with master. Configuration of ADC is such a way that by completing data conversion a pin under the name of data ready $\overline{DRDY}$ goes low and microcontroller is opening the SPI channel to get the acquired data from the TIAs. First byte of the shifted data into the microcontroller is called `Status byte` second byte is maximum significant byte (MSB) and the last one is least significant byte (LSB). First bit from first byte is a flag for microcontroller to show new set of data shifted to microcontroller. Second bit shows overflow, and third bit will show problem in power supply of the ADC. The left bits are for recognition of the address of the registers which is a representative of the channels of ADC. MSB and LSB bytes are the value of the channel which is converted in 16-bit resolution data. This configuration could be summarized in Figure 4.23.

In second configuration, we will need to write the register address in SPI line to read the desired channel value of TIAs. This configuration is by sending command byte in DIN pin of the SPI which is connected to MISO pin of the microcontroller. Thus, Microcontroller by shifting a known byte will read the desired channel value. This configuration is according to Figure 4.24.

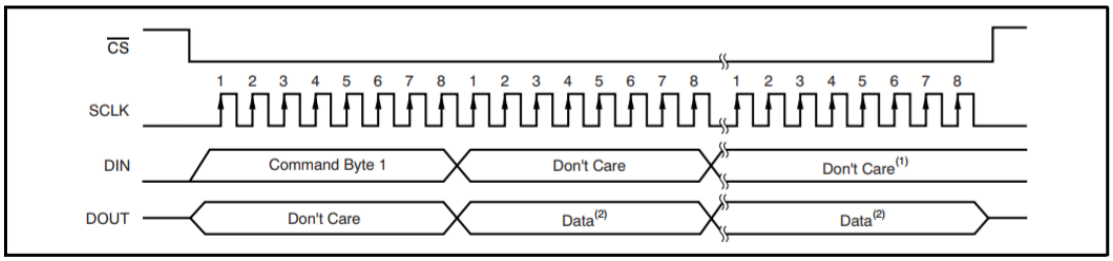

Figure 4.24 - – SPI protocol communication Setting for Channel Data Register Read mode of ADS1158

Obviously, structure of the main software will determine the mode of operation for ADC to take advantage of either first or second configuration.

In MAX5732 as DAC in designed hardware, four-byte set is needed to talk to DAC. MAX5732 provides an ability to put components in load mode by setting a pin low under the name of $\overline{LDAC}$.this pin allows master to hold the component on wait to finish shifting the control law values into the input registers of the DAC and the producing the control signal. Three first bits of the first byte shifted into the DAC is determining the control bits under the name of C2, C1, and C0. Configuration of this 3-control bit will define the mode of operation for DAC. The next 5 bits will be the register addresses of the MAX5732 which according to its value and the command bits, the value of the channel will be shifted out from the slave in line of MOSI. This set of data is for double checking the values as output control laws. This configuration of DAC MAX5732 could be summarized as Figure 4.25.

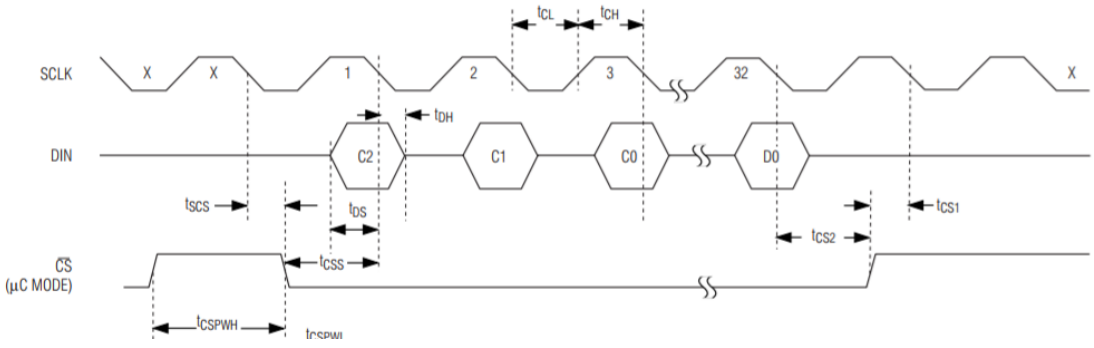

Figure 4.25 - SPI protocol communication Setting for Channel Data Register Read mode of MAX5732

As we see these configurations and timing schedule needs a solid driver structure to avoid data corruption or any fault in the control laws. Regarding that the drivers of the ADC and DAC are reported in Figure 4.26 and finally the main structure of the software will be presented in Figure 4.27.

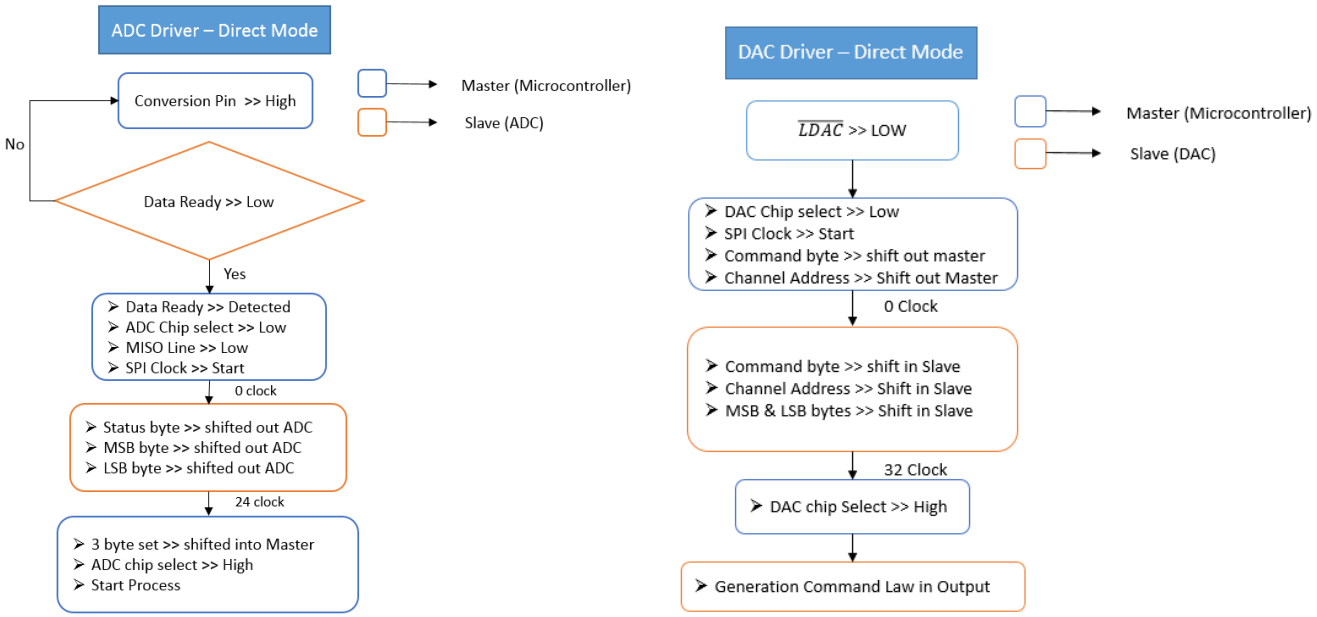

Figure 4.26 – ADC (ADS1158) and DAC(MAX5732) Driver Structure Flow Chart

Main Control Software Structure

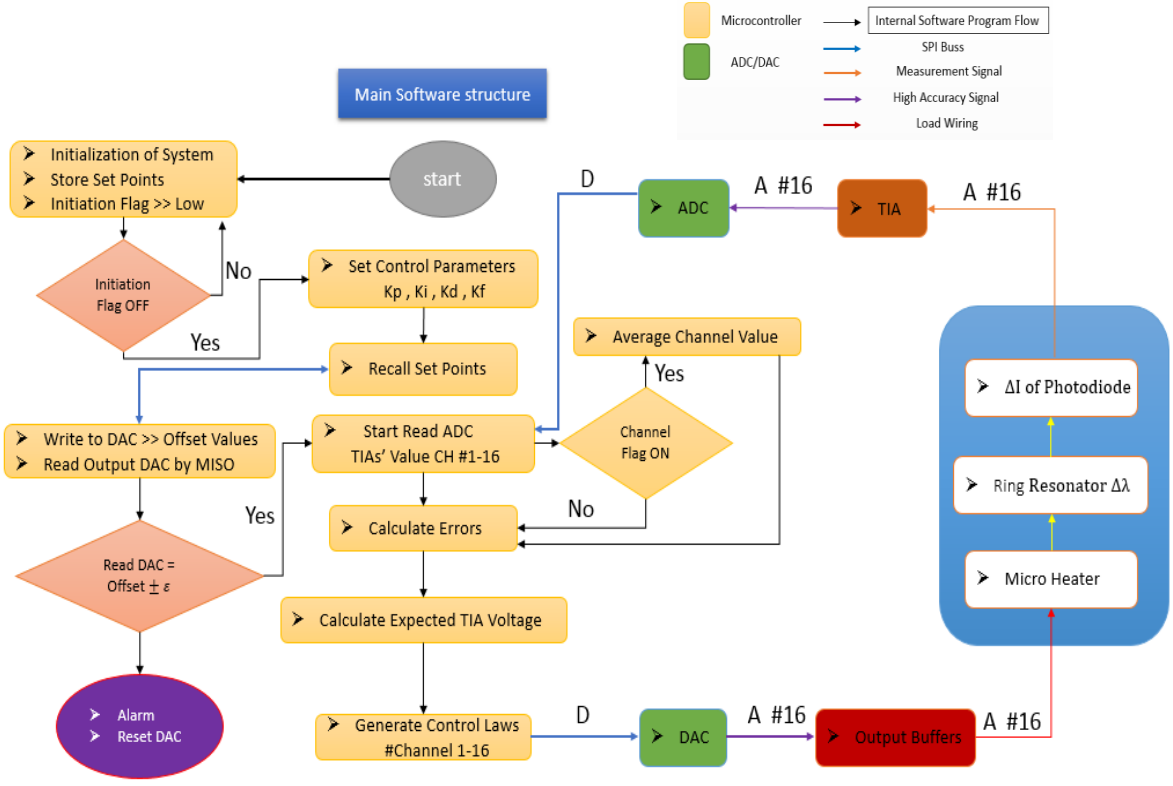

Figure 4.27 – Main Control Software Structure

By realization of the software programmed on the microcontroller, now we can test the performance of the designed controller. Very close relation of the hardware performance and software to reach the desires of the project could be counted as challenges of the project. Because non-ideal behavior of the hardware against the expectations could happen which can be due to a poor programming or a weakness in hardware design, which in both aspects should be debugged to solve the problem and improve the performance of the control process. Next chapter we will summarize the results of the project which is arrangement and tuning of the optical telecommunication channels based on the comb laser lines. And finally, we will have a conclusion about achievements, pros and cons of the accomplishments and prospect of the project and the possible ways of improvements in both hardware and software aspects.

V. Chapter 5: Measurement Results and Conclusion

Overview

As mentioned, aim of the project is to tune and control the optical telecommunication channels based on RRM. As we know our control structure should prepare a situation to tune every channel according to the comb laser lines to prepare ring resonators to modulate or demodulate the RF signal. It is meritorious to mention that RF signal measurement is performed for 6 channels of the transmitter and receiver side. So, the main goal of the control board and software will be focused on the control and tune the 6 channels of TX and RX. The reason of the performing measurement for 6 channels is practical limitations. So, in lambda scan of the laser spectrum we aim to tune the 6 channels of the transmitter and receiver side at the same wave length. In this chapter, the result of the tuning optical channels based on the laser output spectrum and eye diagram of the modulated and demodulated signal based on the tuned ring resonators will be presented. Based on the laser spectrum we can analyze the performance of the hardware and software in initialization procedure. Then, by looking at eye diagram of the RF transmitted signal we can see an improvement of the eye diagrams with control system and without control system. Then the performance of the system under control will be presented.

Measurement Results

Since laser spectrum is a reference for the measurement and control systems, the laser spectrum used in the experiments are reported as Figure 5.1(A). This laser is a mode locked laser and in category of flip chip lasers. The picture of the coupled laser to a lensed fiber is shown in Figure 5.1 (B). This laser after coupling to the optical fiber, will be transmitted to the RF interface board and again will be edge coupled to the silicon chip, which is wire bounded on RF interface board. The laser after coupling into the silicon chip, we can have measurement of the laser spectrum after passing the crow filter and transmitter side. This measurement is performed by commercial spectrum analyzer and the data will be acquired by interface program under the LABVIEW software. The laser name is ACE3 and is biased with 264mA power supply in 20℃.

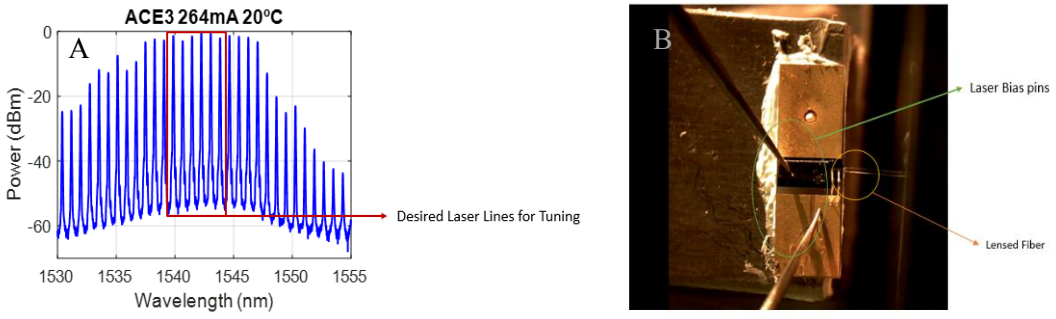

Figure 5.1 – (A) Laser ACE3 Spectrum (B) Laser ACE3 biasing configuration and Coupling to Lensed Fiber

Now by presenting the laser spectrum as a reference of the control and initialization we should evaluate the ring resonators wave length to validate the performance of the initilization procedure which is responsible to put each ring resonatgor in the desired wave length of the laser line and prepare it for starting the RF signal modulation. The laser line wavelengths are according to table xx.

Evaluation of the ring resonator wave length will be after passing laser inside the silicon chip from crow filter and transmitter side and in the reverse path for receiver.so we can present the transmitter and receiver ring resonator wave length before and after the control initialization.

Laser Line	Wave Length[nm]
1	1540.65
2	1541.45
3	1542.24
4	1543.04
5	1543.84
6	1544.64

Transmitter and receiver ring resonator wave length will be measured by spectrum analyzer which is according to Figure 5.2 for transmitter side and Figure 5.3 for receiver side.

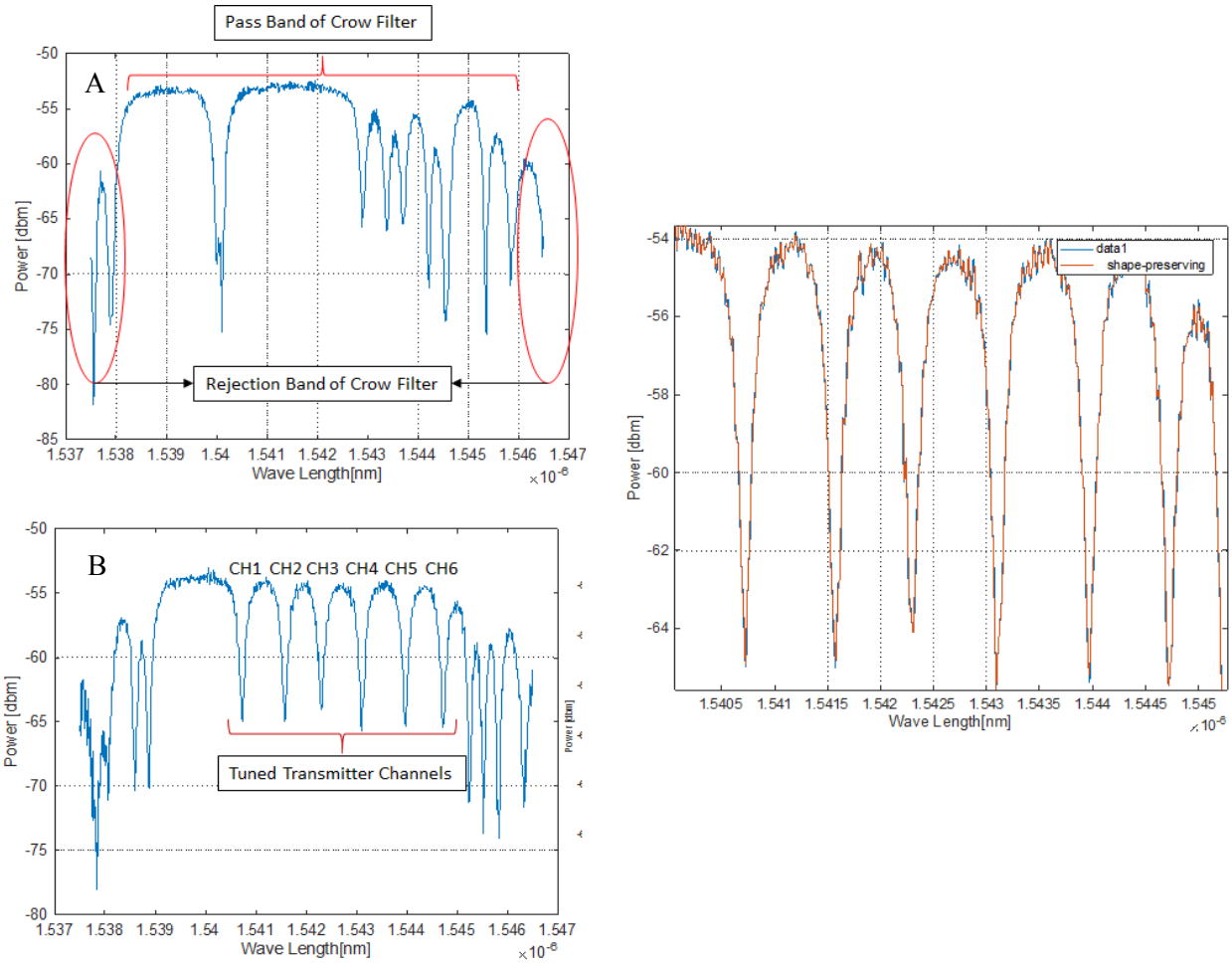

Figure 5.2 – (A) Lambda Scan for Transmitter side laser output spectrum before Initialization (B) Lambda Scan for Transmitter side laser output spectrum after Initialization

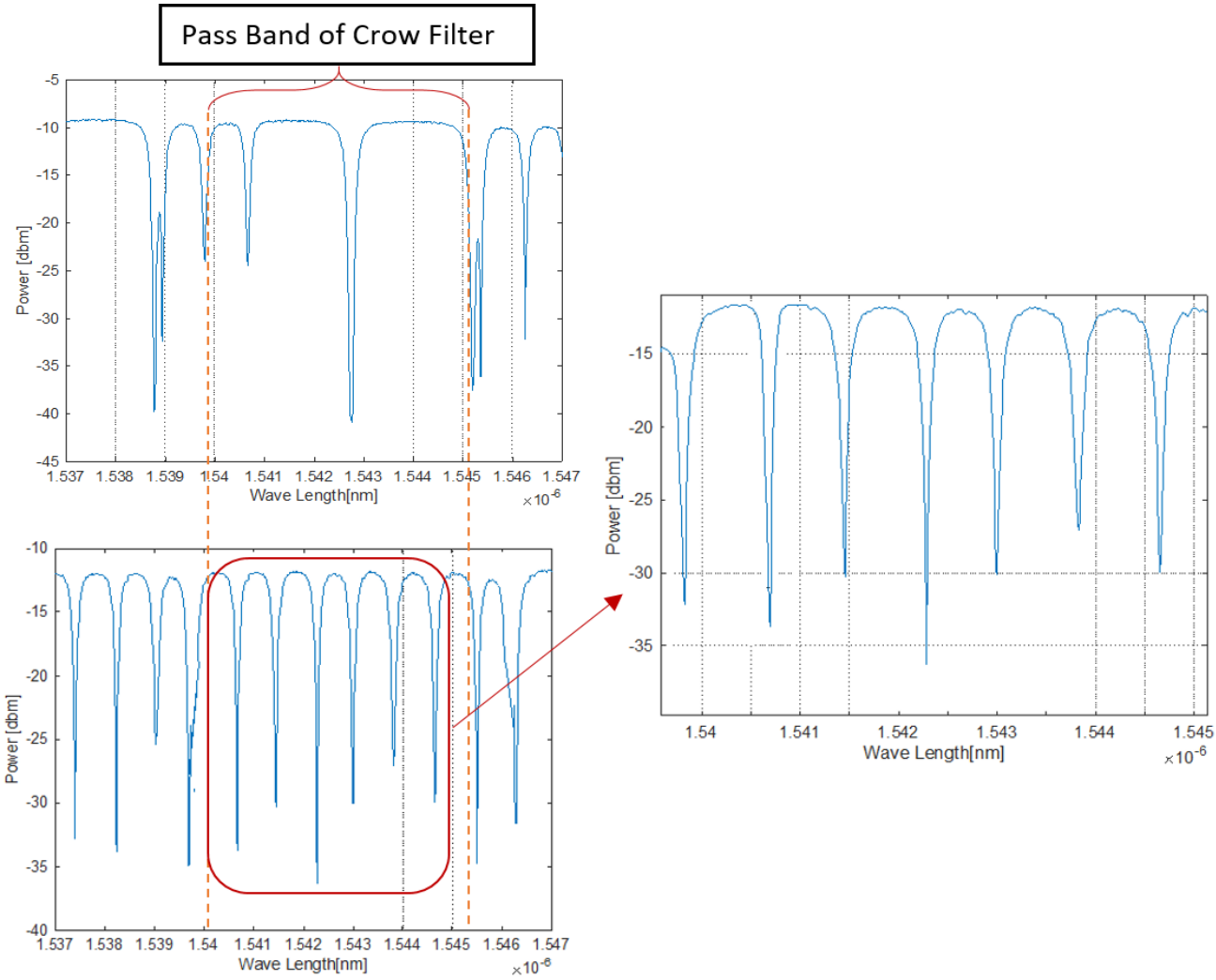

Figure 5.3 - (A) Lambda Scan for Receiver side laser output spectrum before Initialization (B) Lambda Scan for Receiver side laser output spectrum after Initialization

According to the data stored in the microcontroller memory the initialization process is realized according to table 6 for both transmitter and receiver side.

Channel number	Transmitter [mA]	Receiver [mA]
1	1.6	3
2	9.13	3.4
3	9.1	2.3
4	4.7	3.3
5	10.7	3.8
6	8.4	4.2
7	5.8	5.4
8	9.9	3.9

Table 5.1 – offset values calculated by initialization program

As we can see initialization process has been performed by the control structure which makes the system ready for starting the data modulation. For data modulation, we should consider the eye diagram of the transmitter and receiver signals which is a proof of same wavelength of

transmitter and receiver channels. Receiving the same pattern of the transmitted data and then locking the bit error rate analyzer to sync the received data shows the initialization and control procedure is working correctly. Since by starting data modulation in RF interface board we will have an increase of temperature in silicon chip and it induces a shift in rings' resonance. This is the same disturbance which is applied to analog sub system which PID controller tuned by software compensates the deviation from the reference point. The eye diagram, and post processed signa by PRBS[5] averaging, and W-factor of signal for a system under control has been measured and they will be presented as Figure 5.4 and 5.5.

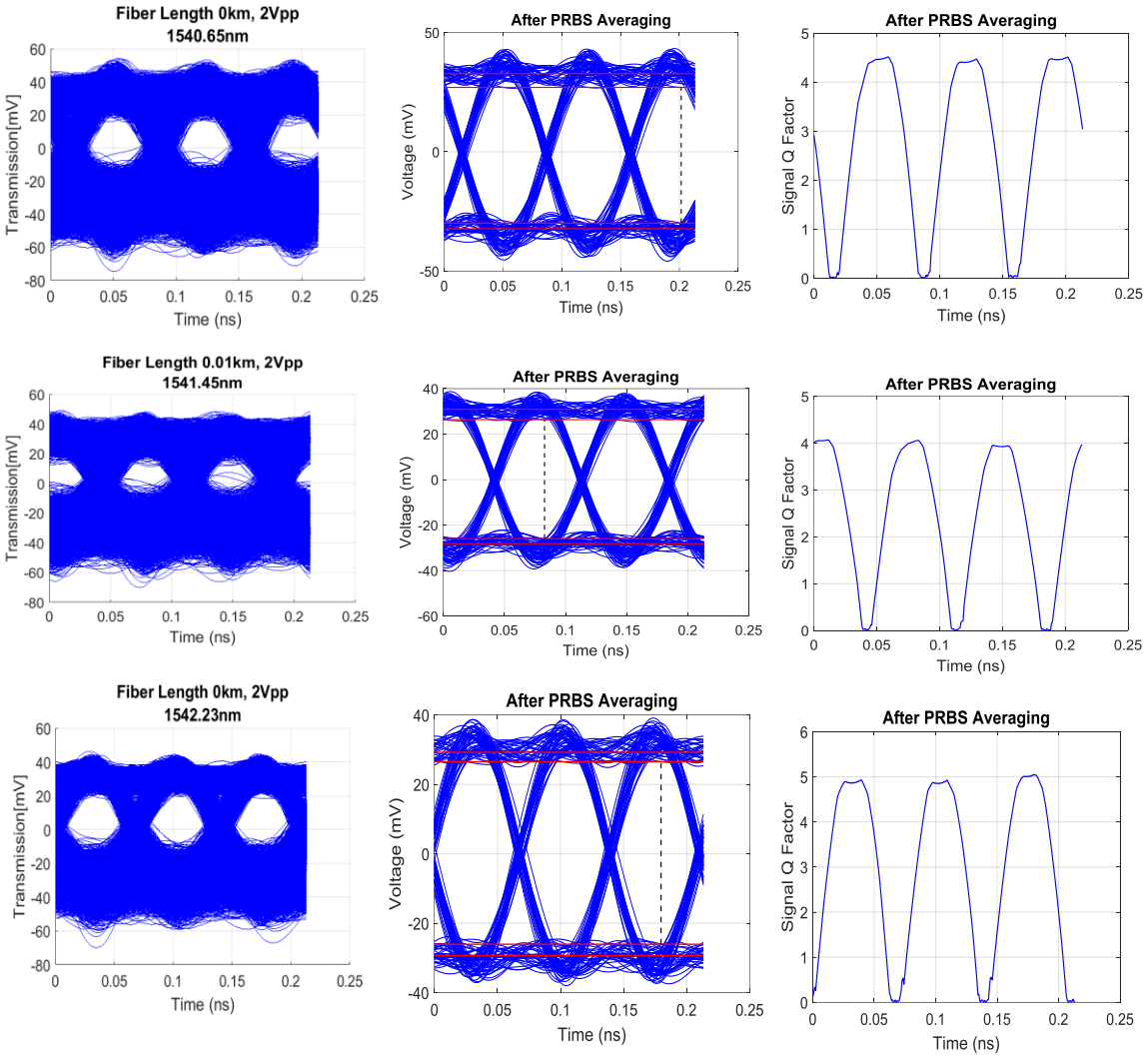

Figure 5.4 – measurement of Eye diagram pattern and post processed measurement by PRBS averaging and Q-Factor computations for transmitter channels number 1, 2, 3

[5] Pseudorandom binary sequence

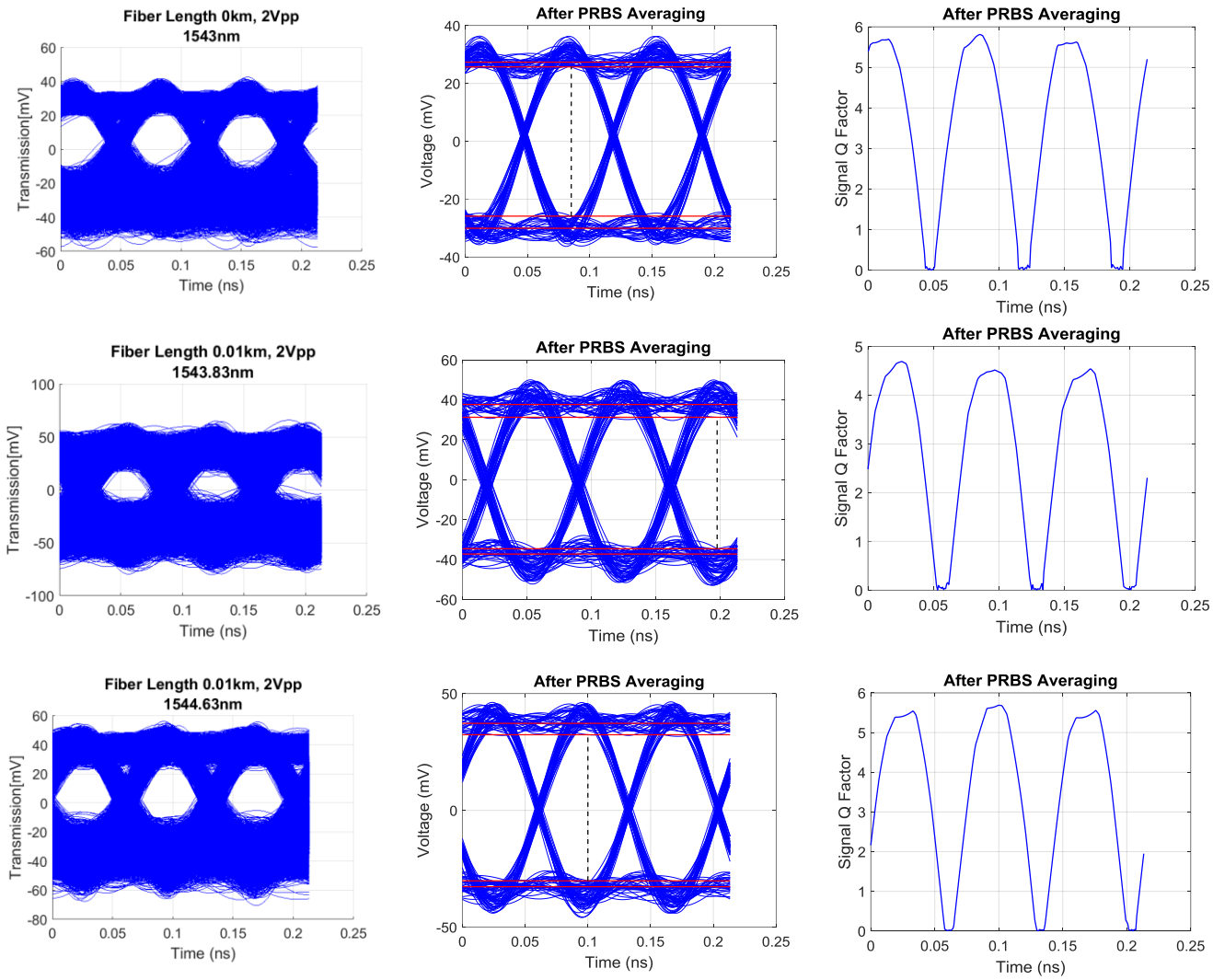

Figure 5.5 - – measurement of Eye diagram pattern and post processed measurement by PRBS averaging and Q-Factor computations for transmitter channels number 4, 5, 6.

During the experiments, it was obvious a system without controller because of the deviation from set point because of internal or external disturbances, we would have whether an asymmetric eye diagram or lower output amplitude in eye diagram. Presented results are the optimal results from the system for 14Gbps data transmission rate. The other criteria which can be considered is the value of BER for a system under control. By having untuned ring resonator the bit error rate cannot sync the received data to calculate the BER of the transmitted and received signal. Lower amplitude of received signal can cause failure in locking of BERT device which one of the reasons could be deviation of the ring resonators from the optimal point. the measurement of the BER for the received signal is performed by 2 kind of receiver which the first one is commercial photoreceiver and the second one is the photoreceivers inside the silicon chips which are under control of control board. The measured BER for a system

Laser Line	Wave Length[nm]	Finisar photoreceiver	Close loop (GePD+Mel_TIA)
1	1540.65	$1e^{-5}$	$2\ e^{-5}$
2	1541.45	$5e^{-5}$	$1\ e^{-5}$
3	1542.24	$6e^{-7}$	$2\ e^{-5}$
4	1543.04	$7e^{-8}$	$8\ e^{-6}$
5	1543.84	$2e^{-6}$	$3\ e^{-4}$
6	1544.64	$1e^{-4}$	$2\ e^{-3}$

under control for both receiver is according to table 7. It should be mentioned that BER as a criterion of the data transmission could be considered. However, BER could change because of other reasons. For example, misalignment of the edge couplers, laser line power and noise value, and indeed the micro ring resonator detuning from an optimal point could affect the BER value.

Conclusion and Prospects

In this master thesis, aim is to study the behavior of the optical telecommunication channels based on ring resonator modulators which are fabricated in silicon chips and tuning the ring resonators by considered micro heaters inside the silicon chip. Ring resonator as a key component are responsible in data transmission cycle of optical telecommunication. Data transmission by transmitter and receiver is realized which ring resonators are a key component there. However, Susceptibility of the ring resonators to temperature fluctuation is one of the challenges of this project which has been dealt by designing a hardware based on microcontroller and a software to run inside the microcontroller to tune and control the ring resonators.

The transmitter and receiver of the silicon chips has been evaluated as control plant and according to the fabrication considerations we are monitoring the light power coupled into the ring resonators from the wave guide which laser is passing through it. As mentioned, resonance wave length of the rings is varying by temperature fluctuations. Temperature fluctuation can be due to ambient temperature, or other electrical or optical components like signal drivers. Thus, after arrangement of the transmitter and receiver channels of the system, we need to control wave length of the ring resonators based on the comb laser lines. In fabricated silicon chips, micro heater on top of each ring resonator is acting as actuator in our control plant which power dissipation causes the resonance shift of the ring resonators.

Moreover, in designed hardware it has been considered to have amplification of the generated current of the monitoring photodiodes. Then an ADC converts the signal to send to the Microcontroller. After processing the measurements by the microcontroller, the control law will be generated and will be sent to the DAC. Control law signal determines the value of the power consumption in micro heater to control and tune the rings.

By generated algorithm for microcontroller, an 8-channel transmitter and receiver have been initialized and controlled. For initialization of the system a unique procedure has been defined which makes the tuning the all transmitter and receiver channels feasible. A comb laser is a reference for our initialization and controlling the ring resonators. For designing a PID controller, an identification of the whole system has been performed by data acquisition and identification by MATLAB tool box. Since the order of the identified model was 5 order, by balanced truncation the obtained model for each channel has been reduced to second order to be appropriate for implementing PID controller inside the microcontroller as a discreet PID controller.

Furthermore, a simulation of the modeled data has been performed to evaluate the functionality of tuned PID controller. This simulation by imposing the modeled system against uniform noise, ramp, step and impulse response, contributed to evaluate control plant and the tuned PID versus the worst possible disturbances. By implementing tuned PID controllers for all channels a series of experiments has been performed to study the functionality of the controller during the real experiments while data transmission.

Finally, the results of the data transmission for a system under control of the designed hardware and software presented to prove the functionality of the designed control process for this plant. Since from the beginning of the project there was a tendency to have functional control system the simplest possible way to implement the control desires are considered. As we know this system is containing the more inputs and outputs which the micro heaters as actuator in silicon chips are in a very small area so in the future for increasing the efficiency of the control system we can study system as MIMO system to evaluate the cross talks of the channels and their response to the other control inputs.

By defining a MIMO system it would be possible to design suitable MIMO controllers for the system which implementation of such control system will be a challenge in both hardware and software term. For improvement of the locking of the laser lines it would be possible to have another signal from the RF interface board to distinguish the optimal point of the tuning point to observe the highest quality signal after transmission in terms of low noise and higher amplitude.

Bibliography

[1] "techpedia," [Online]. Available: https://www.techopedia.com/definition/24942/optical-communication.

[2] G. Breed, "OPTICAL MODULATION," in *High Frequency Design*, From May 2007 High Frequency Electronics, 2007.

[3] [Online]. Available: https://www.rp-photonics.com/wavelength_division_multiplexing.html.

[4] no. ITU Standard G.694.1 (06/02), “Spectral grids for WDM applications: DWDM frequency grid”, International Telecommunication Union (2002).

[5] no. ITU Standard G.694.2 (12/03), “Spectral grids for WDM applications: CWDM wavelength grid”, International Telecommunication Union (2003).

[6] 4. ,. C. R. ,. R. H. ,. A. L. ,. S. S. ,. David Marpaung1, "Integrated microwave photonics," *LASER&PHOTONICS,* 2012.

[7] A. Yariv, "theory of laser osciliation and some specific laser sytems," in *photonics - optical electronics in modern communications*, New york, oxford university press, 2007.

[8] I. D. e. al., "Fundamentals of Optical Communication," in *Coding for Optical Channels*, Springer Science+Business Media, LLC 2010.

[9] "Grating Couplers for Coupling between Optical Fibers and Nanophotonic Waveguides," *Japanese Journal of Applied Physics,* 2006.

[10] [Online]. Available: https://www.rp-photonics.com/waveguides.html.

[11] N. T. e. al., "Silica-based single-mode waveguides on silicon and their application to guided-wave optical interferometers”,," no. J. Lightwave Technol. 6 (6), 1003 (1988).

[12] K. M. D. e. al., "Writing waveguides in glass with a femtosecond laser," no. Opt. Lett. 21 (21), 1729 (1996).

[13] S. C. T. AG, "Tutorial Note #5," Berlin.

[14] "RP Photonics," [Online]. Available: https://www.rp-photonics.com/electroabsorption_modulators.html.

[15] B. S. J. S. a. M. L. Qianfan Xu, "Cascaded silicon micro-ring modulators for," *Optical Society of America,* no. 130.3120, 2006.

[16] "APTechnology," [Online]. Available: https://www.aptechnologies.co.uk/support/photodiodes/photodiode-theory-of-operation.

[17] "rp- photonics," [Online]. Available: https://www.rp-photonics.com/amplifiers.html.

[18] "RP - Photonics - SOA," [Online]. Available: https://www.rp-photonics.com/semiconductor_optical_amplifiers.html.

[19] P. M. M. R. B. Thomas Meynen, "CROW-based Optical Delay Lines : Consequences of Fabrication Limits On Filter Response And Delay," University Ghent.

[20] "wikipedia - OADM," [Online]. Available: https://en.wikipedia.org/wiki/Optical_add-drop_multiplexer.

[21] M. Integrated, *Application Note : Optical Signal-to-Noise Ratio and the Q-Factor in,* HFAN-9.0.2.

[22] R. A. B. e. al, no. ., “Semiconductor optical amplifier (SOA) packaging for scalable and gain-integrated silicon photonic switching platforms,”.

[23] G.M. Malwatkar a, "Tuning PID controllers for higher-order oscillatory systems with," December 2008.

[24] H. I. e. al, "Review and status of wavelength-division-multiplexing technology and its application," J. Lightwave Technol. 2 (4), 448 (1984).

[25] "RP-photonics -EDFA," [Online]. Available: https://www.rp-photonics.com/erbium_doped_fiber_amplifiers.html.

[26] no. A. E. Willner and S.-M. Hwang, “Transmission of many WDM channels through a cascade of EDFA's in long-distance links and ring networks”, J. Lightwave Technol. 13 (5), 802 (1995).

[27] N. S. B. a. C. R. Davidson, "“Wavelength division multiplexing in long-haul transmission systems”," no. J. Lightwave Technol. 14 (6), 1299 (1996).

[28] no. G. E. Keiser, “A review of WDM technology and applications”, Opt. Fiber Technol. 5 (1), 3 (1999).

[29] no. L. F. Mollenauer et al., “Demonstration of massive wavelength-division multiplexing over transoceanic distances by use of dispersion-managed solitons”, Opt. Lett. 25 (10), 704 (2000).

[30] T. S. e. al, “Multichannel and high-density hybrid integrated light source with a laser diode array on a silicon optical waveguide platform.

Figure 1.1 –(A) Block Diagram of Optical Telecommunication Cycle (B) Optical Telecommunication Network 13
Figure 1.2- Functional diagram of an optical modulator 14
Figure 1. 3 - Basic Scheme of WDM 16
Table 1.1 – pros and cons of Silicon photonics 17
Figure 1.4 – Silicon Photonics in Optical data transmission cycle 17
Figure 1.5 - (A) Spontaneous and stimulated emission (B) A four-level laser pumping system (C) Schematic diagram of a basic laser 20
Figure 1.6 - Example of a Laser Spectrum 20
Figure 1.7 - Emission spectra of lasers with single-mode emission (top), multiple axial mode (but single transverse mode) emission (middle), and full multimode emission (bottom). 21
Figure 1.8 - An exemplary optical network identifying key optical components 22
Figure 1.11 – Edge coupler vs. Grating Coupler 23
Figure1. 9 - principle of grating coupler for coupling 23
Figure 1.12 - Wave guide schematics in photonic devices 24
..... 24
Figure 1.13 - Electric field amplitude profiles for all the guided modes of a fiber 24
Figure 1.14 – An illustration of external modulation principle. DFB distributed feedback laser. 27
Figure 1.15 – (a) Mach–Zehnder modulator (b) Electro Absorption Modulator 27
Figure 1.16 - Schematics of a WDM optical interconnection system with cascaded silicon ring resonators as a WDM modulator and demultiplexer. Det: detector. 28
Figure 1.17- Top-view microscopic picture of the fabricated modulators, showing two of the four ring modulators coupled to a straight waveguide. 28
Figure 1.18 - Optical receiver front-end stage schemes (A) high-impedance front-end (B) transimpedance front-end 29
Figure 1.19 – A typical direct detection architecture. O/E optical to electrical and AGC automatic gain control 29
Figure 1.20– Cross section view a Photodiode 30
Figure 1.21 – Equivalent circuit of photodiode 30
Table 1.2 - PD equivalent circuit Parameters 30
Figure 1.22 – Conversion circuits of PD Current to Voltage 31
..... 32
Figure 1.23 - Schematic setup of a simple erbium-doped fiber amplifier. Two laser diodes (LDs) provide the pump power for the erbium-doped fiber. The pump light is injected via dichroic fiber couplers. Pig-tailed optical isolators reduce the sensitivity of the device to back-reflections. 32
Figure 1.24 - Schematic description of possible ring formations. 35
Figure 1.25– Main Scheme of Optical Multiplexer and de-multiplexer 36
Figure 2.1 – Macroscale of the optical telecommunication system 40
Figure 2.2 – (A) Transmitter structure (B)Receiver Structure 41
Figure 2.3 – (A)RRM Modulator driver (B) Filip Chip Photodiode array and TIA (C) Tx and Rx configuration on test bench 41
Figure 2.4 - (A) Tx Integration(B) Tx realization on interface board (C) analysis of the transmission data by the criteria of Q-factor and BER by sweeping laser power 42
Figure 2.5 – (A) RX Integration (B) Rx realization on interface board (C) Analysis of the receiver data by the criteria of BER vs. average power of the receiver 42

Table 2.1 – Comparison of Ge photodiode and flip chip photodiode sensitivity in 14 and 25 Gbps. 43
Figure 2.6 – (A) Full link configuration block diagram of TX and RX (B) Analysis of modulated data and measurement data based on the laser power. 43
Figure 2.7 – Overall view of the optical transmitter and Receiver Module 43
Figure 2.8 – (A) Hybrid Integration structure with an LD array on a silicon Waveguide platform (B) Experimental mounted flip chip Laser (C) Spectrum of the used flip chip in experiments 44
Table 2.2 – Laser and system under experiments main features 44
Figure 2.9 - (A) Fabricated RRM with thermal tuner (B) OMA of the RRM vs. Bandwidth. 45
Figure 2.10 – (A) Optical modulation Amplitude of the RRM in system under experiment (B) RF performance of the RRM modulators 45
Figure 2.11 - (A) fabricated Crow Filter in 50 μm scale (B) fabricated Crow Filter in 200 μm scale 46
Figure 2.12 – (A) Transmission of the crow filter (B)Input laser spectrum of the crow filter (C) Output Spectrum of the Crow Filter 46
Figure 2.13 – (A) Mounted Flip-chip Photodiode (B)Bandwidth of the Flip-chip Photodiode (C) Responsivity of Flip-chip PD 47
Figure 2.14 – (from left to right) 1) sample fabrication 2) Material Structure 3) Gain Bandwidth 4) Responsivity 47
Figure 3.1- Main scheme of Hardware (Left Picture) – Structure of the Micro-ring Resonator (Right Picture) 50
Based on the above descriptions about the hardware, the designed and manufactured hardware is according to block diagram as Figure 3.1. 51
Figure 3.2 – Block Diagram and Pinout 51
Figure 0.2 – Block Diagram and Pinout 51
Table 3.1 _ Main characteristics of XMEGA256A3BU 53
Figure 3.3 – Layout of Designed Microcontroller Circuit 53
Figure 3.4 - 3D View of the designed Microcontroller Circuit 53
Figure 4 - 3D View of the designed Microcontroller Circuit 53
Figure 3.5- Pin Configuration 54
Figure 0.3- Pin Coniguration 54
Figure 3.6- block diagram of ADS1158 54
Figure 0.4- block diagram of ADS1158 54
Table 3.2 - Main Characteristics of ADC Circuit (ADS1158) 55
Figure 3.7 – Layout of the design of ADS1158 55
Figure 5 – Layout of the design of ADS1158 55
Figure 3.8 - 3D View of the Design of ADS1158 55
Figure 0.5 - 3D View of the Design of ADS1158 55
Figure 3.9- Pin configuration of DAC (MAX5732) 56
Figure 0.6 - Pin configuration of DAC (MAX5732) 56
Figure 3.10 - Functional Diagram of DAC (MAX5732) 56
Figure 0.7 - Functional Diagram of DAC (MAX5732) 56
Table 3.3 – main Characteristics of DAC (MAX5732) 57
Figure 3.11 -The Layout of DAC circuit Design (MAX5732) and 3D view of the Designed DAC (Max5732 57
Figure 8 -The Layout of DAC circuit Design (MAX5732) 57
Figure 3.12 (A) Main Scheme of Buck Convertor (B) Off state Mode (C) on state Mode 58

Figure 3.13 - (A) Filtered Buck Convertor (B) Discreet Mode (C) Continuous Mode 58
Figure 0.8 (A)(B)(C) 58
Figure 3.14 – Main scheme of the Designed Power Supply 61
Figure 0.99 – Main scheme of the Designed Power Supply 61
Figure 3.15 – TPS40170 PIN Configuration Configuration 61
Figure 20 – TPS40170 PIN Configuration Configuration 61
Figure 3.16 – Pin configuration of CSD16321Q5 62
Figure 21 - CSD16321Q5 62
Table 3.3 – Main Characteristics of CSD16321Q5 62
Figure 3.17 – (A) Drain Source Impedance vs. Gate source voltage (B) Gate charge vs. Gate source Voltage 62
Figure 22 62
Figure 3.18 - Simplified Schematics of TPS40170 62
Figure 23 - Simplified Schematics of TPS40170 62
Figure 3.19 - Bode plot of the compensation Network of TPS40170 62
Figure 24 - Bode plot of the compensation Network of TPS40170 62
Figure 3.20- Transient Mode Simulation TPS40170 63
Figure 25 - Transient Mode Simulation TPS40170 63
Figure 3.21- Steady State Mode TPS40170 63
Figure 26 - Steady State Mode TPS40170 63
Figure 3.22 - INPUT Transient Mode Simulation TPS40170 63
Figure 27 - INPUT Transient Mode Simulation TPS40170 63
Figure 3.23 - (A) Efficiency of the Power Supply Vs. Load (B) Linear Output Power Vs. Input Voltage 64
Figure 28 (A) Efficiency of the Power Supply Vs. Load (B) Linear Output Power Vs. Input Voltage 64
Figure 3.24 - (A) Junction Temperature for Different input voltage (B) Duty cycle for Different Input Voltage 64
Figure 29 - (A) Junction Temperature for Different input voltage (B) Duty cycle for Different Input Voltage 64
Figure 3.25 - (A) Actual output voltage in different Input Voltages (B) Difference of the output ripple vs. different Input Voltage 64
Figure 30 - (A) (B) 64
Figure 3.26- (A) Input Current vs. Output Current (B) Total Power Dissipation of the power supply TPS40172 64
Figure 31- (A) (B) 64
Figure 3.27 – Pin Configuration of LM3152 65
Figure 32- 65
Figure 3.28- Simplified schematics of LM3152 65
Figure 33- Simplified schematics of LM3152 65
Figure 3.29- (Left picture) Transient of the Output Voltage and Settling In3.3V (Right Picture) Transient of the Output Current and Load Current 66
Figure 34 - (Left picture) Transient of the Output Voltage and Settling In3.3V (Right Picture) Transient of the Output Current and Load Current 66
Figure 31-(Left Picture) Steady State Output Voltage, Output Filter Voltage, Input Voltage. (Right Picture) Steady state Input current, Output Current, Load Current. 66
Figure 36-(Left Picture) Steady State Output Voltage, Output Filter Voltage, Input Voltage. (Right Picture) Steady state Input current, Output Current, Load Current. 66

Figure 3.30 - (Left Picture) Transient of Input Voltage and Output Voltage (Right Picture) Transient of the Load form Max. To Min. and the effects On Output Voltage. 66
Figure 35-(Left Picture) Transient of Input Voltage and Output Voltage (Right Picture) Transient of the Load form Max. To Min. and the effects On Output Voltage. 66
Figure 3.32 (A) Power Supply Efficiency (B) Monotonic Output Power vs. Output current 67
Figure 37 - 67
Figure 3.33 - (A) Output voltage ripple (B) Average Input current vs. output Current in different Input voltages 67
Figure 38 - 67
Figure 3.34 – (A) Total Power Dissipation of LM3152 (B) Power dissipation in Switcher LM3152 67
Figure 39 - 67
Figure 3.35 – (A) max. Junction Temperature (B) Duty Cycle Variation in Different Input Voltages 68
Figure 40 - 68
Table 3.4 – Summary of the Designed Power Supply Main Characteristics 68
Figure 3.36 – (A) Power Supply Final Layout (B) Power Supply 3D View 68
Figure 41- Power Supply Final Layout 68
Figure 3.37 -Main scheme of Reversed Bias TIA 69
Figure 43 -Main scheme of Reversed Bias TIA 69
Figure 3.38– Uncompensated TIA 70
Figure 44– Uncompensated TIA 70
Figure 3.39– Compensated TIA 70
Figure 45– Compensated TIA 70
Figure 40 – Schematics of Designed TIA (OPA380) 71
Figure 46 – Schematics of Designed TIA 71
Figure 42– AC Characteristics of TIA (OPA380) by Swiping R_f from 500K to 2Meg [ohm] 71
Figure 48– AC Characteristics of TIA (OPA380) by Swiping R_f from 500K to 2Meg [ohm] 71
Figure 41 – DC Characteristics of TIA 71
Figure 47 – DC Characteristics of TIA 71
Figure 43– Step Response of TIA (OPA380) Step Input Current 1uA and Max gain 2Mohm .. 71
Figure 49– Step Response of TIA (OPA380) Step Input Current 1uA and Max gain 2Mohm .. 71
Figure 44 – TIA Response to Triangle Input (100 Hz, 1u Amplitude) 71
Figure 50 – TIA Response to Triangle Input (100 Hz, 1u Amplitude) 71
Figure 46 – Noise Analysis of TIA (OPA380) by Swiping Rf 71
Figure 52 – Noise Analysis of TIA (OPA380) by Swiping Rf 71
Figure 45– Steady State Response for Input Step current start at 1ms. 71
Figure 51– Steady State Response for Input Step current start at 1ms. 71
Table 3.5 – Summary of Main characteristics of TIA (OPA380) 72
Figure 3.47– TIA Design Layout (OPA2380) 72
Figure 53 – TIA Design Layout (OPA2380) 72
Figure 3.48– TIA Design - 3D View (OPA2380) – (14xOPA2380) 72
Figure 54– TIA Design - 3D View (OPA2380) – (14xOPA2380) 72
Figure 3.49 – Pin configuration of SMBTA42 73
Figure 55- SMBTA42 73
Figure 3.50 - Output Buffer Schematics 73
Figure 57 - Output Buffer Schematics 73
Figure 3.51– DC Characteristics with 5V DC power Supply 74

Figure 58 – DC Characteristics with 5V DC power Supply 74
Figure 3.52 – Power Dissipation in the Load (400 Ohm Resistance Micro-Heater) 74
Figure 0.10– Power Dissipation in the Load (400 Ohm Resistance Micro-Heater) 74
Figure 3.54- Response of the Buffer to Triangular wave Input with 100Hz Frequency 5V amplitude 74
Figure 61 - Response of the Buffer to Triangular wave Input with 100Hz Frequency 5V amplitude 74
Figure 3.53 - Power Dissipation in the Load (400 Ohm) 74
Figure 60 - Power Dissipation in the Load (400 Ohm) 74
Figure 3.55 - Noise Analysis 74
Figure 64 - Noise Analysis 74
Figure 3.56 - Nominal Maximum Power Dissipation (Supply Voltage 36V) 74
Figure 65 - Nominal Maximum Power Dissipation (Supply Voltage 36V) 74
Figure 3.57 - Response of the Buffer to Square wave Input with 100Hz Frequency 5V amplitude 74
Figure 62 - Response of the Buffer to Square wave Input with 100Hz Frequency 5V amplitude 74
Figure 3.58 – Steady state response to Step Input (5V Amplitude) 74
Figure 63 – Steady state response to Step Input (5V Amplitude) 74
Table 3.6 – Summary of designed Output buffer (OPA4251) 75
Figure 3.59 – Lay out of Output Buffer 75
Figure 66 – Lay out of Output Buffer 75
Figure 3.60 – 3D View of Designed Output Buffer 75
Figure 67– 3D View of Designed Output Buffer 75
Figure 61– Pin Configuration of OPA567 76
Figure 68 – Top View of OPA567 76
Figure 3.62 – Designed OPA567 High Current Buffer Output 76
Figure 3.63 – DC Characteristics of OPA567 76
Figure 3.65 – OPA567 Response to Sinusoidal Wave (500Hz, Amplitude 5V) 77
Figure 3.64 – AC Characteristics of OPA567 77
Table 3.7 - Main Characteristics of Designed High-Current Output Buffer (opa567) 77
Figure 3.66 - OPA567 Layout 77
Figure 3.67 - OPA567 3D View 77
Figure 4.1- Configuration of a digital control system. 79
Figure 4.2 - (A) Ideal sampler model of an ADC (B) Model of a DAC as a zero-order hold 80
Figure 4.3 - Magnitude of the frequency response of the zero-order hold with T = 1 s. 81
Figure 4.4- Cascade of DAC, analog subsystem, and ADC 81
Figure 12- Impulse response of a DAC and analog subsystem. (a) Response of an analog system to 82
Step inputs. (b) Response of an analog system to a unit pulse input. 82
Figure 4.6 - Block diagram of a single-loop digital control system 82
Figure 4.7 - Block diagram of a digital system with an analog disturbance 83
Figure 13 – (A) (B) 84
Figure 4.8 - Model of a basic add–drop single ring resonator filter 85
Figure 4.9 -(A) Notch type ring resonator filter characteristic (B) Add–drop ring resonator filter characteristic 86
Figure 4.11- (A) current Voltage characterization of the micro heaters in Tx (B) Ring resonator wavelength shift versus dissipated power 88

Figure 4.12- (A) current Voltage characterization of the micro heaters in Rx (B) Ring resonator wavelength shift versus dissipated power 88
Table 8 89
Table 4.1 89
Figure 4.13– (A)Responsivity of photodiode to the optical power (B)Generated Dark Current for different Bias voltages (C) Responsivity of the PD in 9dBm (D) bandwidth of monitoring photodiodes with 2 GHz cut off frequency 89
Figure 4.14 – Desired situation for the ring resonators and comb laser lines to satart Data Acquistion 92
Table 4.2 – TX tuning control system transfer Functions 93
Table 4.3 – RX tuning control system transfer Functions 94
Figure 14- Step plot, Bode diagram and Nyquist diagrams of Tx1/Tx2/Tx3/Tx4 95
Figure 15 - Step plot, Bode diagram and Nyquist diagrams of Tx5/Tx6/Tx7/Tx8 96
Figure 16 - Step plot, Bode diagram and Nyquist diagrams of Rx1/Rx2/Rx3/Rx4 97
Figure 17 - Step plot, Bode diagram and Nyquist diagrams of Rx4/Rx5/Rx7/Rx8 98
Figure 4.18 – Simulation configuration and results TX controller for Ramp + uniform Noise and Impulse + uniform Noise 100
Figure 4.19– Simulation results of TX controller for Ramp + uniform Noise and Impulse + uniform Noise 101
Figure 4.20 – Simulation results of Receiver tuning controller for Ramp + uniform Noise and Impulse + uniform Noise 102
Figure 4.21 Simulation results of Receiver tuning controller for Ramp + uniform Noise and Impulse + uniform Noise 103
Figure 4.22 (A) Laser spectrum before crow filter (B) laser Spectrum after crow filter 104
Figure 4.16– Expected initialization outcome for TX & RX 105
Figure 4.17– Initialization Program Structure 105
Figure 4.18– Simulation Configuration for Original and Reduced Order Models of TX & RX 107
Figure 4.19 – Original and reduced order model response to Step / Impulse / Uniform Noise 108
Figure 4.20- – Original and reduced order model response to Step / Impulse / Uniform Noise 109
Table 4.4 – Controller Parameters and Performance Criteria for Original and Reduced Order Model of TX 110
Table 4.5 – Controller Parameters and Performance Criteria for Original and Reduced Order Model of RX 111
Figure 4.22 – SPI Protocol 112
Figure 4.23 – SPI protocol communication setting for Data Read direct mode of ADS1158 113
Figure 4.24 - – SPI protocol communication Setting for Channel Data Register Read mode of ADS1158 114
Figure 4.25 - SPI protocol communication Setting for Channel Data Register Read mode of MAX5732 114
Figure 4.27 – Main Control Software Structure 115
Figure 4.26 – ADC(ADS1158) and DAC(MAX5732) Driver Structure Flow Chart 115
Figure 5.1 – (A) Laser ACE3 Spectrum (B) Laser ACE3 biasing configuration and Coupling to Lensed Fiber 117
Figure 5.2 – (A) Lambda Scan for Transmitter side laser output spectrum before Initialization (B) Lambda Scan for Transmitter side laser output spectrum after Initialization 118

Figure 5.3 - (A) Lambda Scan for Receiver side laser output spectrum before Initialization (B) Lambda Scan for Receiver side laser output spectrum after Initialization 119
Table 5.1 – offset values calculated by initialization program 119
Figure 5.4 – measurement of Eye diagram pattern and post processed measurement by PRBS averaging and Q-Factor computations for transmitter channels number 1,2, 3..... 120
Figure 5.5 - – measurement of Eye diagram pattern and post processed measurement by PRBS averaging and Q-Factor computations for transmitter channels number 4, 5, 6. 121